DESIGN AND CONSTRUCTION OF NEW HONEYCOMB SANDWICH PANELS USING SUPERPLASTIC FORMING AND VACUUM FORMING TECHNIQUE

A THESIS

Presented to

The Faculty of the Division of Graduate Studies

by

Amílcar José Gómez Fermín

In Partial Fulfillment

of the Requirements for the Degree

Doctor of Philosophy

in the School of Mechanical Engineering

Georgia Institute of Technology
December, 1976

DESIGN AND CONSTRUCTION OF NEW HONEYCOMB SANDWICH PANELS USING SUPERPLASTIC FORMING AND VACUUM FORMING TECHNIQUE

Approved:

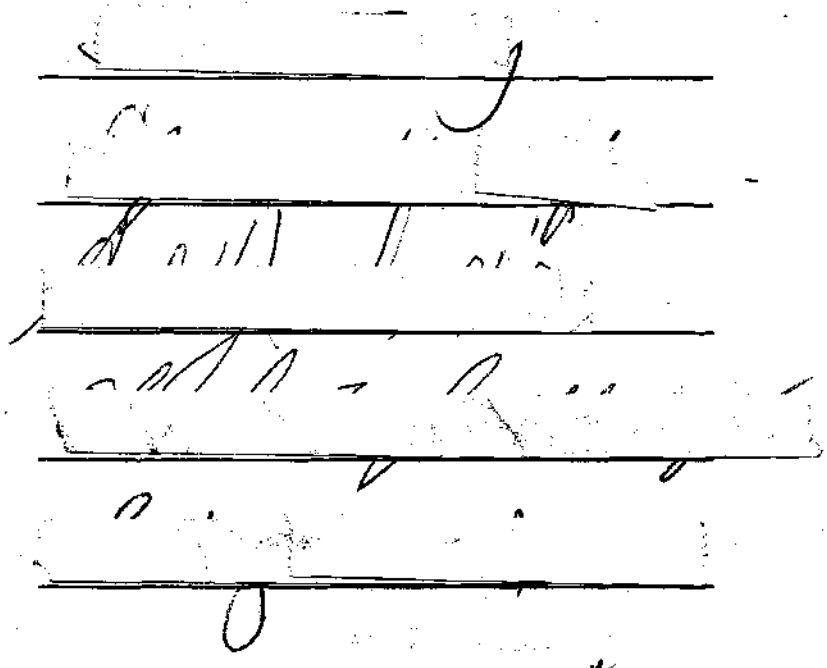

Date Approved by Chairman: 17th Dec. 1976

ACKNOWLEDGMENTS

The author wishes to express his deepest gratitude to Dr. John T. Berry, Chairman of the Reading Committee, academic and thesis advisor, for his encouragement, suggestions, and helpful almost weekly discussions.

Deep appreciation is also expressed to Dr. Ervin E. Underwood, who gave great encouragement to the author in his graduate studies, suggested the research subject material, and the preliminary efforts to make the wire reinforced honeycomb were under his advisorship.

Special thanks are given to Dr. Charles E. Ueng who was very helpful in the preparation of a joint publication together with Dr. E. E. Underwood and the author about the wire reinforced honeycomb, presented in IV InterAmerican Materials Conference, Caracas, June 1975.

Special thanks are due to Dr. Carl Jacobs, Dr. Satya Atluri, and Dr. Edgar E. Starke, for their effort as members of the thesis reading committee.

The author wishes to express his gratitude to Tilden Clopton, William Peel, Louis Cavalli, Clifford Bannister, and to Donald Cabe, for their valuable help in the construction of the equipment and the conduction of the experiments.

The author extends his gratitude to Mr. Olin Dewberry from the Industrial Design Department for his cooperation

in the vacuum forming process; and to Mr. Thomas Mackrovitch for his suggestions about the heating equipment, and willingness to help.

A feeling of indebtedness is expressed to the students Kim Fulkerson, Bud Rosenbach, Sudas Atvur, Richard Schmit, Trot Hunt, Jaime O. Constain, and Marco Chiappina, for their help in relation to this thesis, as part of their requirements in the courses ME 3213 and ME 4085 in the School of Mechanical Engineering.

The author extends sincere words of recognition to Sharon Butler and Annette Plunkett for their join effort in the preparation of the rough and final copies of this thesis.

He wishes to express his gratitude to his wife and their children to whom this thesis is dedicated for their understanding and encouragement.

A final note of gratitude goes to his parents who although they had little money; sought to raise eight children with love and help them play their roles in society.

TABLES OF CONTENTS

Page

LIST OF TABLES

LIST OF ILLUSTRATIONS

SUMMARY

The conventional light weight sandwich structure with a honeycomb core is very weak and unreliable at the fillet bond in the core-facing interface. The manufacturing method of the honeycomb is expensive, and thick cores are also very susceptible to buckling.

Analytical and experimental investigations were carried out to design and construct a new core using the vacuum ore pressure forming technique, in such a way that (a) more area is available for the core-facing bond, (b) inexpensive heat welding can be used for the core bonding, and theoretically (c) the core medhanical properties are not sensitive to buckling and independent of core thickness.

The optimum conditions for maximum shear strength and modulus of rigidity, the core mechanical properties, and the material flow in the various stages in the forming process were investigated, and theoretical estimates developed in this research program.

Cores from both superplastic eutectoid Zn-22Al and High Impact Polystyrene sheets, with Kevlar fibers embedded were manufactured and tested under shear, buckling, and bending; and the results were evaluated accordingly.

The High Impact Polystyrene cores, although in the experimental phase, have comparable mechanical properties

to the non-metallic cores, and it seems that further improvement is quite possible by completely heat welding the core.

A unique and novel detail in WRH cores seems to be the formation of projections with flat top and bottoms interconnected by heat welded webs which have wires or fibers embedded within them for reinformcement.

The thickness distribution within the cores was scrutinized as a function of location and a theoretical justification for the flow behavior was presented. As a consequence of this analysis, an improved projection configuration and arrangement of the wires has been introduced for future investigation.

NOMENCLATURE

Latin Symbols	Definition	Units
A	$(R_o-x_2)/(R_o-x_1)$,	dimensionless
A_o	ab/N, area per projection	m^2
A_1	cross section in sheet number one	m^2
A_2	cross section in sheet number two	m^2
A_c	core cross section	m^2
A_o'	area of undeformed material per projection	m^2
A_s	cross section under shear	m^2
a	length of the core	m
A_{mn}	$16qb^4 (1+\rho\Omega)/(\pi^6 mnD_2\Omega^2)$, coefficient for deflection w_{mn}	m
B	ratio w_o/w_1	dimensionless
b	width of the core	m
c	core thickness	m
D	flexural rigidity	N-m
D_2	$Etdc/(1-\nu^2)$, approximate flexural rigidity	N-m
d	c + t, conventional sandwich thickness	m
E	U + V, total energy	N-m
E	Young's modulus of elasticity	MPa
E_c	core Young's modulus of elasticity	MPa
E_s	sheet modulus of elasticity	MPa
E_x	core modulus of elasticity in the x-direction	MPa

Latin Symbols	Definition	Units
E_y	core modulus of elasticity in the y-direction	MPa
E_α	core modulus of elasticity in the α direction	MPa
F	loading force in the shear test	N
F	$m^2b^2/a^2 + 1$, sandwich factor	dimensionless
F_1	internal force in sheet number one	N
F_2	internal force in sheet number two	N
F_N	normal force component in a shear test	N
F_x	shear force component in a shear test	N
F_s	force applied to a core sheet	N
F_w	force applied to the embedded wires	N
f_s	F_s/N, shear force per projection	N
G	facing modulus of rigidity	MPa
G_c	core modulus of rigidity	MPa
G'	core material modulus of rigidity	MPa
H	height of projection in mathematical model	m
h	height of experimental projections	m
K_1	$(mb/a + a/mb)/(1 + \rho[(mb/a)^2 + 1])$, sandwich parameter	dimensionless
k	stress constant	Pa
k_1	$(R_o - x)$ Gw, constant, solution of differential equation	N
L	length of plate	m
ℓ	distance between projections center	m
ℓ_1	spearation between projections, length of webs	m

Latin Symbols	Definition	Units
m	integer number	dimensionless
m	strain rate sensitivity factor	dimensionless
N	number of projections in a core	dimensionless
N_x	force per unit length in the x-direction	N/m
n	integer number	dimensionless
P	maximum load before plate buckling failure	N
P_E	maximum load before plate buckling failure, assuming infinite shear modulus	N
p	applied forming pressure	Pa
p_1	applied pressure in sheet one	Pa
p_2	applied pressure in sheet two	Pa
Q	-dM/dx, shear load	N
q(x)	normal load per unit length	N/m
q_n	coefficient in load infinite series	N/m
R_o	maximum radius of formed sheet	m
r	radius of curvature	m
r*	radius of curvature at the end of second forming stage	m
s	length of deformed element at time t	m
s^+	length of a deformed element at time t + dt	m
s*	length of deformed element at the end of second forming stage	m
t	time	see

Latin Symbols	Definition	Units
t_o	initial sheet thickness	m
t_1	time elapsed forming sheet one	see
t_2	corresponding time forming sheet two	see
U	strain energy	N-m
U_c	strain energy of the core	N-m
U_f	strain energy of the facings	N-m
u	displacement in the x-direction	m
V	potential energy of the sandwich	N-m
V_1	potential energy due to edgewise load	N-m
V_2	potential energy due to normal load q	N-m
V_p	effective volume of material per projection	m^3
v	displacement in the y direction	m
x	distance in the undeformed sheet or sandwich	m
x_1	distance in sheet one at time t	m
x_2	distance in sheet two at time t	m
y	distance in the undeformed sheet, perperdicular to x	m
y	w_2/w_1 ratio	dimensionless
w	displacement in the z-direction	m
w	sheet thickness at time t	m
w^+	sheet thickness at time t + dt	m
w_o	initial sheet thickness	m
w_x	sheet thickness at a distance x	m

Latin Symbols	Definitions	Units
w^*	thickness at the end of second forming step	m
w_1	thickness of sheet number one at time t	m
w_2	thickness of sheet number two at time t	m
$w_1(0)$	initial thickness in sheet number one	m
$w_2(0)$	initial thickness in sheet number two	m
w_{mn}	coefficient in the infinite series of deflection	m
w'	deflection due to core properties only	m
w''	deflection independent of core properties	m
z	direction perpendicular to the sandwich facing	m

Greek Symbols	Definition	Units
α	angle between the load F and the loading plates	dimensionless
γ	shear strain	dimensionless
γ_{zx}	shear strain in the zx plane	dimensionless
γ_{xy}	shear strain in the xy plane	dimensionless
γ_{yz}	shear strain in the yz plane	dimensionless
ε	strain	dimensionless
ε_x	strain in the x direction	dimensionless
ε_y	strain in the y direction	dimensionless
$\dot{\varepsilon}$	strain rate	sec^{-1}
$\dot{\varepsilon}_A$	strain rate at position A	sec^{-1}

Greek Symbols	Definition	Units
$\dot{\epsilon}_B$	strain rate at position B	sec^{-1}
ξ	$\pi^2 Ect/2L^2 G_c$, sandwich constant	dimensionless
λ	$\lambda(\partial w/\partial x)$, coefficient of slope	dimensionless
λ	Lagrange multiplier	m^{-1}
μ	friction coefficient	dimensionless
μ	$\mu(\partial w/\partial y)$, coefficient of slope	dimensionless
ν	Poisson's ratio	dimensionless
ρ	$\pi^2 Etc/2(1-\nu^2)Gb^2$, sandwich parameter	dimensionless
ρ	material density	gr/cm^3
ρ_c	core density	gr/cm^3
σ	internal stress	Pa
σ_1	internal stress in sheet number one at time t_1	Pa
σ_2	internal stress in sheet number two at corresponding time t_2	Pa
σ_A	internal stress at point A	Pa
σ_B	internal stress at point B	Pa
σ_f	Mz/DE_f, stress at the facing	Pa
σ_x	stress in a section normal to the x-direction	Pa
σ_y	stress in a section normal to the y-direction	Pa
τ	shear stress	Pa
τ'	f_s/A, average shear stress at a section A-A in the core	Pa
τ_{xy}	shear stress in a plane normal to the x direction, and oriented in the y direction	Pa

Greek Symbols	Definition	Units
Ω	$(m^2b^2/a^2) + n^2$, sandwich parameter	dimensionless

CHAPTER I

INTRODUCTION

The need for faster air transportation with greater effective load per pound of thrust led to the development of the sandwich construction having a very light core bonded to a strong facing on each side. The most currently used cores are made from aluminum foils, glass reinforced plastic, polyurethane or other foams, balsa wood, and paper honeycombs. Although it possesses good shear strength τ_c and modulus of rigidity G_c, the conventional core requires a fillet bond to secure it to the facing sheets. This results in a decrease in reliability and core mechanical properties, especially under fatigue. As the honeycomb cells have no internal surfaces parallel to the facings, they are extremely susceptible to buckling and the shear strength is drastically reduced in the thicker core range. Finally, the manufacturing method of the honeycomb requires an excessive amount of expensive, consecutive bonding and curing operations, rendering its use prohibitive in a number of applications.

Balsa wood and paper are excellent core materials in terms of strength to weight ratio, but their properties are very unreliable and susceptible to drastic changes as

function of the moisture content and aging.

In an attempt to improve the weak fillet bond of the standard honeycomb, plastic cellular cores have been recently introduced in the market. They are frequently manufactured by transforming heated plastic sheets into three dimensional shells possessing flat tops and bottoms; however, they do not have cells interconnected and this is very detrimental to the shear strength and the modulus of rigidity of the core.

A critical evaluation of the manufacturing methods and mechanical properties of the commercial cores led to the recognition of the following principal areas which were the object of the present research: (1) Improvement of the core facing bonding areas, (2) Development of a core resistant to buckling, and (3) Methods to reduce adhesive bonding operations. Starting from this frame of reference, the author developed an apparently novel core manufacturing technique*, by which a strain rate sensitive plastic or metallic sheet can be formed around wires or fibers and projections disposed in different arrangements, as the sheets are heated to a characteristic temperature and formed by either vacuum or pressure against a die. In this way, a composite shell is generated, having the appearance

---

*A patent covering this technique has recently been filed.

of a wire reinforced honeycomb (WRH) core, incorporating a group of surface of revolution projections disposed in a regular fashion and interconnected by vertical webs in which wires are embedded. The core presents flat tops and bottoms, as shown in Figure 1-1, which permits a good bonding area and limits the cell height to a fixed value, making the core insensitive to buckling, unlike the conventional honeycomb.

The most effective bonding method, in applying the WRH process to plastic sheets, seems to be heat welding, since no adhesive is required except for bonding the core to the facings. Heat welding not only optimizes the core strength, but as the energy required has already been transmitted to the material for the forming process, heat welding may be economically highly advantageous.

As the technique of the WRH cores was mastered, new ideas were generated up to optimize the core shear strength and the modulus of rigidity. So, in the second phase of the investigation, formulations were developed (a) for the thickness distribution in the various stages of the forming process, (b) for the optimum flow, and (c) for estimating the core mechanical properties. A series of shear, buckling, bending and thickness distribution tests were conducted in an attempt to determine the core mechanical properties and to confirm the theoretical analysis.

Heat welded cores can be manufactured in a wide density range, and strength to weight ratios would be expected to increase markedly through further improvement of core-facing bond, the use of other plastics materials, and optimization of projection shape and arrangement, following the lines discussed in the present work.

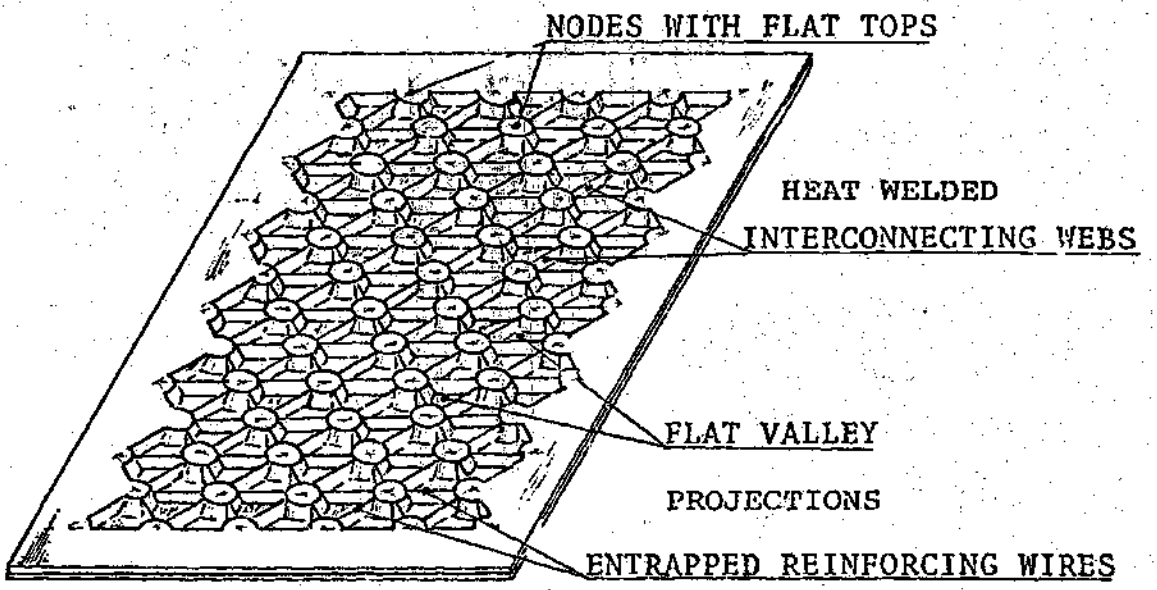

Figure 1-1. Wire Reinforcing Honeycomb (WRH) Cores Made from Plastics or Metallic Sheets.

CHAPTER II

LITERATURE REVIEW

To process and characterize the wire reinforced honeycomb, it is in order to make a literature survey referring to the conventional honeycomb manufacturing process, to materials currently used in sandwich construction, and to the mechanical behavior of those materials, such as polymers and superplastic Zinc-22Al which might be used for processing wire reinforced honeycomb.

The following literature survey therefore relates to previous studies pertaining to sandwich construction characterization and testing procedures, bonding methods, reinforcing fibers, as well as superplastic materials.

Sandwich Construction

Sandwich construction is a relatively novel structural element, having its origin during World War II. It has principally been used in the air and space vehicles. Although of fairly recent origin, many researchers have devoted effort to the characterization of the mechanical properties of the light weight structures, and have attempted, for design purposes, to understand the behavior of the core as a function of configuration and materials properties.

Most of the work to date has dealt with aluminum honeycomb, which seems to be the type of core most currently used. For example, Kuenzi [2,3,5,7,8], Voss [1], Stevens [6,7], and Jenkinson [5,10], have all been productive in the study of the aluminum honeycomb, as well as low density cores such as those made from Kraft paper, polyimide and polyester films. Topics reviewed include the strength of the core, manufacturing processes and also test procedures. Some of these may briefly be summarized as follows.

Voss [1] studied the mechanical properties of low density sandwich cores made out of materials such as foam resins and glass-fiber deformed mats impregnated with resins having a waffle pattern. He found wide variations in the mechanical properties for otherwise similar cores. The mechanical properties of commercially available honeycombs used in structural sandwich construction have been studied by Kuenzi [2]. The analysis of the experimental data included methods for predicting average strength and stiffness values from basic material properties and core configuration. It is interesting to note that Kuenzi reports shear modulus variations for the aluminum honeycomb as much as 500 percent.

Paper honeycomb for structural building panels was evaluated by Seidl, Kuenzi and Fahey [3]. They investigated the effect of the decay, acidity, alkalinity and aging on the shear and compressive strength of paper cores. The weight percent of the phenolic resin, urea, and sodium

silicate adhesives were varied in an attempt to determine optimum proportions of base material (Kraft paper) and adhesive for core manufacturing.

The use of resin impregnated paper to make sandwich cores has also been studied by Markwardt and Wood [4]. By glueing together large numbers of flat and corrugated sheets in different configurations, a variety of combinations were made available. The sandwich panels made from this type of material has an application in building construction.

Turning to metallic light weight structures, Jenkinson and Kuenzi [5] made a series of experiments to characterize the shear strength of aluminum honeycomb cores as a function of core thickness. They found that (1) tension and compression shear tests generate similar values for shear strength and (2) as the core thickness increases the shear strength decreases for the same honeycomb density.

An evaluation of the compressive and shear properties of corrugated foil sandwich cores was performed by Stevens [6]. The crossbanded cores were tested and compared with conventional aluminum honeycomb for the same density. The aluminum hexagonal honeycomb proved to have higher modulus of rigidity G_c and shear strength.

Stevens and Kuenzi [7] also made a series of experimental determinations of mechanical properties of hexagonal honeycomb cores and proposed a series of linear empirical equations relating compressive strength to density,

compressive strength to shear strength and an equation correlating the shear strengths in the length and in the width directions of the core.

Kuenzi [8] went on to discuss how a series of tests were conducted to assess the structural capability of titanium alloy sandwich construction having the facings and the honeycomb core bonded by diffusion. Results in flatwise tension and compression, edgewise compression and shear tests were presented.

Turning to testing techniques, Kommers and Norris [9] designed an apparatus for evaluating sandwich plates where the load is applied normal to the facing as a vacuum pump is connected to an evacuated box that has knife edges where the sandwich rests. Although this is not a standardized test, it can be used in a rather convenient way to determine the shear properties of a sandwich construction. Comparison of the analytical and experimental deflection as a result of shear in the sandwich are possible using the described testing apparatus.

Again, referring to polymeric materials, Jenkinson [10] has determined the shear strength of polyimide and polyester film honeycombs. The specimens were prepared by dipping the core edges in epoxy resins to form reinforcing fillets about 1.5 mm thick around the boundary of the cells.

Most recently, Baldanza [11] made a state-of-the-art survey of plastic sandwich construction to provide general

and technical information for the designer in tank and automotive components such as vehicle bodies, fire walls, ballistic resistant panels and flotation units. He appears to favor the use of honeycomb for vehicle bodies provided that cells are filled with a suitable close cell foam. He reported that sandwich construction in general appears to have definite advantages over solid materials for ground transportation applications as it is evident from its high strength to weight ratio and stiffness factor.

With the intention to fabricate a sandwich core with higher strength-to-density ratio than the aluminum honeycomb and with manufacturing technique involving no adhesive bonding, Ogden, Abraham and Taffee [12] developed a process for production of sandwich structures which can be formed to complex contours without detrimental effects at the core-facing interface. The core is made by roll-bonding Ti-6 Al-4 V alloy sheets and subsequently diffusion bonding the core to the facings. During the bonding process the core is supported by filling the empty spaces with suitable materials that are later removed by a leaching operation, however, a more reliable method to eliminate the filler material had yet to be found.

Looking at more recent evaluations of honeycombs, Bendix Corporation [13] investigated the energy absorption characteristics of several types of aluminum honeycomb cores under a range of pressure and temperature conditions to

determine the feasibility of light weight structures as shock attenuators in the soft landing of space vehicles. The Bendix report seems to convey the idea that crushable materials in capsule form may be the best choice to counteract meteorite and landing impact, variation of friction with environment, and maintenance of close tolerances in the space ships.

Turning to the analysis of the behavior of sandwich structures, following Reissner's theory of plates, Ueng [14] has developed a set of equations for the generalized forces acting on a sandwich plate. These equations together with the equilibrium equation represent a system of equations for the generalized forces and displacement variables. Ueng reported the similarity in the analysis of sandwich plates and homogeneous plates and provided an example problem to demonstrate the simplicity of his approach for special cases compared to other methods.

A series of basic analyses in monograph form about sandwich structures have been compiled by both Allen [15] and Plantema [16]. The theory, in its more complete form, can be considered as an extension of beam and plate theory for homogeneous materials. It was noted that the deflection of the sandwich as a result of core shear while disregarded in plate theory, it is considered quite significant in sandwich analysis.

Bonding

The bonding of the strips to make a sandwich core, as well as the core-facing bond seems to be an area of intensive research because excessive deformation due to bending and buckling and fatigue failures can be traced back to cohesive or adhesive characteristics of the bonding medium.

Effort has been dedicated to the improvement of adhesive life and strength, resistance to high temperature, non-adhesive bonding methods such as diffusion bonding and heat welding, and also surface preparation and adhesive application.

A study of how the surface of both the core and facings of a sandwich structure should be prepared for better bonding has been made by Eickner [17], Black and Blomquist [18]. The chemical solutions and surface preparation methods in industry today follow closely Eickner's recommendations. Tension tests with a bonded area of 12.5 mm x 101.6 mm (1/2 in x 4 in) according to ASTM Standards to determine the strength of the bond were conducted.

Fan [19] went on to disclose that the quality of the adhesive to join the facings and the core is a very significant factor in the final results of the sandwich edgewise compression strength. The implications for these findings in the actual engineering design is that the core modulus of rigidity G_c may not be considered as an invariant in the

evaluation of the critical buckling stress of the sandwich. Fan suggested that the testing technique should be improved to include specific data of the bonding medium. To obtain more reliable results for G_c, a shear test may also be done for comparison purposes.

The procedure to clean the surface of aluminum sheets prior to bonding has been examined by Cagle [20]. The design of various types of joints has been considered and a series of bond strength tests were proposed.

The possibility of bonding plastic to itself by applying heat and pressure has been discussed by Skeist [21]. He has indicated that most plastics, except cellulose nitrate, can be heat welded between 325°F and 400°F.

Debruyne [22] has made a comprehensive study of the adhesion mechanism, adhesion and cohesion and the preparation and uses of epoxy resin adhesives. In reference to the plastic sheet forming technology, Bernhardt [23] has made an extensive review about plastics hot forming. Many variations of the vacuum forming process are discussed as well as aspects of parts design and limitations. Details regarding heating and optimum forming temperature for most plastics and in particular for High Impact Polystyrene are given.

Reinforcing Fibers

In an effort to increase the core-facing bonding area

in a sandwich, the author developed the idea of using thin wires or organic fibers to form webs to join surface of revolution projection shells in a regular fashion, as a metallic or polymeric sheet is transformed into a sandwich core by pressure or vacuum forming against a die and a wire or fiber mesh, as illustrated later in Figure 3-2. Kevlar 49 aramid seems to be about the most promising fiber used for that purpose. Riewald and Venkatachalam [24] have evaluated the excellent properties of "Kevlar" strengthening fibers and determined the maximum temperature that this organic material can stand without appreciable degradation. A tensile strength of 3.3 MPa (500,000 lbs/in^2) has been reported for Kevlar 29 and Kevlar 49.

Superplastic Materials

To make the wire reinforced honeycomb, the sheets area must be increased in the order of 200 percent and the material must flow fairly uniform. For this reason, a superplastic alloy sheet must be used. What follows is a quick literature survey of the most relevant development in the field of superplasticity. This subject is covered in greater detail in the Appendix F.

It was observed in the 1920's by Rosenhain [25] and Sauveur [26] that some materials like zinc, copper, aluminum eutectic alloy and iron had mechanical characteristics closely resembling hot polymers or glass at the transformation

temperature. This type of behavior was later identified as "superplasticity" by Bochvar.

Underwood [27] is distinguished by producing an extensive review of the subject and, in fact, introduced the term "superplasticity" to the United States. Rossard [28] demonstrated analytically that superplasticity is the result of an equilibrium between hardening and recovery above the half melting point for some alloys; therefore strain rate must be a basic parameter that controls the superplastic characteristics of such materials. He determined the minimum value that the strain rate sensitivity factor m should have for significant superplastic deformation to take place. This was proved experimentally by Backofen, Turner and Avery [29].

Rossard [28] also showed that for stable superplastic flow of material, the stress in the equation of state should be a function of strain, strain rate, a strain rate sensitivity index m, and a strain hardening index N. To this regard, Holt [30] theorized that, provided that the strain hardening index N is a material constant, Rossard's equation of state can be reduced to an expression where strain rate but not strain is the independent variable controlling the flow stress. In such case, the constitutive equation could be written as

$$\sigma = k\dot{\varepsilon}^{m}$$

According to Ragab and Duncan [31,32] the strain rate sensitivity factor can also affect the equation of state for backward extrusion of superplastic Zn-22Al alloy, and for uniaxial torsion tests on Zn-22Al and Sn-Sb alloys. They made some theoretical analyses substantiated by experimental evidences on this line.

Headley, Kalish, and Underwood [33] have studied the microstructure, the forming technique, and industrial applications of commercially available superplastic alloys. They have considered that ultrafine-grain size is the most important characteristic of superplastic materials.

Regarding the manufacturing of superplastic materials, Holt [34] has studied the conditions to produce a superplastic alloy. Basically the grain should be between 1-10μm, the material should be multiphase, and the stability of the grain structure is provided by low interphase boundary mobility.

Looking for some basic explanations for the ductile behavior of some materials, Honeycombe [15] has proposed that the main factors that govern maximum ductility in single crystal are (1) only one slip system, (2) alloy purity, (3) free movement and high elimination rate of dislocations, and (4) uniform plastic deformation throughout the specimen.

The deformation characteristics of conventionally plastic alloys and superplastic alloys has been compared by

Nicholson [36]. Emphasis was put in zinc and magnesium superplastic alloys and its wide range for possible applications.

The deformation characteristics of eutectoid Zn-22Al alloy at room temperature has been studied by Nuttall [31]. He found that both the tensile strength and the hardness of eutectoid An-22Al amazingly diminish with cold work. Nuttall's findings seem to suggest that the effect of grain size upon the flow stress and presumably on hardness in superplastic materials may be quite the opposite as compared with the effect on common alloys.

Turning to industrial applications, Naziri and Pearce [38] have discussed the advantages and disadvantages of using superplastic materials for production. They have put emphasis in the possibility of manufacturing complex parts in small presses in a few operations.

A group of researchers from IBM led by Fields [39] investigated the mechanical properties, forming ability, and applications of Zn-22Al alloy. Underwood, Gomez and Ueng [40] analyzed the use of vacuum forming as a new method to fabricate sandwich cores using superplastic materials. They put emphasis in the relatively inexpensive equipment required for the core manufacturing.

CHAPTER III

INSTRUMENTATION AND EXPERIMENTAL APPARATUS

In order to make the wire reinforced sandwich core, High Impact Polystyrene sheets were processed in a laboratory type vacuum forming machine, Figure 3-1; while the Zn-22Al sheets were pressure formed in an integral furnace-pressure forming assembly specially made for that purpose, Figure 3-3. In both cases the sheets conformed to the shape of a die which was made with interchangable projections, Figure 3-2. Sandwich panels were made by placing a facing on each side of the core.

Tensile shear, compression shear, edgewise compression, and bending tests, Figure 3-8 to Figure 3-12, were made following ASTM specification guidelines [50]. An Instron universal testing machine, Figure 3-4, was used for these tests in conjunction with a Sanborn recorder, Figure 3-7, which was used for registering strain in the edgewise compression and bending tests.

The above instrumentation and apparatus are described in detail in the present chapter.

Vacuum Forming Machine

A vacuum forming machine was used for the formation of the polystyrene sheets into sandwich cores. The machine

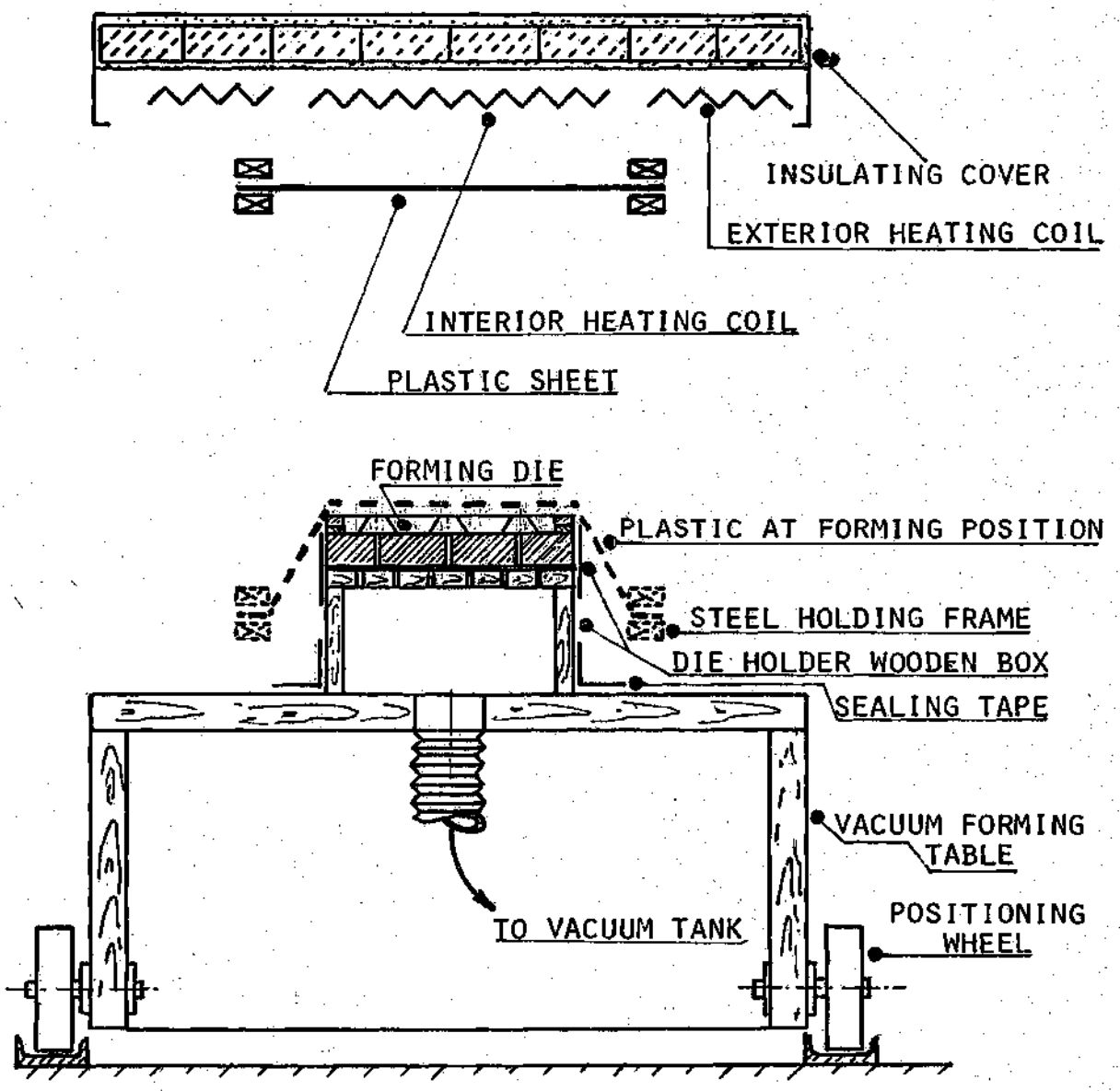

Figure 3-1. Schematic Representation of Vacuum Forming Machine.

has a heating table of 2.1m x 1.8m with two sets of electrical heating coils covering an area of 1.8m x 1.5m; but only the interior set of coils which covers a space of 0.9m x 1.5m and has a power consumption of 420 KW was used throughout this research. A steel holding frame with vertical motion brings the plastic sheet to a fixed distance from the heating coils, as illustrated in Figure 3-1. The frame is attached to the vacuum forming table which has a backward and forward horizontal motion. The positioning of the frame in the horizontal and vertical directions with respect to the heating coils is controlled by limit switches. The vacuum forming table is connected to the 0.13 m^3 evacuating tank by 7.5 cm (3 in.) flexible hose. The purpose of the tank is to provide and sustain sufficient vacuum during the entire plastic forming process. After several forming cycles, a limit switch activated by the tank pressure turns on the vacuum pump motion to reduce the tank pressure to working levels, about 1.3 KPa. The machine is located in an enclosed area to avoid chilling of the plastic sheets as they are formed. The polystyrene cores are made as the heated plastic sheet is brought into contact with an aluminum die that is placed in the vacuum forming table and the air between the die and the plastic is evacuated.

Forming Die

The forming die illustrated in Figure 3-2 has general dimensions of 21.5cm x 29cm x 2.54cm. It comprises a base plate, a set of boundary frames, boundary pins, interior pins, small lateral cylindrical pins for wire fastening, and an electrical circuit to indicate the end of the forming process. The die is made out of 2024 aluminum alloy which is very easy to machine, has good corrosion resistance at the working temperature and it has high heat conduction coefficient compared with steel. The base plate has a series of 6.25mm (1/4 in.) holes disposed in triangular pattern, 12.5mm apart, in which both the boundary and interior pins fit. There are also ten 2mm holes in the base plate for air evacuation during both vacuum and pressure forming. While the boundary pins have a cylindrical projection to allow fit in the boundary frame without major gaps, the interior pins are shaped like truncated cones. The boundary frame has an internal zig-zag contour, which proved to be essential for both pressure and vacuum forming. In this way the sheet material is stressed the same at all locations, and tearing of the sheets, due to thinning and stress concentration at the boundary, is avoided. All the pins and the boundary plates can be removed easily from the base plate so that experimental cores with different configuration and height can be made. Three small 0.125mm deep grooves are placed on each pin to

provide space for the reinforcing wires; but this turned out to be unnecessary when the Kevlar 49 bundles are used as reinforcing fibers, since they flatten out when they are placed on top of the projecting pins. Consequently, the top and bottom bonding surfaces of the core are essentially flat. A series of small grooves are machined in the boundary frame and 1mm steel pins are inserted in the frame in a horizontal position in alignment with the boundary grooves. In this way a mesh of Kevlar fibers can be readily woven on top of the die. As there is no visible way to tell when the forming process is completed, an open electrical circuit is installed in the die. Two thermocouple wires with ceramic insulation were inserted in the base plate and connected to contact points at the upper surface of the plate. The wires are connected to a 3 volt battery-power light source. As the metallic sheet reaches the bottom of the die, the electrical circuit is closed and the light source indicates that the pressure forming process is near completion.

Pressure Forming Furnace

The Zinc-22Al sheets were formed in a furnace with a heating space of 30cm x 30cm x 20cm, as illustrated in Figure 3-3. Stainless steel 3mm tubing connects the furnace to the main air line. The pressure to form the sheet can be varied from 34 KPa (5 psi) to 690 KPa (100 psi)

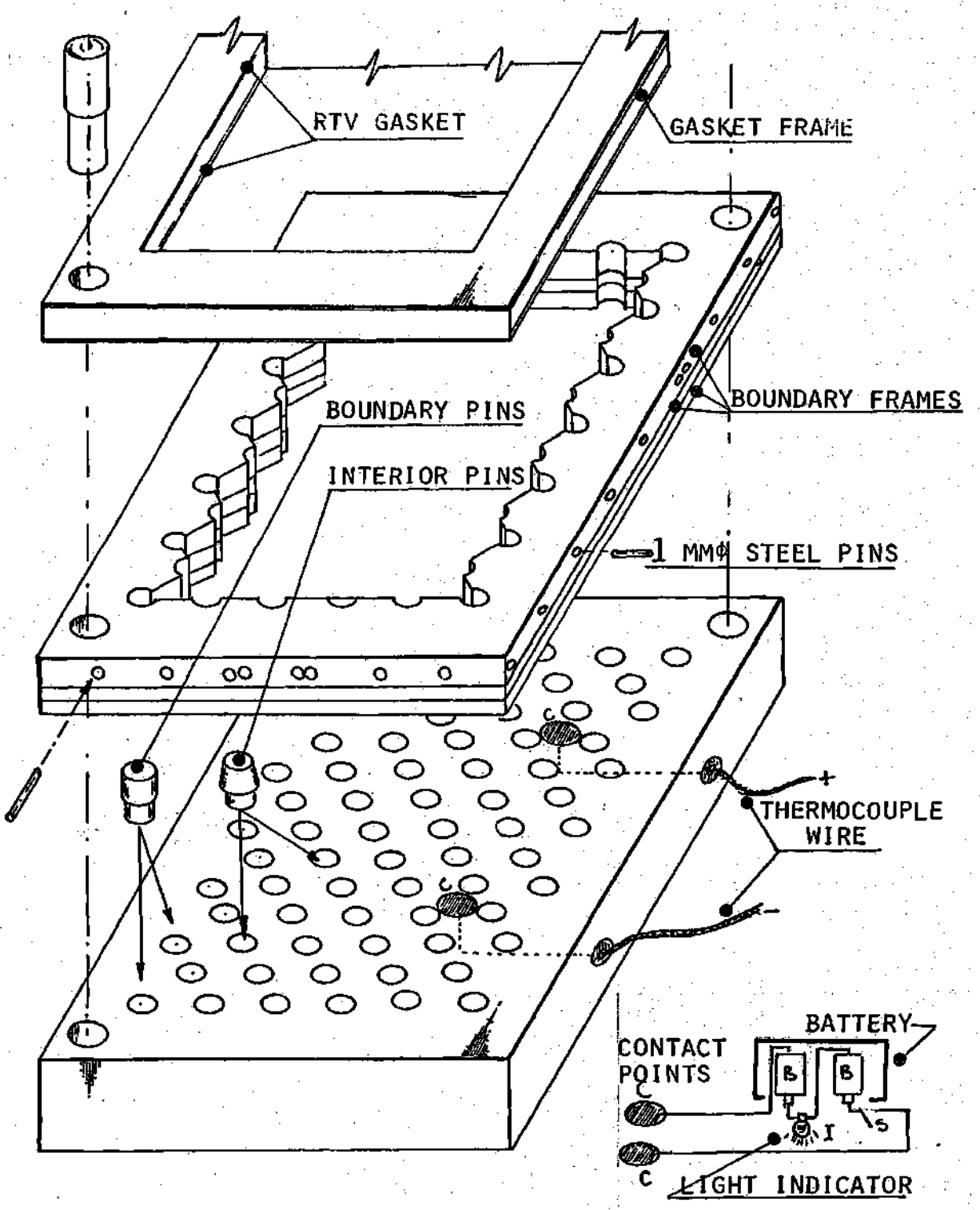

Figure 3-2. Pressure and Vacuum Forming Die.

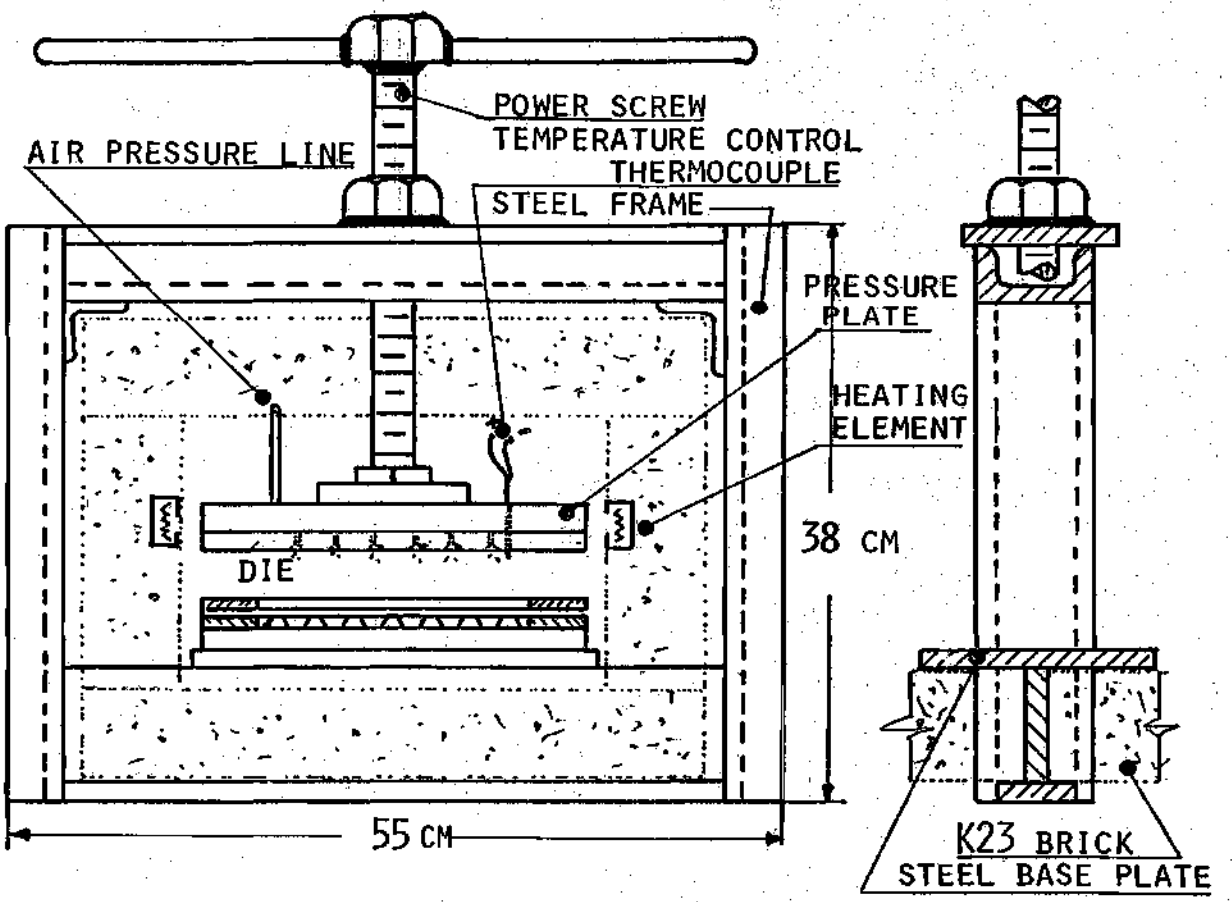

Figure 3-3. Pressure Forming Furnace.

by means of an air pressure regulator. A gasket made from a 6.25mm thick 2024 aluminum frame covered with a 2mm thick layer of RTV (silicon rubber), seals the air pressure chamber that is above the superplastic sheets to be formed. The chamber is closed as a 25.4mm manually driven power screw tightens down the upper portion of the die against the forming sheet. The air is brought into the pressure chamber through a 6.25mm thick 2024 aluminum perforated plate with 1mm holes, placed 6.25mm apart. In this way, as the chamber is pressurized, no transient high air flow takes place that may blow and tear abruptly the forming sheet. The furnace temperature is regulated by an on-off control circuit which is connected to an iron-constantan thermocouple installed in the upper portion of the die. The furnace is heated by two 1500 Watt coils installed on the side walls of the furnace. The walls were made with 7.5cm x 15cm x 45cm K23 light weight porous alumina B and W bricks, good for a maximum temperature of 2300 °F. These fire bricks were selected because they are very soft and they can be cut and machined very easily with ordinary machine shop tools. For safety reasons, the furnace is installed under a hood with a constant draft. When the furnace is in operation, the hood door is lowered almost to a closed position, so that the positive air pressure in the laboratory helps to remove, through the hood, the gases generated during the curing of any adhesive.

The Instron Universal Testing Machine

All the tests to determine the mechanical properties of the sandwich core were performed in a universal testing machine, model TTC standard, manufactured by the Instron Corporation. This testing instrument has a sensitive, electronic weighing system with load cells that use strain gages arranged in a Wheatstone bridge to detect and record tensile or compressive loads. The moving crosshead is operated by two vertical drive screws, as shown in Figure 3-4. At low velocity the machine can be operated in a number of positions from 0.0508 cm/min (0.02 in/min) to 5.08 cm/min (2 in/min). The load cells used for all the experiments had an operating range zero to 200, 500, 1,000, 5,000, and 10,000 lbs. The strain gages on any load cell are excited by a stabilized oscillator. An applied load on the cell causes a proportional change in the resistance of the strain gages, and the resulting signal is amplified, rectified to DC and fed to the driving circuit of a null-balance, high speed recorder. The sensitivity of the amplifier may be changed in calibrated steps of 1, 2, 5, 10, 20, 50, and 100, enabling the load cell to provide a number of full scale ranges. The manufacturer claims an accuracy of the overall weighing system of ±0.5% of the indicated load or ±0.25% of the recorder scale, whichever is greater. The machine has a compression accessary that permits application of a compressive load on the specimen

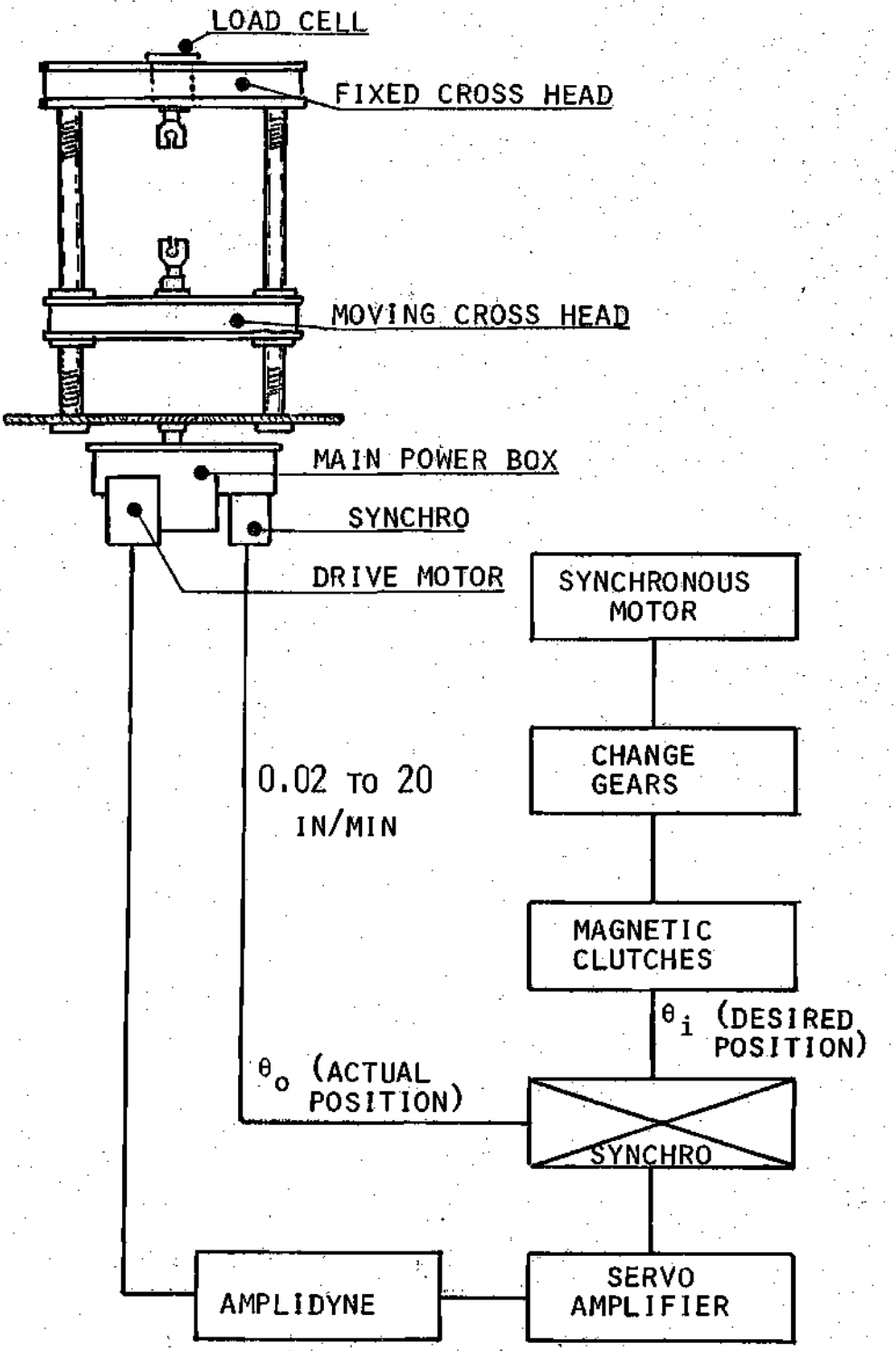

Figure 3-4. The Instron Universal Testing Machine Schematic Diagram.

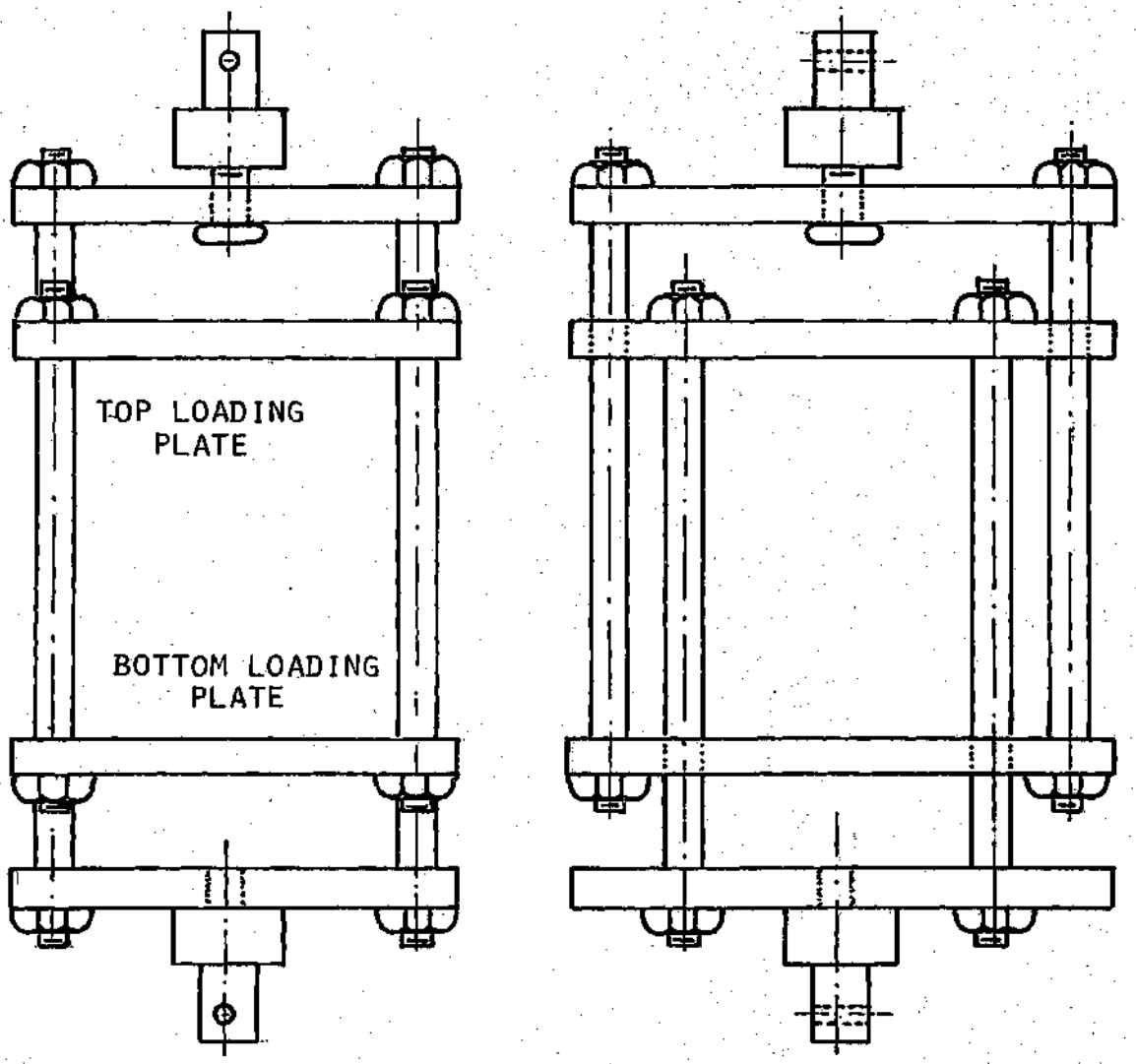

Figure 3-5. The Instron Compression Accessory. The bottom plate moves down at the cross heat velocity. Top plate remains stationary.

as the load cell registers a tensile load acting on the moving crosshead, as shown in Figure 3-5. The simply supported loaded end and four supported edge buckling tests, the compression shear test and the four point bending test required the use of the compression accessory.

The Sanborn Strain Recorder

In order to read the strain on the facing sheets of a sandwich construction as the bending and buckling tests were performed, a number of strain gages were mounted on the sandwich facings. The strain gages were connected in a full Wheatstone bridge circuit, as shown in Figure 3-6. The change in resistance of the active strain gage unbalances the circuit. A carrier preamplifier Model 150-1100, manufactured by Sanborn Company, measures the strain on the facing sheets by measuring the unbalance voltage from the bridge. The carrier preamplifier supplies an excitation voltage to the transducer (Wheatstone bridge); in turn, as the load is applied to the cell, the transducer generates a voltage signal (produced by the active arm of the bridge) that is picked up by the Sanborn carrier preamplifier 150-1100. The preamplifier interprets the transducer output in terms of the physical load and moves the galvanometer stylus across the recording paper, as shown diagramtically in Figure 3-7. The carrier preamplifier includes a zero suppression control which can suppress the indication of a

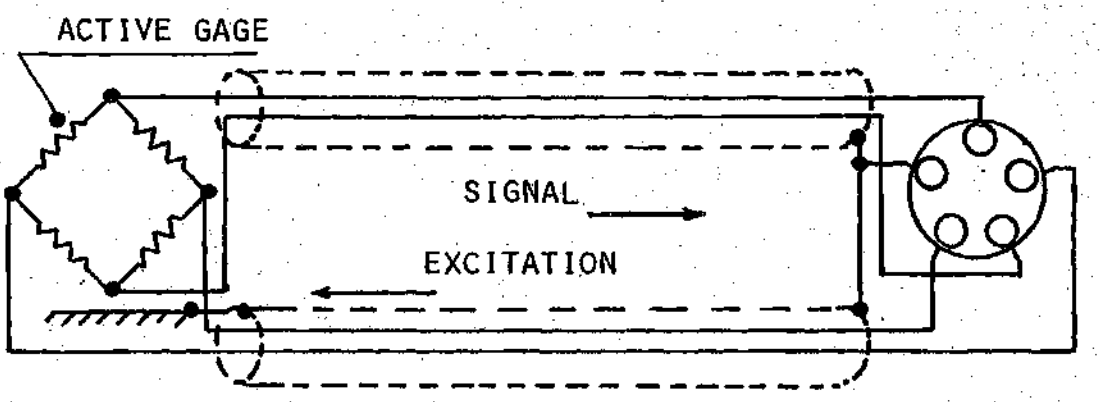

Figure 3-6. Full Bridge Connections to Carrier Preamplifier.

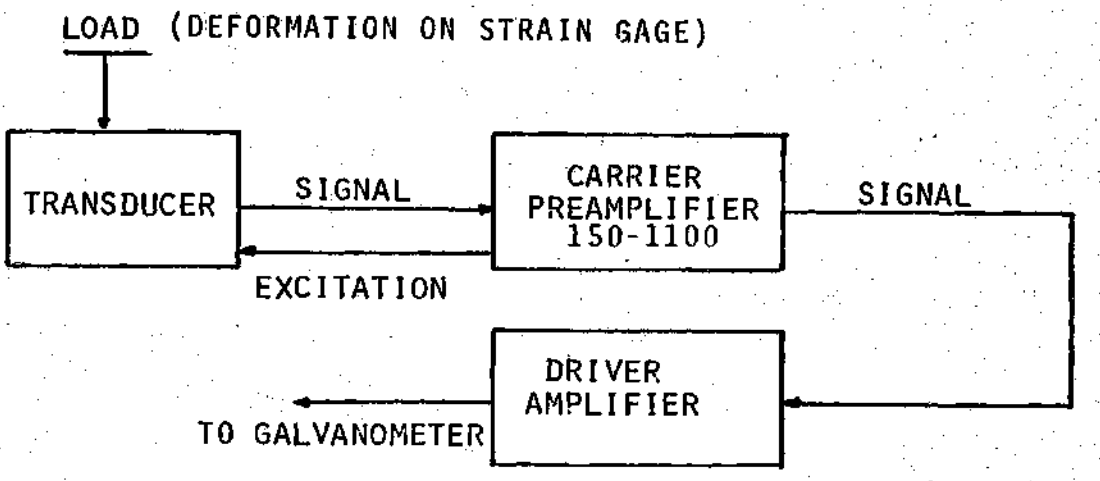

Figure 3-7. Operation of Sanborn Carrier Preamplifier, Model 150-1100.

static load. This allows the readings of small changes in load which might be obscured by a larger load.

Compression Shear Test Apparatus

The compression shear test apparatus was used to determine the shear strength and the modulus of rigidity of the core G_c, following ASTM procedures [50]. These two mechanical properties are probably the most important properties of a core and they have direct bearing on the sandwich performance. The shearing load is applied to the core through two 0.625cm x 15cm x 21.5cm low carbon steel plates that are directly bonded to the core, as shown in Figure 3-8. Each plate has two knife edges, so that the core can be tested in two perpendicular directions. The knife edges fit into two 0.625cm x 2.54cm x 7.5cm guiding plates, having each a 2mm V groove in the center. The guiding plates are bonded to the compression device by a double coated polyurethane adhesive foam. In this way the shear fixture can be aligned and mounted with relative ease at the center of the compression device. A 10mm range Starrett deflection dial gage is installed on one of the shearing plates. A 12.5mm x 12.5mm x 18mm aluminum stop is mounted in a 0.625cm in diameter x 5cm N.F. bolt that is fixed to the other shearing plate. Before the shear test is conducted, the dial gage is loaded against the aluminum stop. As the test proceeds, the relative movement between the two shearing steel plates can be measured as the

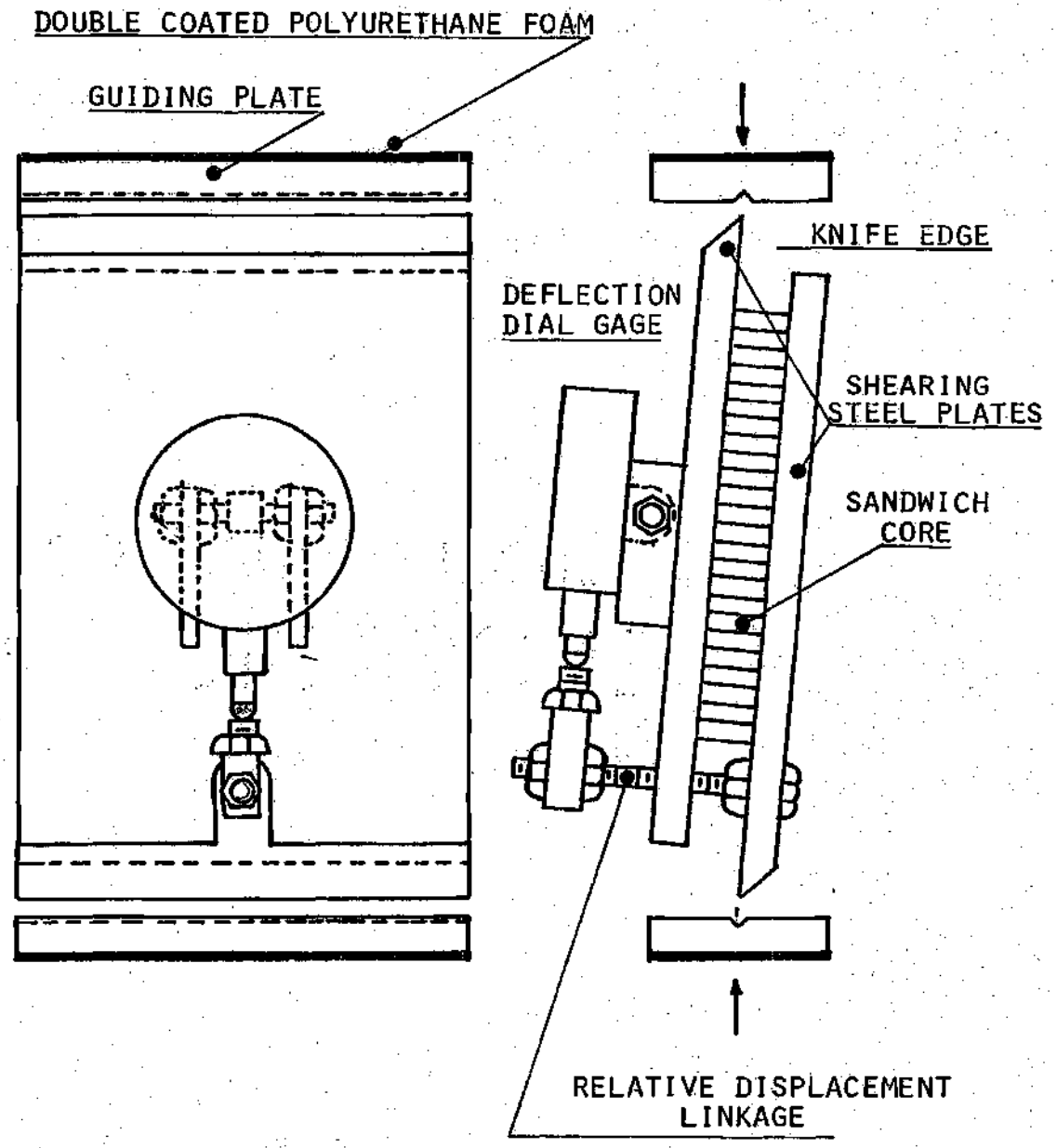

Figure 3-8. Compression Shear Test Apparatus.

gage spring maintains the sensor pin and the aluminum stop in contact. Both the gage and the aluminum stop supports can be easily removed from the shearing plates during the application and curing of the adhesive that bonds the core to the plates.

Tension Shear Test Apparatus

As in the compression shear test, the tension shear test may be used to determine both the shearing strength and the modulus of rigidity of the core. In this case the loading plates have 5cm hinges bolted to their ends and no knife edge is required. Each hinge has two small 0.625cm x 0.625cm x 5cm steel bars attached to it, as shown in Figure 3-9; so that there is good gripping and no slippage occurring at the crosshead, as the specimen is loaded. As in the compression shear test, a dial gage and aluminum stop mechanism could indicate the relative motion between the two loading shear plates; however, as tension shear tests were designed to determine the shear strength of the core, there was no need for relative deflection readings. While the compression shear test fixture is mounted in the compression accessory, the fixture for the tension shear test is directly mounted on the tensile test machine and alignment is automatic.

Bending Test Apparatus

The four point bending test apparatus is for testing

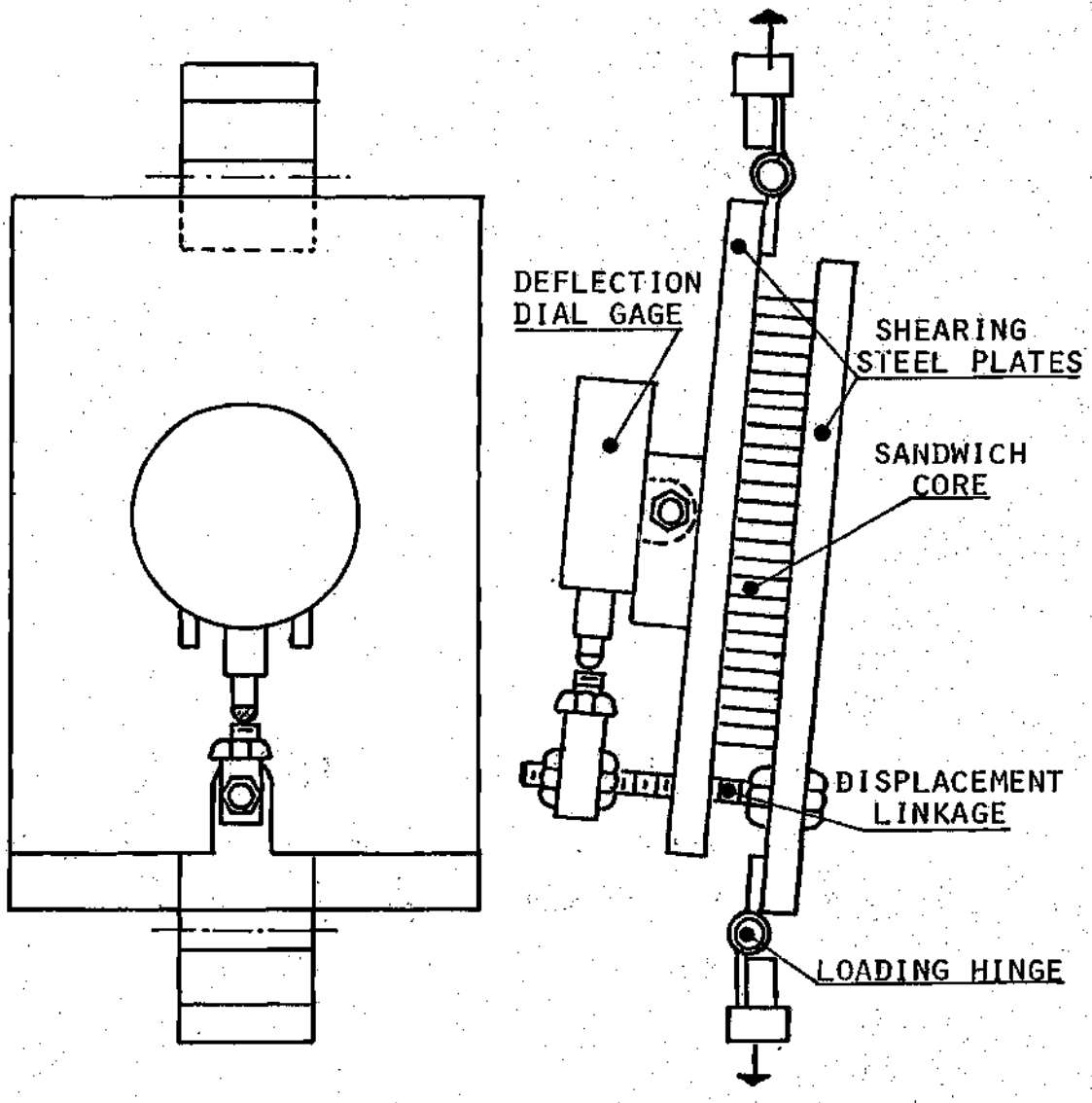

Figure 3-9. Tensile Shear Test Apparatus.

the deflection of the central portion of a lightweight sandwich beam under the effect of a constant bending moment applied in that portion of the beam, as shown in Figure 3-10. The apparatus has a 15cm x 35cm x 0.625cm high carbon steel base plate. The plate has been grounded so that the loading surfaces are essentially flat. The load in the upper facing of the sandwich is applied by two 12.7mm round steel bars that are fixed to the steel plate, and placed 27.3cms apart (10.75 in.). Two 12.7mm (0.5 in.) round bars apply the load to the lower facing of the sandwich construction. To avoid rotation or misalignment of the lower bars during loading, they are bolted down to two 0.625cm x 2.54cm x 15cm guiding steel plates. The lower bars can be moved to different positions so that the sandwich can be loaded at different locations. To prevent uneven loading, both the guiding plates and the round bars have a cushion of double coated polyurethane adhesive foam, 1.5mm thick. Neither the deformation of the soft adhesive nor the bending of the loading device will affect the sandwich deflection reading; in fact, they are not read directly from the universal testing machine output graph, but from a set of two strain gages mounted in the sandwich facings on the section of constant bending moment. To load the sandwich, the bending fixture is installed in the universal testing machine compression accessory, as indicated in Figure 3-10. This compression device has two 2.54cm x 20cm

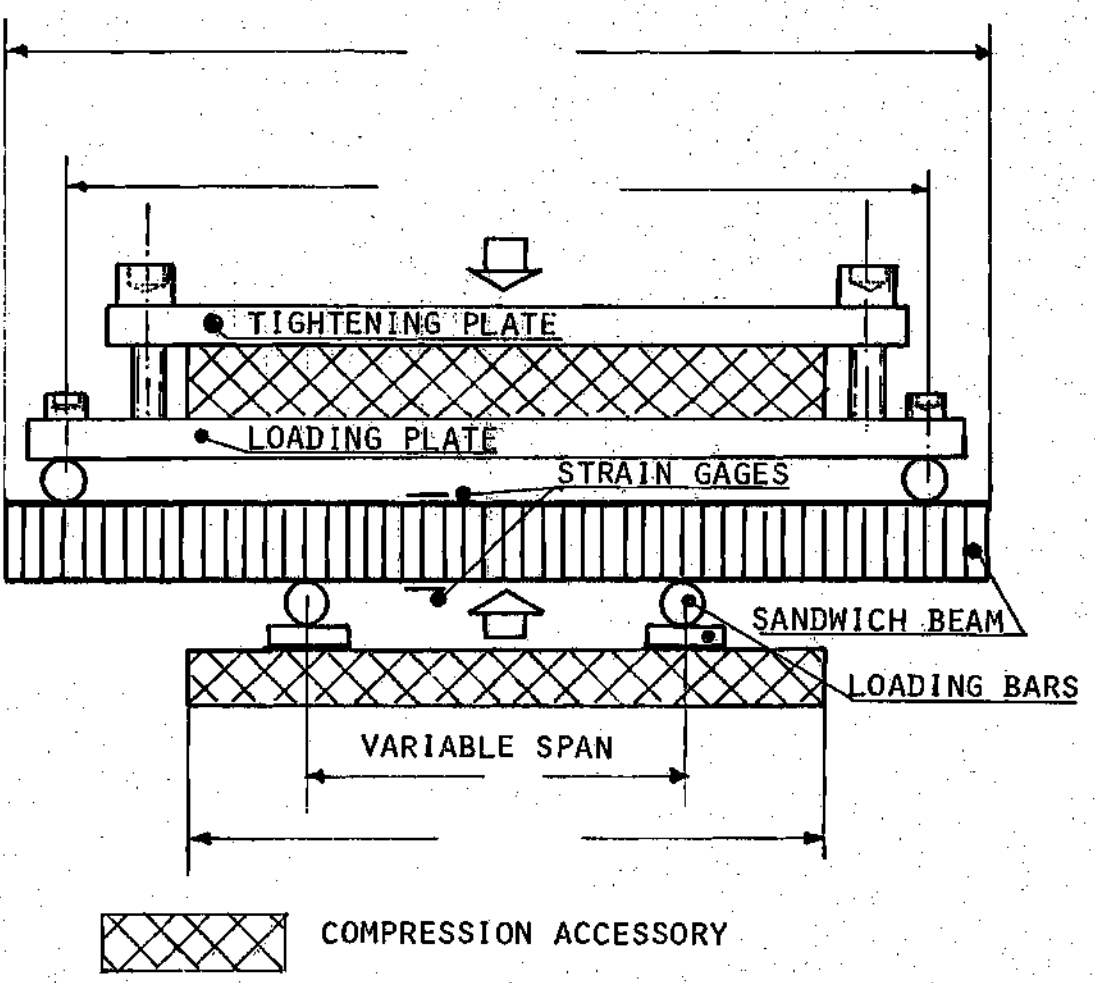

Figure 3-10. Bending Test Apparatus.

x 16cm parallel plates that can be brought closer together at a constant speed as the crosshead of the universal testing machine applies a tensile load. As the tension is applied, the sandwich beam is loaded by the four round steel bars in the bending fixture. The strain gages installed in the upper and lower facing of the sandwich measure the facings strain which is converted into a graph by the Sanborn recorder.

Buckling Test Fixture

The buckling fixture is used to test the edgewise compressive strength of flat sandwich construction as specified by the ASTM Designation C364-61. The sandwich is loaded inside the universal testing machine compression accessory, as shown in Figure 3-11. The two base plates at each end of the sandwich are fastened by 0.625mm NC bolts to the top and bottom loading plates of the compression accessory. The lateral bearings are bolted down to the base plates. A 0.625cm in diameter pivoting pin is inserted at each end of the pivot plate through the lateral bearings. As the aligning plates are moved laterally by sliding the fastening bolts in the aligning guide plate, the sandwich is tested with small loads for even force distribution on each facing. This can be checked out until the strain gages mounted on each facing give about the same output. To reduce concentrated stresses on the facing at the loading contacts, (1) the sandwich ends are covered

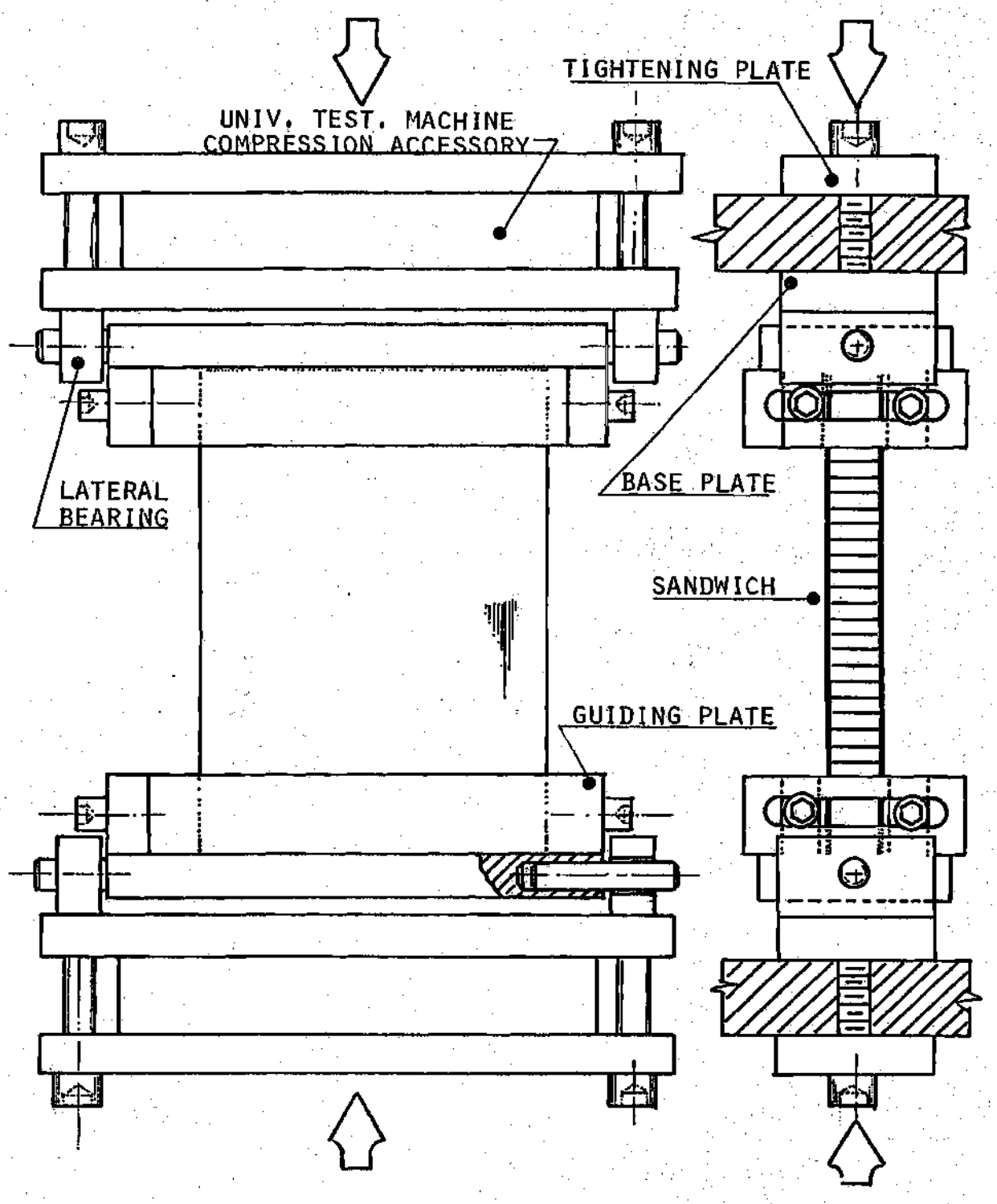

Figure 3-11. Buckling Test Fixture.

with room temperature curing epoxy and (2) the load is transmitted to the sandwich from the pivot plate through a double coated polyurethane adhesive foam which levels out misalignments and irregularities in the loading surfaces. As the loading plates in the compression accessory approach each other, the sandwich is compressed edgewise, and the beam is subjected to a buckling load with simply supported loading ends.

Fixture for Four Edges Simply Supported Test

The buckling fixture with simply supported loading ends proved to be rather difficult to align during the buckling test and one of the two facings was frequently unevenly loaded, as could be determined from the strain gages readout. For this reason it was thought that a four edges simply supported fixture might be easier to load and that the edgewise compressive strength of the flat sandwich construction could be readily determined. The apparatus consisted of two bolted aluminum frames, as shown in Figure 3-12. The frames are made of four 1.26cm x 2.54cm aluminum bars bolted together and prevented from relative rotation. The frame has a 8.75cm x 12.5cm x 2mm wide ground supporting edge, so that the sandwich has all four edges simply supported. The frames are hand tight against the sandwich, so that vertical motion of the facings with respect to the frame can take plate without friction at the edge supports. As the frame is mounted, there is a 0.626cm gap at the

upper and lower ends of the sandwich, so that the loading ends can be reinforced with a 0.312cm x 2.54cm x 12.7cm aluminum strip which is bonded to the structure with room temperature curing (RTC) Epoxy. Again, in an attempt to load the facings evenly, the force is applied to the sandwich through a strip of polyurethane double coated adhesive foam.

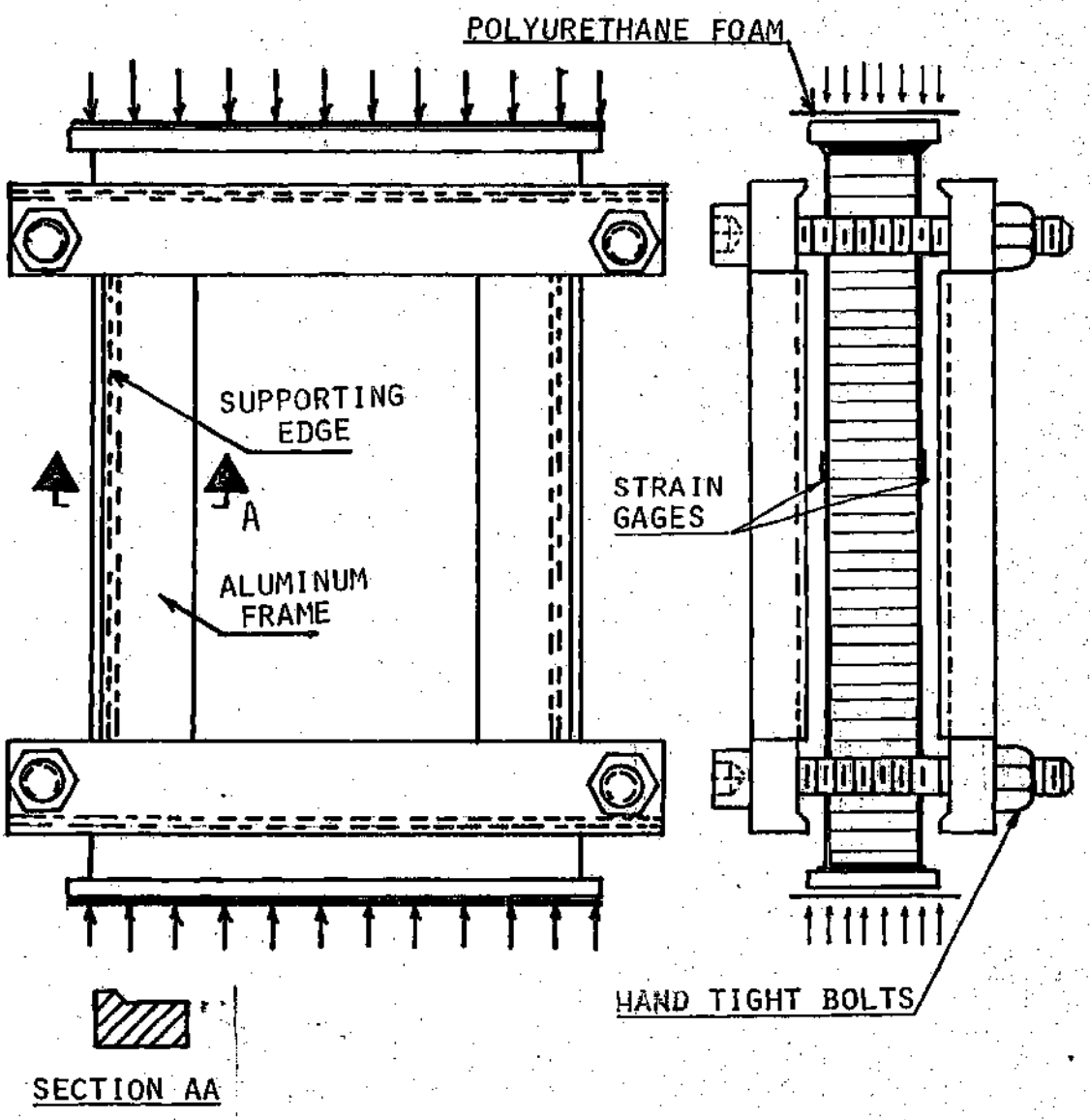

Figure 3-12. Fixture for Four Edges Simply Supported Test.

CHAPTER IV

THEORETICAL ANALYSIS

The subject material presented in this chapter can be divided in two main areas of studies: (a) sheet forming analysis and (b) sandwich stress analysis.

Our main concern in the first part is to derive analytical expressions that may help to explain the way the sheet material flows into a given configuration and the thinning that takes place as a function of the process variables such as pressure, temperature, stock thickness, and initial point coordinates of the material. Cases such as bulging a superplastic sheet into hemispherical or cylindrical shape have been studied theoretically and correlated with the experimental work [45]; however, the deformation of a plastic or metallic sheet into a sandwich core upon the application of heat and pressure would seem to require a more elaborate analysis because the material flow is not symmetric. For the particular case of Zn-22Al, the modified equation of state governing the superplastic forming process will be systematically taken into consideration [34].

In the second part of this chapter, equations are developed in an attempt to correlate core mechanical properties to the core solid materials properties. The

applicability of this analysis may be of special interest to the core manufacturer as he could anticipate the strength of the core for a given material, sheet thickness, and core configuration. For the conventional honeycomb similar studies have been done and empirical equations have been developed [48]. The sandwich core analysis also includes a study of the deflection of the sandwich as a function of the loading mode and the core mechanical properties such as shear strength, elastic and shear modulus. The work of Allen [15] and Plantema [16] is followed closely in the sandwich stress analysis. The equations developed in this section can be used to determine the core characteristics as tests are conducted where deflection and forces or bending moments are directly measured.

Sheet Forming

The following analysis refers to the effect that the die friction may have on the sheet thickness distribution in the transient and final state during vacuum or pressure forming. Our curiosity has been around on this subject because in the processing of reinforced honeycomb structures two distinct types of surfaces are developed. In one surface the material flows against a solid projection, as indicated in Figure 4-1. In the other surface, the material drapes around the reinforcing wires and is free to stretch until the form touches the upper surface of the die, as

shown in Figure 4-1.

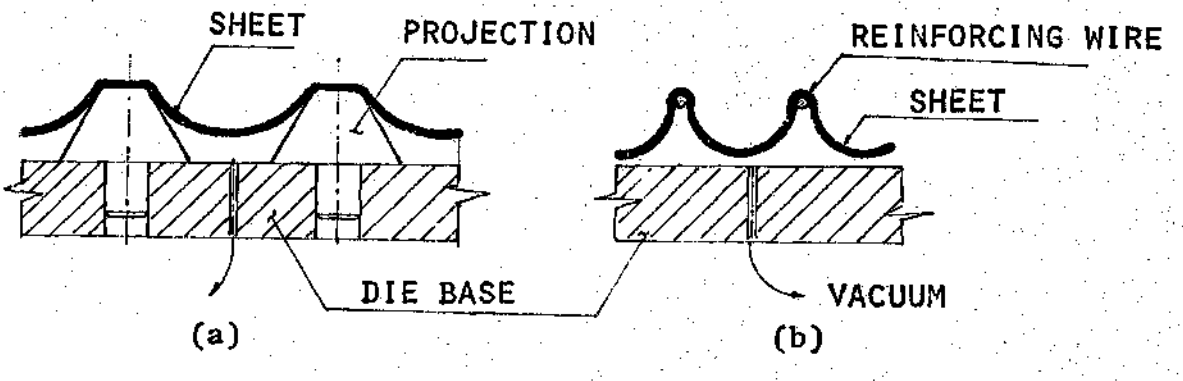

Figure 4-1. Forming Conditions.
(a) Friction Restricted Stretching;
(b) Stretching around the Wires, No Friction.

The analysis of the flow of material for the complete reinforced light weight structure appears to be rather complex; and as the boundary conditions are irregular, there is no evident way that an exact solution for thickness distribution valid for the whole panel can be found. However, the case at hand can be split into much simpler two-dimensional flow models, as described in Figure 4-2, where the final and intermediate shapes are periodic and the specimens are considered infinitely long in the direction normal to the paper. The advantage of making this simpler mathematically approximated model is that we may obtain an exact solution that could be used as an indicator to predict the material flow in the more complicated real case.

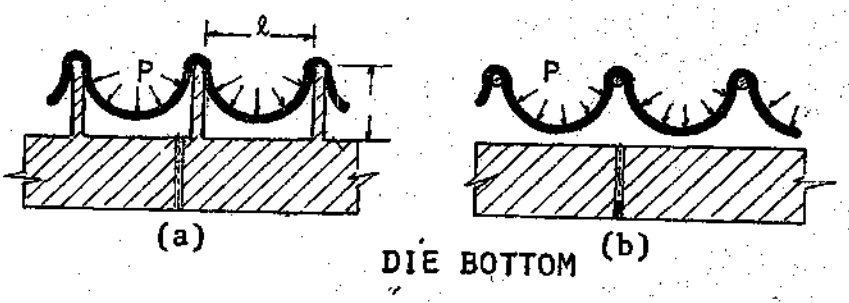

Figure 4-2. Models for Two-Dimensional Forming.
(a) 2-D Restricted Stretching Model;
(b) 2-D Free Stretching Model.

2-D Friction Restricted Forming

As shown in Figure 4-2a, the material displacement is a result of uniformly applied pressure p. As the forming is made at temperatures where the thin sheets can only support tensile stresses, the sheets can be treated as a membrane. Let us assume that the sheet has an initial and intermediate thickness w_o and w(s, t), where s is the instantaneous coordinate of a small element of unit length and width ds at time t, as shown in Figure 4-3.

From the force balance in the direction of p of the small element of width ds, we obtain:

$$(1)pr(d\phi) = (1)2\sigma w(d\phi)/2 \qquad (4\text{-}1)$$

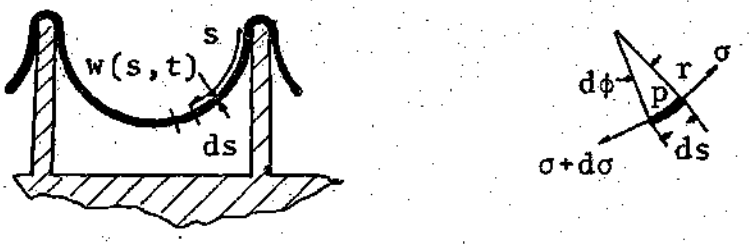

Figure 4-3. 2-D Friction Restricted Forming.
(a) Instantaneous Sheet Shape;
(b) Free Body Diagram of an Element of Width ds

$$p = w\sigma/r \tag{4-2}$$

The force balance in the tangential direction gives:

$$(1)w\sigma = 1(w+dw)(\sigma+d\sigma) \tag{4-3}$$

or,

$$\sigma w = \text{constant} = \text{independent of } s \tag{4-4}$$

From Eq. 4-4, Eq. 4-2 and since p is independent of s, we may conclude that r does not change with s. In other words, the material will be shaped at time t as a circular cylinder or radius r = r(t). Considering at this point the fact that the material exhibits a uniform thickness w_o at the beginning of the forming process, from Eq. 4-4 we may say that the

sheet is uniformly stressed with $\sigma = \sigma_{t=o}$, independent of location s. This consideration implies that at the conclusion of the first increment of time dt, the same strain increment $d\varepsilon$ has occurred everywhere, as it can be deduced from the stress-strain rate relation governing the superplastic forming process:

$$\sigma = k\dot{\varepsilon}^{m} \tag{4-5}$$

Assuming that the material is incompressible in this non-elastic process, the uniform straining in the s direction can be interpreted as a uniform thickness variation dw. Therefore, after the first time interval dt, we have returned to a condition of uniform thickness. As this process is repeated over and over, we can reasonably predict that at time t, the material that is free to stretch will exhibit a cylindrical shape of radius $r = r(t)$, and uniform thickness $w = w(t)$.

In an ideal situation, that is homogeneous material properties, stock thickness and uniform heating seems to be all it is required to ensure uniform thickness distribution. However, as soon as there are small variations in the sheet thickness, conventional materials will flow unevenly because the flow stress is essentially a function of the forming temperature only and necking will most probably take place. On the other hand, when a superplastic alloy is considered, the whole sheet may stretch at roughly the same rate

because the weakness of smaller cross sectional areas at some locations may be compensated by the higher flow stress required [43], as can be verified by Eq. 4-5.

To shape the material into its final form as shown in the die of Figure 4-2, we may recognize three distinct forming steps, as shown in Figure 4-4.

In the first step the material is free to stretch until the radius r(t) becomes $r = \ell/2$, in which case the material next to the supports touches the vertical surface.

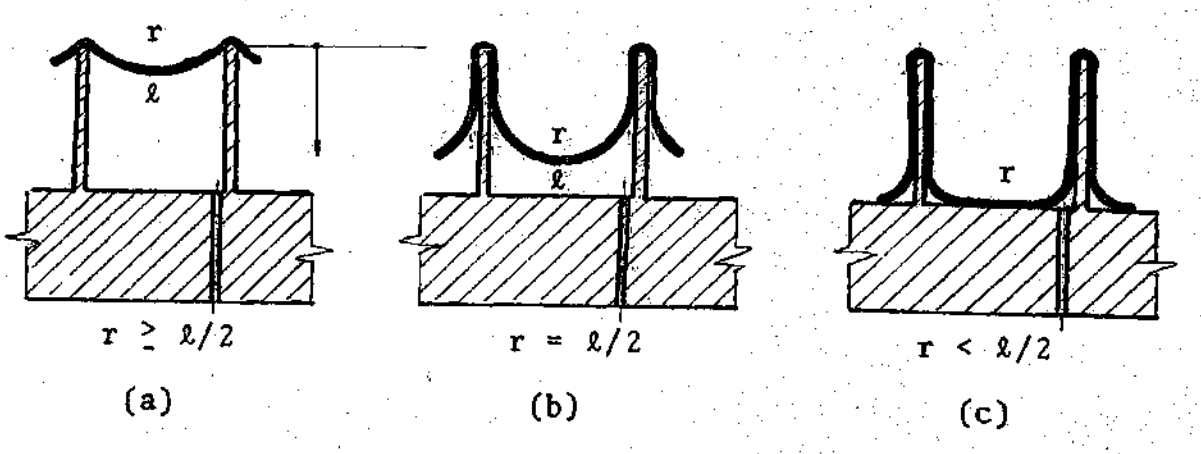

Figure 4-4. Steps in Two-Dimensional Forming
(a) Unrestricted Stretching;
(b) Stretching Essentially Stops at the Vertical Surfaces; (c) Stretching Stops at Vertical and Horizontal Surfaces.

The first element of width dx and thickness $w_{x=o}$ that is formed will be subjected to diminishing tension forces with time because as the forming progresses, the frictional force F per unit length will greatly reduce the resultant stress applied to this element, as illustrated in Figure 4-5 where F is:

$$F = \int_{o}^{h} \mu p(1)dx = \mu ph \qquad (4\text{-}6)$$

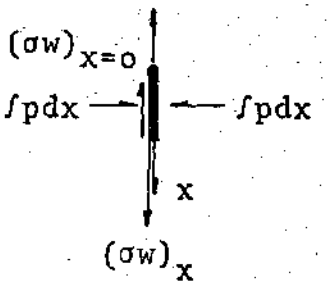

Figure 4-5. Force Balance of Element Under Restricted Vertical Stretching.

As the sheet is formed against a vertical portion of the die to a depth x = h, the stress σ at x=o is obtained from the force balance:

$$(\sigma w)_{x=o} = (\sigma w)_{x=h} - \mu ph \qquad (4\text{-}7)$$

As a first approximation, we may neglect the stress $\sigma_{x=o}$ and consider that once the sheet material touches the die surface, further stretching becomes insignificant. In that case, using the incompressibility and uniform thickness conditions in the first step, we may conclude that $w_{x=o}$ is given by:

$$w_{x=o} = \frac{w_o \ell}{\pi \ell/2} = 2w_o/\pi \qquad (4\text{-}8)$$

where w_o and $w_{x=o}$ are the initial and final thickness of the sheet at x=o. To determine the thickness at any other position x during the second step as depicted in Figure 3b, we may use the incompressibility criterion in a time increment dt, where the material in the half cylinder at the bottom with thickness w, as shown in Fgiure 4-6, is modified into a half cylinder with thickness (w + dw) and two small strips of length dx.

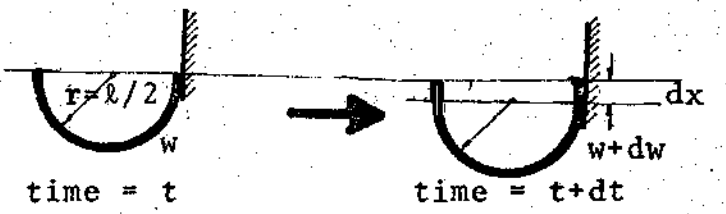

Figure 4-6. Second Forming Step.

Equating the volumes at times t and t + dt, the following expression results:

$$(w\pi\ell/2)_t = (w\pi\ell/2)_{t+dt} + 2wdx \qquad (4\text{-}9)$$

or

$$dw/w = -4dx/\pi\ell \qquad (4\text{-}10)$$

Integrating Eq. 4-10 and replacing the value of $w_{x=0}$ from Eq. 4-8,

$$\ell n(w/w_{x=o}) = \ell n(\pi w/2w_o) = -4x/\pi\ell \qquad (4\text{-}11)$$

or

$$w/w_o = \frac{2}{\pi}\, e^{-4x/\pi\ell} \qquad (4\text{-}12)$$

where w represents the sheet thickness at a forming depth equal to x, as shown in Figure 4-3b, or Figure 4-4.

The third and last forming step occurs when the sheet material is touching both the vertical and horizontal surface of the die. Again, let us consider a small change in shape the material may undergo during the small time interval dt, as illustrated in Figure 4-7.

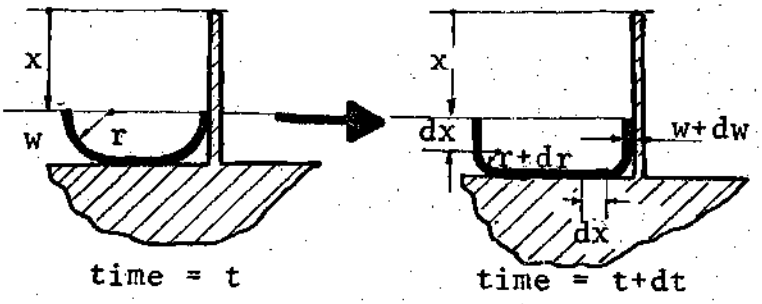

Figure 4-7. Third Forming Step.

It is simple to show that the material free of friction has uniform thickness w and (w+dw) at times t and (t+dt), as may be anticipated by the anlaysis in the first

forming step. Also, from the symmetry of the load, the small elements formed vertically and horizontally are of the same length dx. Under these circumstances, the incompressibility condition can be written as:

$$(\pi\ r/2\ w)_t = (\pi\ r/2\ w)_{t+dt} + 2dxw \qquad (4\text{-}13)$$

Also, from geometry, we have that:

$$r = H-x;\ dr = -dx \qquad (4\text{-}14)$$

Replacing dx from Eq. 4-14 into Eq. 4-12, we obtain:

$$\frac{d(rw)}{rw} = \frac{4}{\pi}\frac{dr}{r} \qquad (4\text{-}15)$$

or:

$$\ell n(rw/(rw)^*) = \frac{4}{\pi}\ \ell n(r/r^*) \qquad (4\text{-}16)$$

Solving for w/w^*, we obtain:

$$w/w^* = (r/r^*)^{(4/\pi-1)} \qquad (4\text{-}17)$$

where r^* is the radius when the first element touches the bottom surface, indicating the beginning of the third forming step. The value of r^* is obviously given by $r = \ell/2$ and $x^* = H-\ell/2$. It may be recognized also that w^* also represents the thickness of the last element formed in the second step; that is, using Eq. 4-12:

$$w^*/w_o = \frac{1}{\pi} e^{-4(H-\ell/2)\ell\pi} \qquad (4\text{-}18)$$

Using 4-17, 4-18, and 4-14, we may develop a final relation valid for $x > H-\ell/2$:

$$\frac{w}{w_o} = \left(\frac{w}{w^*}\right)\ (w^*/w_o) = \frac{1}{\pi} e^{-4(H-\ell/2)\pi\ell\left(2\frac{H-x}{\ell}\right)^{(4/\pi-1)}} \qquad (4\text{-}19)$$

We can recognize from Eq. 4-19 or Eq. 4-17 that as the radius grows smaller in the third step, w also becomes smaller. We should, therefore, expect a rather critical condition in the last elements formed if the final radius is very small. This phenomenon, however, may be attenuated in the actual process, as thinning may occur at the vertical portion of material after the sheet comes in contact with the die surface, and the actual forming time should be less than what could be predicted here. In consequence, the final thickness of the most strained element, the one to form last, should be somewhat higher than the estimate given by Eq. 4-19.

Two Dimensional Friction Free Forming

It was mentioned before that even with the restricted stretching, the material that comes in contact with the die will be strained at a diminishing rate with time during the rest of the forming process. In fact, although the frictional force F increases with time, it may not be sufficient

to balance the applied tension in the free end. For this reason it is proposed here to study the material redistribution in the other extreme case, namely: unrestricted thinning where the friction coefficient is zero in the vertical portion of the forms. We may divide the process again into the same three distinct steps described in Figure 4-3. We may notice that the thickness of the material at x = o, when the sheet first reaches the radius r = $\ell/2$ at time t = t_1, is the same as in the previous case given in Eq. 4-8, only that w here is no longer considered a function of position only, but also varies with time. We know then that:

$$w(0,\ t_1) = \frac{w_o \ell}{\pi\ \ell/2} = \frac{2}{\pi}\ w_o$$

From the incompressibility condition, at time (t_1 + dt), the new thickness (w + dw) is constrained to the following relation:

$$(w+dw)\ [\pi\ \ell/2 + 2dx] = w\pi\ \ell/2 \qquad (4\text{-}20)$$

The thickness of the two newly formed small vertical elements of length dx and the thickness of the curved material will be the same, as shown in Figure 4-8.

But from a force balance, it is easy to show that the tension $\sigma_{x=o}$ acting during time dt in the element dx and the tension σ acting in the curved material are the same

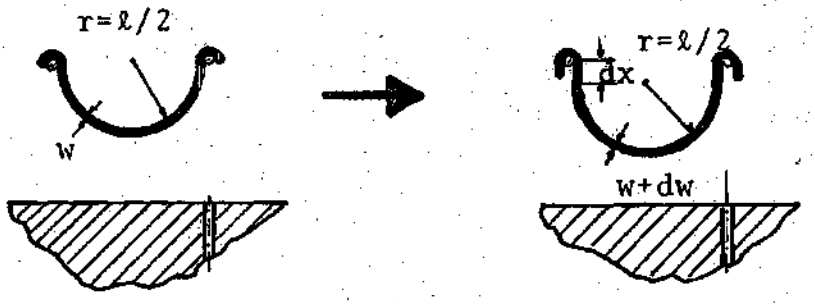

Figure 4-8. Beginning of the Second Forming Step.

and are given by expression:

$$\sigma = p\ell/2w \qquad (4\text{-}21)$$

Using now the stress-strain rate relationship given in Eq. 4-5, we can predict that both the two small vertical elements dx and the curved material are strained the same amount $d\varepsilon$ in the small time interval dt. Repeating this argument indefinitely, we can conclude that any small vertical element during the second forming step has been stretched the same amount as any element in the free half cylinder. Therefore, at the end of the second step, the thickness of the material w* is uniform and is given by:

$$w^* = w_o/(\frac{\pi}{2} - 1 + 2H/\ell) \qquad (4\text{-}22)$$

For the third step, from the force balance and the stress-strain rate relationship, we can see that both the curved and vertical material would have uniform thickness as shown in Figure 4-9. For this reason, using the incompressibility criterion again, the following relation results for times t and t-dt.

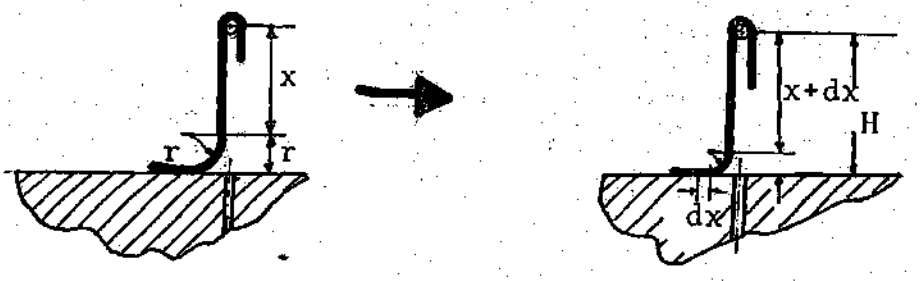

Figure 4-9. Third Forming Step

$$(\pi \frac{r}{2} + H-r)w\Big|_t = wdx + [\pi(\frac{r}{2}) + H-r]w\Big|_{t+dt} \qquad (4-23)$$

From geometry considerations we can write:

$$H-r = x \quad \text{and} \quad dx = -dr \qquad (4-24)$$

For convenience, let us also call the length of the free material in one side s, then we have that:

$$s = H+r\ (\pi/2-1) \qquad (4-25)$$

and

$$ds = (\pi/2-1)dr \tag{4-26}$$

Replacing dx in (23) we obtain the following expression

$$\frac{ds}{(\frac{\pi}{2} - 1)s} = \frac{d(ws)}{ws} \tag{4-27}$$

or

$$(s/s^*)^{(\frac{1}{\pi/2-1})} = (ws/ws^*) \tag{4-28}$$

Solving for w/w*, we obtain

$$w/w^* = (s/s^*)^{(4-\pi)/(\pi-2)} \tag{4-29}$$

where s* and w* correspond to the values of s and w at the beginning of the third step; w* was defined in Eq. (4-22) and s* is given by

$$s^* = H + (\frac{\pi}{2} - 1)\ell/2 \tag{4-30}$$

The final expression then for the thickness of the material not touching the die is

$$\frac{w}{w_o} = \frac{L}{(\frac{\pi}{2} - 1 + \frac{2H}{\ell})} \left(\frac{s}{H+(\pi/2-1)\ell/2}\right)^{(4-\pi)/(\pi-2)} \tag{4-31}$$

where the quantities H, ℓ, and w_o are constant for a given forming process.

It is interesting to see that the restrained stretching, as studied in the previous section, presented a critical thinning situation if the final radius in the third step was very small. However, the formulation for this free stretching problem indicates that thinning will not be greatly affected if the final radius is very small. The obvious explanation for the contrast is that in the free stretching there is plenty of material available that is equally strained until the final shape is obtained; but in the restricted thinning this is not the case. It should also be recognized that since the vertical and curved material is stretched all the time in the free forming, the metal that is formed first in the vicinity of the wire will be thinner than the material close to the top of the projections in the restricted forming. This observation explains now why the material close to the wires and half-way between projections in the wire reinforced cores had a tendency to thin down more than the material at the end of the wires, close to the projections. This phenomenon was obvserved when the metal sheet was very thin 0.075mm (.003 in), and the projections were high and very close. Another important argument that can be brought up in the light of Eq. 4-31 is the need for a well lubricated die with very good surface finish if one is interested in allowing the material to flow more freely and thereby allowing it to posses a more uniform final thickness.

3-D Symmetric Forming

The analysis of material flow as a sheet is formed into a general shape shell appears to be a rather complex problem. In fact, as displacements are large, the boundaries of the formed pieces are irregular in general, and the thickness of the material does not change uniformly, there is no analytical means to determine the path that each material point follows during the plastic deformation process; consequently, the thinning of the sheet cannot be predicted easily. But as our interest lies in characterizing the tendency for the material to flow, a good start in the analysis could be to study what happens to a sheet as it is formed under tension into a surface of revolution shell. In such a case, one may be able to reduce the complexity of the analysis and still gain some insight on the most general case. Let us consider a circular metallic sheet that is clamped at the edges and is deformed under the action of a truncated cone punch, as indicated in Figure 4-10 where the initial and final position of the sheet are represented.

As the forming progresses, at a time t, the sheet may take the shape indicated in Figure 4-9, where the material is considered to behave like a membrane and to be under superplastic conditions. The balance of forces in the free body diagram of the small element shown in Figure 4-11b gives:

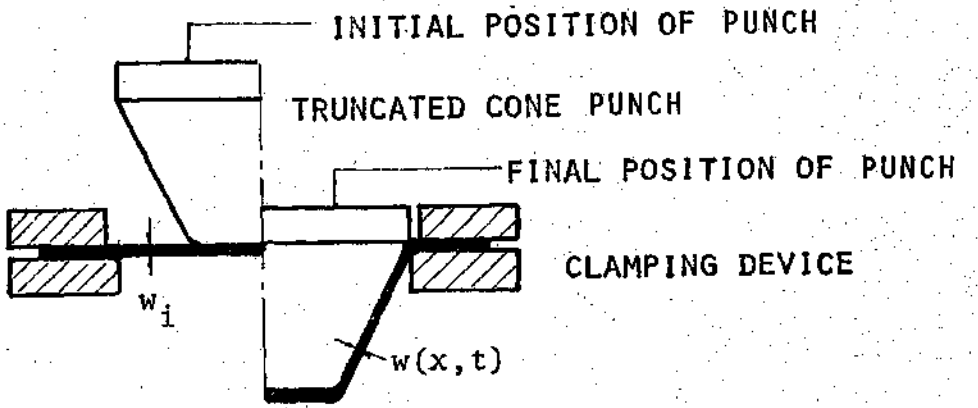

Figure 4-10. Initial and Final Position of Punch in 3-D Symmetric Stretching.

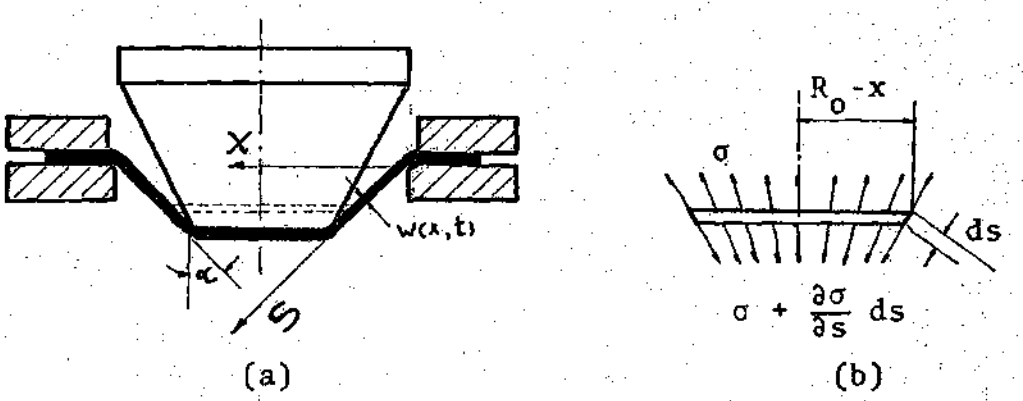

Figure 4-11. (a) Intermediate Deformation Stage; (b) Free Body Diagram

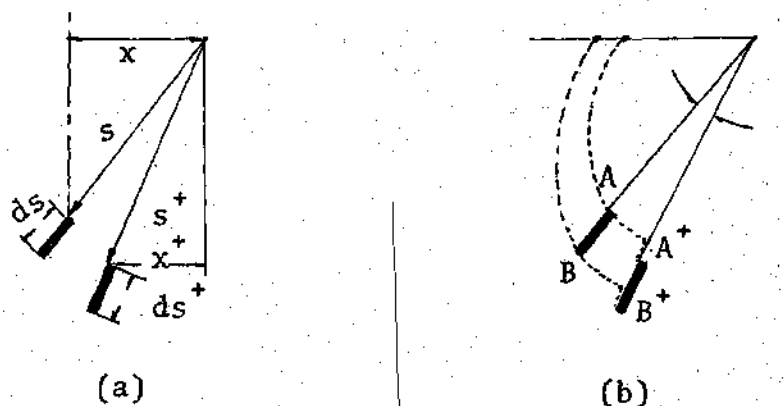

Figure 4-12. Deformation During Forming. (a) Change in Position of a Small Element as Time dt Elapses; (b) Path Followed by the Element from Time = 0 to Time = t+dt.

$$2\pi(R_o-x)\sigma(\cos\alpha)w-2\pi(R_o-x-dx)(\sigma+d\sigma)(w+dw)\cos\alpha = 0 \quad (4-32)$$

Eliminating the differentials of higher order, we obtain:

$$(R_o-x)d(\sigma w) + \sigma w d(R-x) = 0 \quad (4-33)$$

which has a solution:

$$(R_o-x)\sigma w = k_1 \quad (4-34)$$

where k_1 does not change with x but is a function of time $k_1(t)$. Replacing σ using the stress-strain rate relationship, Eq. (4-34) can be written as follows:

$$(R_o-x)k\dot{\epsilon}^m w = k_1(t) \quad (4-35)$$

Let us concentrate our attention now in the change in length and position of the element indicated in Figure 4-12b, as an increment of time dt elapses. Consider that at time t the length of the element is ds as shown in Figure 4-12. A material point A with coordinates x, s at time t will advance to a new position of coordinates x^+, s^+, at time t+dt. Let us call w and w^+ the average thickness of the element shown in Figure 4-12 at times t and t+dt respectively. Neglecting terms of higher order, the incompressibility condition requires that:

$$2\pi(R-x)wds = 2\pi(R-x^+)w^+ds^+ \quad (4-36)$$

where x^+, w^+, and ds^+ can be written as:

$$x^+ = x + \frac{\partial x}{\partial t}\, dt$$

$$w^+ = w+dw = w + \frac{\partial w}{\partial t}\, dt$$

The variables ds and w are also related to the true strain in the longitudinal and transversal direction as shown below

$$\frac{ds^+}{ds} = 1 + \frac{ds^+-ds}{ds} = 1 + d\varepsilon \qquad (4\text{-}37)$$

and

$$\frac{w^+}{w} = 1 + \frac{w^+-w}{w} = 1 + dw/w \qquad (4\text{-}38)$$

where the quantities $d\varepsilon$ and dw/w represent differential change of the true strain in the longitudinal and transverse direction that occur to the small element of length ds during the elapsed time dt.

Eliminating terms of higher order, Eq. 4-36 can be written as:

$$\frac{\frac{-\partial x}{\partial t}\, dt}{R-x} + \frac{\frac{\partial w}{\partial t}}{w} + d\varepsilon = 0 \qquad (4\text{-}39)$$

or

$$\dot{\varepsilon}^m = \left[\frac{\frac{\partial x}{\partial t}}{R-X} - \frac{\partial w/\partial t}{w}\right]^m \qquad (4\text{-}40)$$

Combining now Eq. 4-40 with Eq. 4-35, we obtain a relation between x, w and t as follows.

$$(R_o-x)kw\left[\frac{\partial x/\partial t}{R-x} - \frac{\partial w/\partial t}{w}\right]^m = k_1(t) \qquad (4\text{-}41)$$

It is interesting to evaluate the influence of the terms appearing in Eq. 4-41 from a practical viewpoint considering typical dimensions. In that order, it can be said that since the value of w is only at most 0.05-0.127mm (0.002 in.-0.005 in.), and as the material is forced mostly to flow downward, the magnitude of $(\partial x/\partial t)$ is probably much smaller than $\frac{-1}{w}\,\partial w/\partial t$ at some distance away from punch bottom. In other words, Eq. 4-41 could be simplified into the following expression:

$$(R_o-x)kw(\dot{w}/w)^m = k_1(t) \qquad (4\text{-}42)$$

where negative sign of $\dot{w}$ has been eliminated and by $\dot{w}$ is meant $|\partial w/\partial t|$.

Let us study the significance of this equation when two material points of initial coordinates x_1 and x_2 $(x_1<x_2)$ are considered. For this case Eq. 4-42 reduces to

$$\frac{R_o-x_1}{R_o-x_2}\left(\frac{w_1}{w_2}\right)^{1-m} = (\dot{w}_2/\dot{w}_1)^m \qquad (4\text{-}43)$$

As w_1 and w_2 are equal at the beginning of the process, it can be deduced from Eq. 4-43 and from the condition $x_1 < x_2$ imposed above that at time t = 0, $\dot{w}_2/\dot{w}_1 > 1$. Repeating this argument for every increment of time and assuming that the ratio $(R_o-x_1)/(R_o-x_2)$ does not vary much with time, Eq. 4-43 indicates that the tendency for the material away from the clamping device to thin down faster than at the outer boundary is more pronounced as time increases.

Although the case presented here refers to a sheet that is stretched by the action of a punch as it moves down, the analysis should remain roughly valid for when a case as depicted in Figure 4-13 is analyzed, in which not only tensile load but also normal pressure could be applied to the sheet.

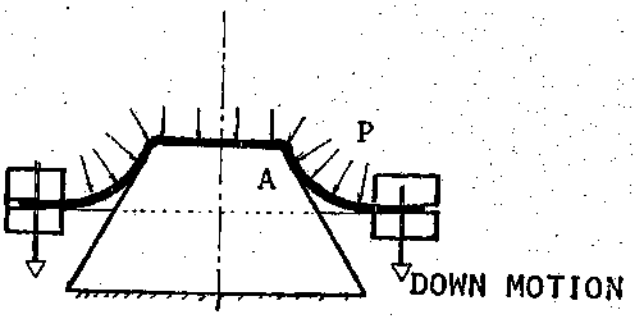

Figure 4-13. Sheet Formed Under the Action of Tension and Pressure.

In the light of Eq. 4-43, it is interesting to observe that the final thickness distribution of the surface of revolution shell is not greatly affected by the downward

speed of the punch in Figure 4-11. In fact, Eq. 4-43 can always be written in the following manner:

$$\frac{R_o-x_1}{R_o-x_2}\,(w_1/w_2)^{1-m} = (dw_2/dw_1)^m \qquad (4\text{-}44)$$

where dw_1 and dw_2 are the change in thickness at locations x_1 and x_2 during time dt. Following the history of the thickness reduction at the two locations which initially may have been $x_1(0)$, $x_2(0)$, admitting that the ratio $(R_o-x_1)/(R_o-x_2)$ does not change significantly, we can see from Eq. 4-44 that from the beginning of the process, the ratio (dw_2/dw_1) will be essentially the same for corresponding time increments.

A similar argument can be introduced in reference to thickness variations at two different locations, if we rewrite Eq. 4-42 in the following form:

$$w^{1/m-1}\,dw = \frac{[k_1(t)]^{1/m}}{(R_o-x)^{1/m}}\,\frac{dt}{k^{1/m}} \qquad (4\text{-}45)$$

Considering small variation of (R_o-x) and integrating Eq. 4-45, we obtain:

$$m(w^{1/m} - w_o^{1/m}) = \frac{F_1(t) - F_1(0)}{(R_o-x)^{1/mk^{1/m}}} \qquad (4\text{-}46)$$

where $F_1(t)$ is a time function characterized by the punch

speed, sheet material, and forming temperature, as can be anticipated from Eq. 4-35 where we can see the nature of k_1 from the stress-strain rate relationship.

From Eq. 4-46 we can compare the final thickness at two locations x_1 and x_2 as follows:

$$\frac{w_1^{1/m} - w_o^{1/m}}{w_2^{1/m} - w_o^{1/m}} = \left(\frac{R_o - x_2}{R_o - x_1}\right)^{1/m} \qquad (4\text{-}47)$$

It can be inferred from this equation that variations of the punch speed should not appreciably affect the material redistribution in the final form. A practical consequence of this fortunate phenomenon is that we can afford higher strain rates to increase production levels without affecting negatively the permissible thickness variations in the parts.

From Eq. 4-47 we perhaps can also study the significance of the strain sensitivity factor m over the material redistribution. Let us assume that we have two sheets of same initial thickness w, but with strain rates sensitivities m and (m+dm). We are interested in comparing the thickness of the sheet at a location of coordinate x_2, after both sheets have reduced their thicknesses at a particular location of coordinate $x_1 < x_2$ to the same value w_1. For convenience, let us define the following quantities:

$$(R_o - x_2)/(R_o - x_1) = A < 1$$

$$w_o/w_1 = B > 1$$

$$w_2/w_1 = y < 1$$

$$m < 1$$

We can write now Eq. 4-47 as

$$(1-B^{1/m})A^{1/m} = (y^{1/m} - B^{1/m}) \qquad (4\text{-}48)$$

where y and m are the dependent and independent variables respectively. Putting equation 4-48 in a differential form, we have

$$[A^{-1/m} \frac{\ln A}{m^2} (1-B^{1/m}) + B^{1/m} \frac{\ln B}{m^2} (\frac{1}{A^{1/m}} - 1) - y^{1/m} \frac{\ln y}{m^2}]dm$$

$$= y^{(1/m-1)}dy \qquad (4\text{-}48)$$

Knowing the limitations of A, B, y and m assigned above, it is easy to see from Eq. 4-48 that if $dm > 0$, then $dy > 0$ and $dw_2 > 0$. A practical interpretation of this analysis is that higher the strain rate sensitivity factor m, the more uniform the thickness distribution of the final product, which is indeed gratifying.

Forming Time

The time consumed to form a piece by pressure forming is a very important production factor. We have previously

shown that material redistribution is basically independent of time, therefore, we can safely increase strain rate and reduce the forming time. But as the strain rate depends on the applied external pressure, our interest lies in determining how the time to form a part is affected by the applied pressure p. Let us consider the manufacture of two identical parts from same stock material of equal thickness ($w_1 = w_2$), as the metallic superplastic sheets are subjected to pressures p_1 and p_2 [$p_1 > p_2$]. Let us focus the attention at corresponding material points in both parts and study the flow pattern which should be the same for corresponding times t_1 and t_2 in which the material is equally strained and under stresses σ_1 and σ_2. The stress-strain rate relationship can be written as:

$$(\sigma_1/\sigma_2) = [(d\varepsilon_1/dt_1)/d\varepsilon_2/dt_2)]^m \qquad (4\text{-}49)$$

Since both pieces were strained the same amount $d\varepsilon_1 = d\varepsilon_2$ during the corresponding time dt_1 and dt_2, Eq. 4-49 can be reduced to:

$$(\sigma_1/\sigma_2)^{1/m}\, dt_1 = dt_2 \qquad (4\text{-}50)$$

But, since the geometry of a differential element is the same for both cases, as illustrated in Figure 4-14, the internal stress σ is related to the external load p as follows:

$$\sigma_1/\sigma_2 = p_1/p_2 \qquad (4\text{-}51)$$

Replacing (σ_1/σ_2) in Eq. 4-50 and integrating, we finally obtain

$$(p_1/p_2)^{1/m} = t_2/t_1 \qquad (4\text{-}52)$$

For the case of Zn-22Al which has a strain rate sensitivity factor of m = 0.48, Eq. 4-52 seems to indicate that if the forming pressure is doubled, the forming time is reduced to 1/4, as it has been observed by Fields [39].

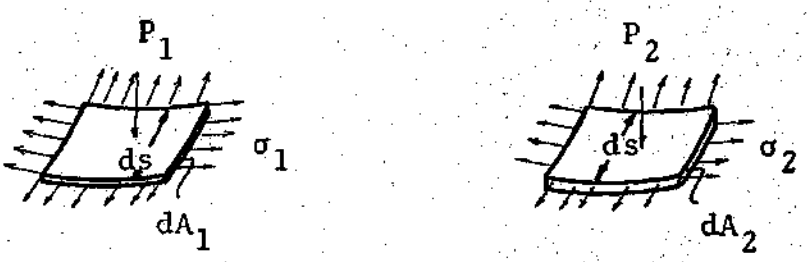

Figure 4-14. Small Equal Elements Subjected to Different External Pressures $p_1 > p_2$.

In a production situation, however, a maximum pressure will be limited by the size of the equipment and clamping forces. This brings up the second problem of interest which is to find the time vs. thickness relationship when the applied pressure stays constant but the

thickness of the stock changes. In that case, for corresponding times t_1 and t_2 giving the same strain, the force balance of corresponding sections dA_1 and dA_2 as shown in Figure 4-15 indicates that $dF_1 = dF_2$. The cross sectional areas dA_1 and dA_2 are related to σ_1 and σ_2 by:

$$dF_1 = dA_1\sigma_1 = ds_1 w_1 \sigma_1 = dF_2 = ds_2 w_2 \sigma_2 \qquad (4\text{-}53)$$

Since the small arc length ds_1 and ds_2 are equal because the forms are identical, Eq. 4-53 can be simplified as:

$$w_2/w_1 = \sigma_1/\sigma_2 = w_2(0)/w_1(0) \qquad (4\text{-}54)$$

where w_1 and w_2 are the instantaneous sheet thickness and $w_1(0)$, $w_2(0)$ are the initial thicknesses. Combining Eq. 54 with Eq. 4-50, and integrating Eq. 4-50, results in:

$$[w_2(0)/w_1(0)]^{1/m}\, t_1 = t_2 \qquad (4\text{-}55)$$

In terms of the Zn-22Al properties, since $1/m \simeq 2$, Eq. 4-55 implies that if the thickness is doubled, the forming time is increased by a factor of 4.

In an effort to relate Eq. 4-43 to a practical situation, the forming example illustrated in Figure 4-15 is presented at this point. The material close to point A in Figure 4-13 should experience the largest change in thickness, as suggested by Eq. 4-43 and failure may occur at a region close to A before the sheet has a chance to take the

final configuration. One way to avoid sheet failure should be then by putting a small radius at the top of the forming die as indicated in Figure 4-15, so that the material subjected to the highest strain rate in the forming process comes to rest the fastest,and, from friction considerations, no further significant straining is possible.

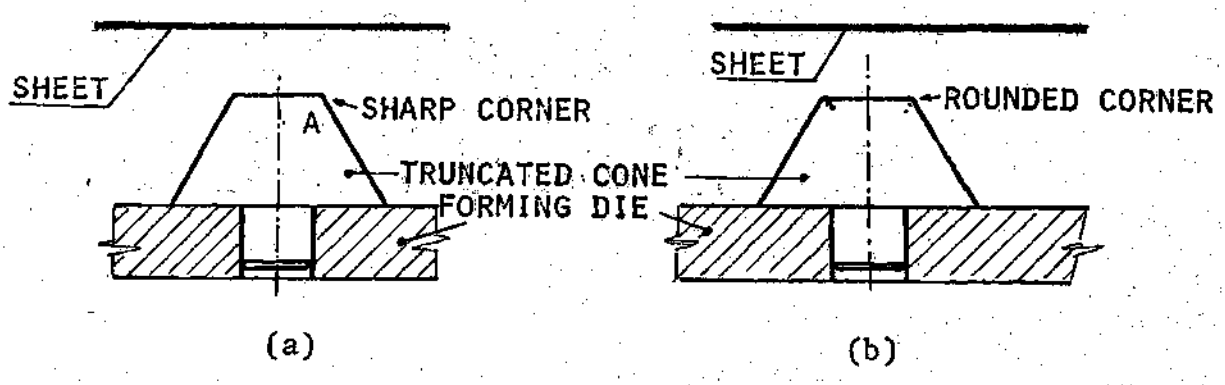

Figure 4-15. Forming Around a Projection.
(a) Failure May Occur at the Sharp Corner;
(b) Rounding the Corner for a Successful Forming.

Sandwich Stress Analysis

The main object of this analysis is to examine the relative importance of the core mechanical properties in the performance of a sandwich structure considered as a composite material. Relations between sandwich deflection and sandwich properties will be developed, such that as a sandwich is subjected to external loading, criteria to predict the core properties can be advanced. These predictions will be related to the results of the standard testing methods described earlier.

The analysis comprises deformation of panels under bending and buckling, edge wise simply supported beams, prediction of effective elastic modulus in the flatwise direction and edgewise direction, effective core shear modulus, and shear strength.

Sandwich Bending and Buckling Behavior

The stress analysis presented here corresponds to the case of a simply supported sandwich panel with very thin facing. The structure is subjected to edgewise load per unit width N_x and uniform load per unit area q normal to the plane of the plate, as shown in Figure 4-16. The condition of "very thin facing" implies the following assumptions:

(1) Stresses in the z direction in the facing can be neglected

(2) Local bending stiffness of the facing is

negligible.

(3) The dimensions d and c of the sandwich, as given in Figure 4-16, can be interchanged.

In addition, it is also assumed that (a) the deflections are small, (b) the faces are isotropic, and (c) the sandwich core is much less stiff than the faces.

The shearing strain can be written following Allen [15] as:

$$\sigma_{zx} = (1-\lambda)\ \frac{\partial w}{\partial x} \qquad (4\text{-}56)$$

where w is the displacement in the direction perpendicular to the sandwich palne xy, see Figure 4-16. The quantity λ will vary between +1 for completely rigid cores and zero for completely flexible cores.

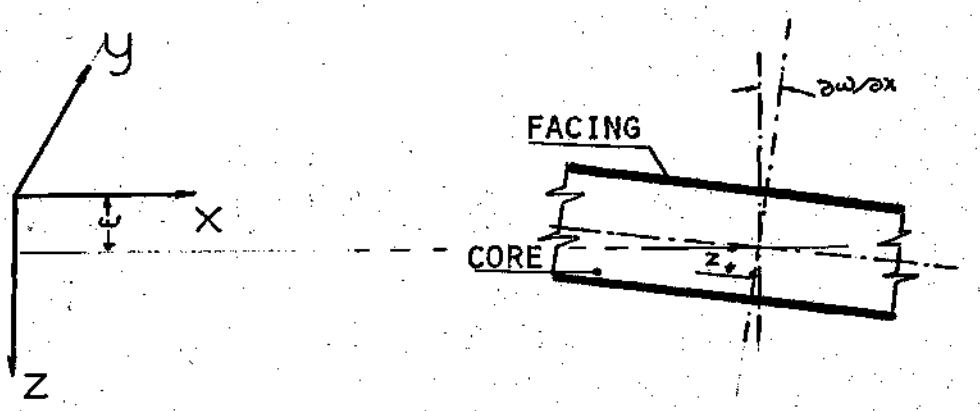

Figure 4-16. Deflection w(x,y) of a Loaded Sandwich Panel.

The displacement u in the x-direction for a point at a distance z from the neutral axis is

$$u = -z\lambda\frac{\partial w}{\partial x} \qquad (4\text{-}57)$$

In a similar manner, the shear strain γ_{zy} in the zy plane and the displacement v in the y-direction can be expressed as

$$\gamma_{zy} = (1-\mu)\frac{\partial w}{\partial y} \tag{4-58}$$

$$\gamma_v = -z\mu\frac{\partial w}{\partial y} \tag{4-59}$$

The strain γ_{xy} in the xy plane is related to u and v by

$$\gamma_{xy} = \frac{\partial u}{\partial y} + \frac{\partial v}{\partial x}$$

Replacing u and v above from Eq. 4-57 and Eq. 4-59,

$$\gamma_{xy} = -z(\lambda+\mu)\frac{\partial^2 w}{\partial x \partial y} \tag{4-60}$$

As the sandwich is simply supported, the displacement w can be expressed as a sine series [16], i.e.,

$$w = \sum_{n=1}^{\infty} \sum_{m=1} a_{mn} \sin\frac{m\pi x}{a} \sin\frac{n\pi y}{b} \tag{4-61}$$

where a is the length of the plate along the x axis and b is the width in the y direction, as given in Figure 4-17.

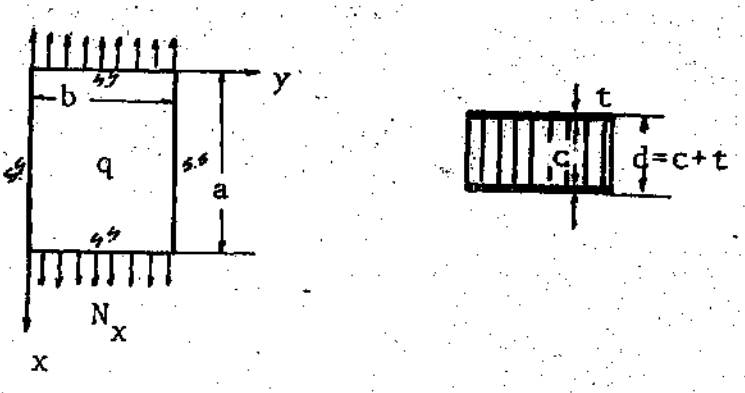

Figure 4-17. Simply Supported Sandwich Plate Loaded Edgewise and Normal to the Facing.

It will be noticed that the assumed displacement w satisfies the zero boundary condition.

Let us call the strain energy of the core and the faces U_c and U_f respectively. Then the total energy E of the system can be written, following references [2] and [3]:

$$E = U+V = U_c + U_f + V \tag{4-62}$$

where U represents the total strain energy of the system and V the potential energy of the loads. Using the definition of strain energy, and replacing the strains as functions of w, provided that the effective core shear modulus is negligible, i.e., condition (c) is satisfied, U_c can be expressed following Allen [15] as:

$$U_c = G_c \frac{d}{2} \int_0^a \int_0^b [(1-\mu)^2 (\frac{\partial w}{\partial y})^2 + (1-\lambda)^2 (\frac{\partial w}{\partial x})^2] dy\, dx\, dz \tag{4-63}$$

where d is c+t, as shown in Figure 4-17, G_c is the effective core shear modulus, and μ and λ are inherent characteristic of the core that indicate how rigid is the core in the y and x direction under shear.

In a similar manner, the faces strain energy U_f can be computed according to Allen [15] as:

$$U_f = E_f \frac{d^2 t}{4(1-\nu_f^2)} \int_o^a \int_o^b \{\lambda^2(\partial^2 w/\partial x^2)^2 + \mu^2(\partial^2 w/\partial y^2)^2 + \quad (4\text{-}64)$$

$$+ 2\nu\lambda\mu \frac{\partial^2 w}{\partial x^2}\frac{\partial^2 w}{\partial y^2} + \frac{1-\nu_f}{2}(\lambda+\mu)^2(\partial^2 w/\partial x \partial y)^2\} dx\, dy$$

where ν_f and E_f are the Poisson's ratio and Young's modulus for the face material.

The potential energy V of the system when the plate is subjected to uniform normal load per unit area q and to a tensile load per unit length N_x in the x direction as indicated in Figure 4-17, is given by Allen [15] as

$$V = V_1 + V_2 = \frac{N_x}{2} \int_o^a \int_o^b \left(\frac{\partial w}{\partial x}\right)^2 dy\, dx - \int_o^a \int_o^b wq\, dy\, dx \quad (4\text{-}65)$$

For w, as given in Eq. (4-61), to be the solution for the plate displacement it is required that the total energy of the system (U + V) be stationary with respect to any of the unknown coefficients a_{mn}, λ, and μ. That is,

$$\frac{\partial(U+V)}{\partial\lambda} = \frac{\partial(U+V)}{\partial\mu} = \frac{\partial(U+V)}{\partial a_{mn}} = 0 \quad (4\text{-}66)$$

Putting U and V as functions of w in Eq. (4-66), the following expression is obtained:

$$\frac{\partial(U+V)}{\partial a_{mn}} = \left(Gd \frac{\pi^2}{4}\frac{a}{b} \frac{\Omega^2}{1+\rho\Omega} + N_x \pi^2 \frac{ab}{4}\frac{m^2}{a^2}\right) a_{mn} - \frac{4q}{\pi^2}\frac{ab}{mn} = 0 \quad (4\text{-}67)$$

where Ω and ρ are given by:

$$\Omega = m^2 \frac{b^2}{a^2} + n^2 \tag{4-68}$$

$$\rho = \frac{\pi^2 Etc}{2(1-\nu^2)Gb^2} \tag{4-69}$$

E and ν here are the elastic modulus and Poisson's ratio of the facings.

Let us assume now that there is an interest in predicting the behavior of the plate when loaded as in edgewise simply sypported compressive tests. For that particular case, there is no normal load q, and the condition for Eq. (4-67) to be satisfied is that the coefficient of a_{mn} is zero. This condition determines the value of N_x, the force per unit length to produce a plate failure in the (m, n)th mode, as follows

$$N_x = \frac{Gd}{m^2} \left(\frac{a}{b}\right)^2 \frac{\rho\Omega^2}{1+\rho\Omega} \tag{4-70}$$

From equation (4-68) and (4-70) it may be inferred that for any given m, the smallest value of N_x is obtained when n is equal to one. Therefore, Eq. (4-70) can be rewritten as

$$N_{xm} = \frac{\pi^2 D_2}{b^2} K_1 \tag{4-71}$$

where

$$K_1 = \frac{(mb/a + a/mb)^2}{1+\rho[(mb/a)^2+1]} \qquad (4\text{-}72)$$

and D_2 is the flexural rigidity of the sandwich, defined as

$$\{D_2 = Etdc/(1-\nu^2)\} \qquad (4\text{-}73)$$

Scrutinizing the independent variables that are involved in Eq. 4-72 and Eq. 4-73, it is interesting to notice that the maximum compressive load N_{xm} before buckling takes place is related in a complex manner to the geometric factor a/b, to the core height c, elastic modulus and thickness of the facing, and to the shear modulus of rigidity G_c of the core.

For the edgewise compression test the values of D_2, b, a, and ρ will be known in every case; therefore, the minimum load N_x that can be applied to the sandwich structure before buckling occurs may be predicted using Eq. (4-71). This minimum load should correspond in general to either the first, the second or third failure mode [48].

The value D_2 for the conventional honeycomb, for all practical purposes, depends entirely on the characterisitcs of the facing materials; however, that may not be the case for the wire reinforced honeycomb. In fact, as mentioned in previous chapters, this new core may be significantly more rigid than the conventional ones and it may be bonded to thinner faces. When no edgewise load ($N_x = 0$) is

applied, but only a constant load q normal to the plate plane, Eq. (4-67) is reduced to

$$\frac{\partial(U+V)}{\partial a_{mn}} = \{Gd\ \frac{\pi^2 a}{4b}\ \frac{\rho\Omega^2}{1+\rho\Omega}\ a_{mn} - \frac{4q\ ab}{\pi^2 mn}\} = 0 \qquad (4\text{-}74)$$

or

$$a_{mn} = \frac{16qb^4}{\pi^6 mn}\ \frac{(1+\rho\Omega)}{D_2\Omega^2} \quad \text{(for m, n odd)} \qquad (4\text{-}75)$$

where again ρ and Ω take the values as given by Eq. (4-69) and (4-68) respectively. To find the stresses in the core and faces, the strains are determined first as a function of w, as indicated below

$$\begin{aligned} \varepsilon_x &= \partial u/\partial x = -\lambda z\ \partial^2 w/\partial x^2 \\ \varepsilon_y &= \partial v/\partial x = -\lambda z\ \partial^2 w/\partial y^2 \\ \gamma_{xy} &= \frac{\partial u}{\partial y} + \frac{\partial v}{\partial x} = -z(\lambda+\mu)\,\partial^2 w/\partial x \partial y \end{aligned} \qquad (4\text{-}76)$$

Then, using the stress strain relationship and solving for the stresses, we obtain:

$$\begin{aligned} \sigma_x &= \frac{E}{2(1-\nu^2)}(\varepsilon_x+\nu\varepsilon_y) = \\ \sigma_y &= \frac{E}{2(1-\nu^2)}\ (\varepsilon_y+\nu\varepsilon_x) \\ \tau_{xy} &= G\gamma_{xy} \end{aligned} \qquad (4\text{-}77)$$

replacing the values of ϵ_x, ϵ_y and γ_{xy} in Eq. 4-77, a final expression for the stresses on the plate facings is given in terms of w as follows:

$$\sigma_x = +E \frac{d\theta}{2(1-\nu^2)} \left(\frac{\partial^2 w}{\partial x^2} + \frac{\nu d^2 w}{\sigma y^2}\right.$$

$$\sigma_y = + E \frac{d\theta}{2(1-\nu^2)} \left(\frac{\partial^2 w}{\partial y^2} + \frac{\partial^2 w}{\partial x^2}\right) \qquad (4\text{-}78)$$

$$\tau_{xy} = \frac{Edx}{2(1+\nu)} \frac{\partial^2 w}{\partial x \partial y}$$

where $$\theta = \frac{1}{1+\rho\Omega}$$

Since w will be a known function because the coefficients a_{mn} will be determined as functions of q, then the set of equations given in 4-78 represents the solution for the facing stresses for the prescribed uniform normal load.

As in the previous case, it can be seen from Eq. 4-75 that the deflection w and consequently the strains and the stresses in the sandwich are linked through ρ and Ω to the core dimensions, properties and thickness of the facings, and to the core modulus of rigidity G_c.

It is possible through this kind of analysis to determine the core shear modulus if a test is performed where the deflection or the strain is measured at convenient locations and the approximate solution for w is taken as

proposed in Eq. 4-61, and solution for a_{mn} is taken from Eq. 4-75.

The Core Young's Modulus

The conventional stress analysis for a sandwich structure neglects the contribution that the core may have in carrying tensile load in the xy sandwich plane. This criterion implies that the effective core Young's Modulus E_c is negligible compared to the facing modulus, as illustrated in Figure 4-18, but for the wire reinforced sandwich core, it may not be reasonable to assume that $E_c << E_f$ for all cases. In fact, since this new core is rigid by itself, some applications may required the use of a core with very thin facings, or even just the core alone. Consequently, it is appropriate to consider an effective core Young's Modulus which is a function of the core geometry and core and wire material properties.

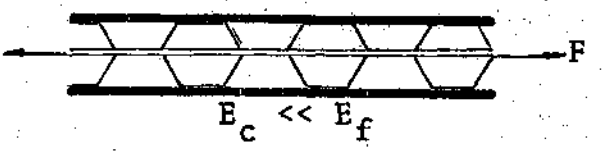

Figure 4-18. Sandwich Under the Action of a Tensile Load.

As the wires are firmly embedded in the core, for the purpose of estimating E_c without embarking upon a complex analysis which implies the study of the material behavior at the interface, it will be considered that both sheet forms and the wire are subjected to the same displacement. Inasmuch, as the object of the analysis is to predict an average modulus E_c along prescribed directions and as the facing restricts the displacement of the core, rendering it more uniform, it will be assumed that plane sections in the core perpendicular to the sandwich plane remain plane after an elastic deformation. The core considered in this analysis comprises two sheets pressure or vacuum formed and bonded together as illustrated in Figure 4-19. The first

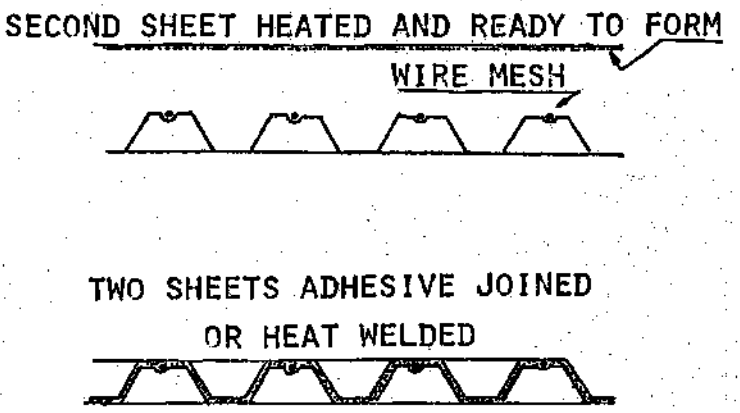

Figure 4-19. Wire Reinforced Core.
(a) Core in Process;
(b) Finished Product.

sheet is formed without the wires and the second one has the embedded wires in. Both sheets are bonded together either by an adhesive or by heat welding.

From the stated conditions, it is expected that the effective core Young's Modulus to be a function of the wires reinforcement orientation with respect to the stress system. Consequently, it is convenient to determine the effective elastic modulus as the wires reinforcement is oriented in various directions. Three basic orientations can be distinguished, namely: (a) the load is applied in the sandwich plane and perpendicular to one of the wire orientations; (b) the load is parallel to one set of wire orientations; and the most general case, (c) when the load is at an angle α from a wire orientation, as shown in Figure 4-20.

Case a: Ey. To determine Ey the load is applied perpendicular to one of the wire directions, as shown in Figure 4-20a.

From the assumption that planes remain planes and considering that the flow of material during the forming process is rather uniform, the deformation of the complex shell-like core can be conceived in a form more convenient to work with, i.e., the displacement in the y direction should be approximately the same as if the two sheets were only joined together without being formed but having the wires embedded. The argument that follows is based on this mathematical model.

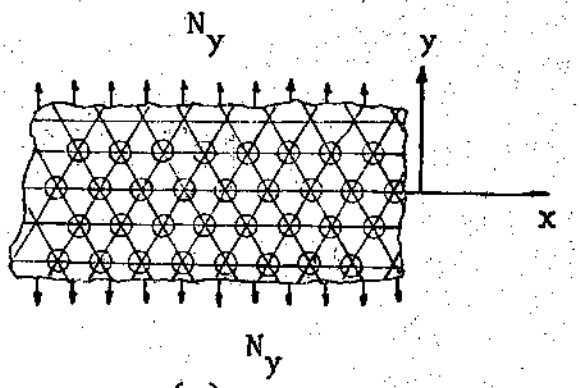

(a)

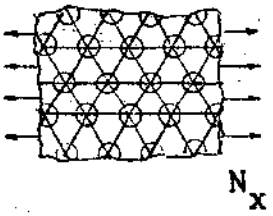

(b)

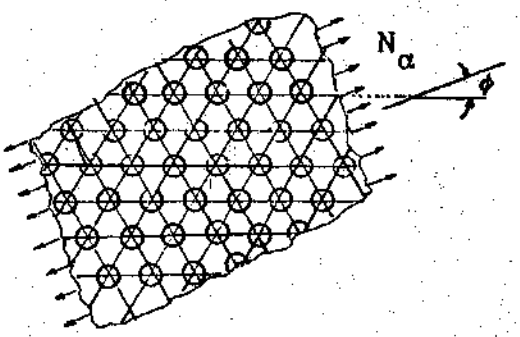

(c)

Figure 4-20. Different Modes of Loading in the xy Plane.
(a) Loading Perpendicular to One Set of Wires
(b) Loading Along the Direction of a Set of Wires
(c) Loading Along a General Direction at an Angle α.

Let us consider a portion of a sandwich core and its corresponding mathematical model as shown in Figure 4-21.

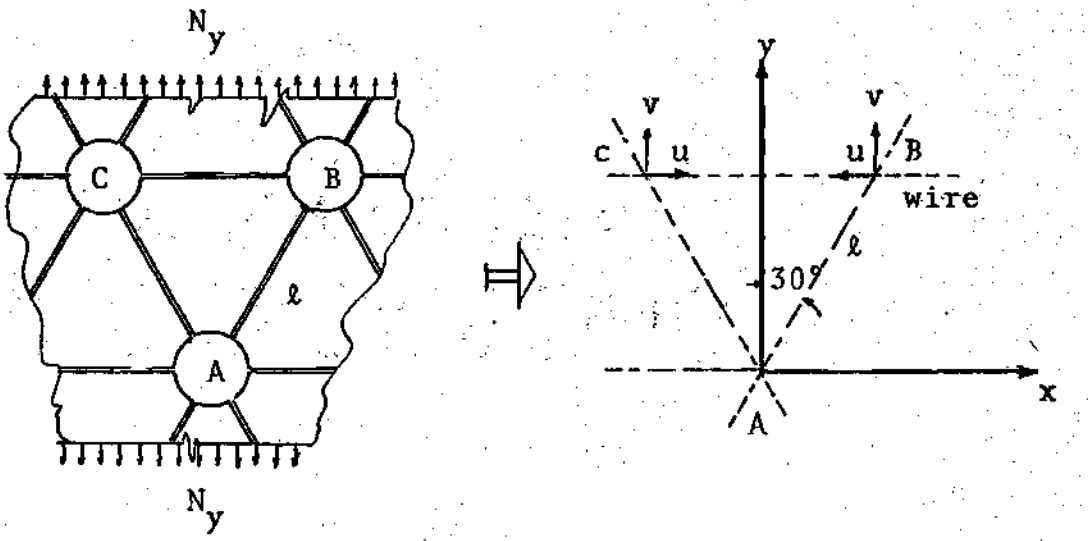

Figure 4-21. Loading a Core in the y-Direction. (a) Portion of a Sandwich Core Made by Either Pressure or Vacuum Forming; (b) Sandwich Core Model Made by Bonding Together Two Plane Sheets and Embedded Wires.

The points labeled A, B, and C define the intercept of the three wires which is located in the projections axis of symmetry. As the uniform load N_y is applied, the points B and C are displaced in respect to A in the x and y directions the distances u and v.

The resultant strains in the sheets in the y and x direction are:

$$\varepsilon_y = \frac{\partial v}{\partial y} = \frac{v}{\ell \cos 30°} \qquad (4\text{-}79)$$

$$\varepsilon_x = \frac{\partial u}{\partial y} = -\frac{u}{\ell/2} \qquad (4\text{-}80)$$

where ℓ represents the distance between projections.

The load F_s that can be carried by the two sheets in a strip of width CB = ℓ would be

$$F_s = 2\ t_o \ell\ \varepsilon_y E_s = 2\ t_o \frac{v}{\cos\ 30°} E_s \qquad (4\text{-}81)$$

where t_o is the thickness of one sheet and E_x is the elastic modulus of the sheet. The load F_w in the direction y that can be carried by the two wires that are embedded in the strip bounded by C and B is

$$F_w = 2\ E_w \frac{\Delta\ell}{\ell} \cos\ 30°\ A_w \qquad (4\text{-}82)$$

where E_w is the wire modulus, $\Delta\ell$ is the increase in length of each wire and A_w is the wire cross sectional area.

But from Figure 4-21, $\Delta\ell$ is

$$\Delta\ell = v \cos\ 30° - u \sin\ 30° \qquad (4\text{-}83)$$

However, the displacements u and v are not independent of each other; they are related through the sheet Poisson's ratio ν in the following manner.

$$\varepsilon_x = -\nu\varepsilon_y = \frac{\partial u}{\partial x} = -\frac{u}{\ell/2} = -\nu\ \frac{v}{\ell\ \cos\ 30°}$$

We obtain,

$$u = \nu\ v/2\ \cos\ 30° \qquad (4\text{-}84)$$

Therefore, Eq. 4-83 can now be written in terms of v only as

$$\Delta \ell = v \left(\cos 30° - \frac{\nu}{2} \tan 30°\right) \tag{4-85}$$

Referring back to Eq. 4-82, F_w can be written as

$$F_w = 2E_w \, v \, \frac{\cos 30°}{\ell} \, A_w \left(\cos 30° - \frac{\nu}{2} \tan 30°\right) \tag{4-86}$$

where A_w is the wire cross sectional area. The total F carried by the sheet and the wire can now be estimated as

$$F = \left[2 \, t_o \, \frac{E_s}{\cos 30°} + 2E_w A_w \, \frac{\cos 30°}{\ell} \left(\cos 30° - \frac{\nu}{2} \tan 30°\right)\right] \tag{4-87}$$

Both the force F and the strain ε_y computed in the above manner for the mathematical model correspond to the F and ε_y of the real sandwich core. However, the correspondence between stress and strain for the real core is given by

$$\sigma_c = F/A_c = E_y \varepsilon_y \tag{4.88}$$

where E_y is defined as the effective core elastic modulus, F is the force given by the expression in Eq. 4-87 and σ_c is computed on the basis of the cross sectional area A_c of the core strip which is

$$A_c = \ell h \tag{4-89}$$

where h is the height of the core projections. Replacing now the values of σ_c and ε_y in Eq. 4-88, the final expression for E_y is obtained

$$E_y = \frac{t_o}{h} \left[2E_s + 2E_w \frac{A_w}{\ell t_o} \cos^2 30° \left(\cos 30° - \frac{\nu}{2} \tan 30°\right)\right] \quad (4\text{-}90)$$

The nature of this equation indicates that E_y does not only depend on the material properties E_s, E_w, and ν, but it is also a function of the cross sectional areas ratio $A_w/\ell t_o$ which determines the wire to sheet weight ratio, and a function of h which determines the core density.

Case b: E_x. In this case the load is applied in the direction parallel to one of the wires as shown in Figure 4-22, and we wish to determine the effective Young's modulus of the core in the direction of the applied load.

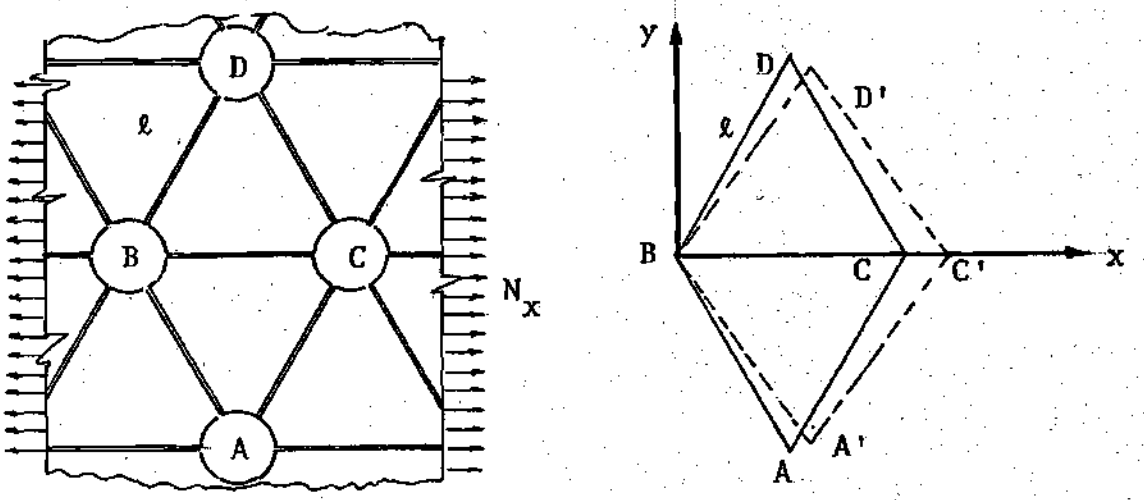

Figure 4-22. (a) Sandwich Core Loaded in a Direction Parallel to One of the Wires; (b) Initial and Final Orientation of the Wires.

Again, consider a core strip bounded by A and D projections, loaded with a force F_x and been strained the amount ε_x and ε_y. As the wire arrangement cannot prevent any sheet deformation in the y direction, ε_y can be estimated as $\nu\ \varepsilon_x$.

Under these circumstances, the load carried by the wire BC is $F_1 = \varepsilon_x A_w E_w$. The strain in the wires BD and BA is:

$$\varepsilon_2 = \left(-\frac{\sqrt{3}}{2}\ \ell\varepsilon_y \sin 60° + \varepsilon_x \frac{\ell}{2} \sin 30°\right)/\ell$$

or

$$\varepsilon_2 = \varepsilon_x \frac{\sqrt{3}}{4}\ (1-\nu)$$

and the force carried by each of these two wires is

$$F_2 = A_w\ \varepsilon_2\ E_w \tag{4-91}$$

The total force F_x in the x direction is given by

$$F_x = F_1 + 2F_2 \cos 60° + A_s\ \varepsilon_x\ E_S \tag{4-92}$$

where A_s is the solid cross sectional area of two sheets, i.e.,

$$A_s = \ell\sqrt{3}\ 2t_o \tag{4-93}$$

Defining now the core elastic modulus in the x direction as

$$E_x = \frac{F_x}{A_c \epsilon_x} ,$$

where A_c is the cross sectional area of the strip of width AD, the following expression is obtained:

$$E_x = \frac{\epsilon_x A_w E_w + 2A_w \epsilon_x \frac{\sqrt{3}}{4} (1-\nu) E_w \cos 60° + A_s \epsilon_x E_s}{h\ell\sqrt{3}\ \epsilon_x}$$

or

$$E_x = \frac{\pi}{4\sqrt{3}h\ell} d_w^2 E_w \left[1 + \frac{\sqrt{3}}{4} (1-\nu)\right] + \frac{2t_o}{w} E_s \qquad (4-94)$$

where d_w is diameter of the wire or reinforcing fiber.

Case c: E. To determine the modulus E at an angle α from one of the reinforcing fiber orientation, it is necessary to assume that the core is loaded with a force F_1, applied in the direction α. The corresponding stresses σ_1, $\sigma_2 = 0$, and $\tau_{12} = 0$ that are developed, as well as σ_x, σ_y, and τ_{xy} are shown in Figure 4-23.

Calling σ_x, σ_y and τ_{xy} the equivalent stresses generated in the element as it is oriented like in Figure 4-23b, the following expression results from the Mohr's circle [49].

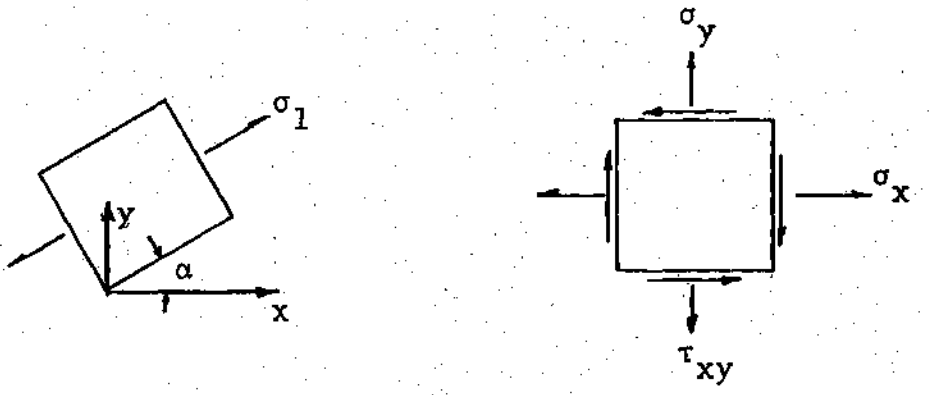

Figure 4-23. Stress State Diagram.
(a) Stress State in the Directions 1 and 2;
(b) Equivalent xy Stress State

$$\sigma_1 = \sigma_x \cos^2\alpha + \sigma_y \sin^2\alpha - 2\tau_{xy} \sin\alpha \cos\alpha$$

$$\sigma_2 = 0 = \sigma_x \sin^2\alpha + \sigma_y \cos^2\alpha + 2\tau_{xy} \sin\alpha \cos\alpha$$

$$\tau_{12} = 0 = \sigma_x \sin\alpha \cos\alpha - \sigma_y \sin\alpha \cos\alpha + \tau_{xy} (\cos^2\alpha - \sin^2\alpha)$$

It is found from this set of equations that

$$\sigma_1 = \sigma_y/\sin^2\alpha = \sigma_x/\cos^2\alpha$$

$$\tau_{xy} = \sigma_y \sin\alpha \cos\alpha/-\sin^2\alpha \qquad (4\text{-}95)$$

In the same way the transformed strains ε_1, ε_2, and γ_{12} can be written as

$$\varepsilon_1 = \varepsilon_x \cos^2\alpha + \varepsilon_y \sin^2\alpha - \gamma_{xy} \sin\alpha \cos\alpha$$

$$\varepsilon_2 = \varepsilon_x \sin^2\alpha + \varepsilon_y \cos^2\alpha + \gamma_{xy} \sin\alpha \cos\alpha \qquad (4\text{-}96)$$

$$\varepsilon_{12} = 2\varepsilon_x \sin\alpha \cos\alpha - 2\varepsilon_y \sin\alpha \cos\alpha + \gamma_{xy} (\cos^2\alpha - \sin^2\alpha)$$

The strains ε_x, ε_y, and γ_{xy} are related to σ_x, σ_y and τ_{xy} by the Hooke's Law in the following manner.

$$\varepsilon_x = \frac{\sigma_x}{E_x} - \nu_{xy}\ \sigma_y/E_y$$

$$\varepsilon_y = \sigma_y/E_y - \nu_{yx}\ x/E_x$$

$$\gamma_{xy} = \tau_{xy}/\sigma_{xy}$$

Replacing these values in Eq. 4-96, a final expression for E_1 is found [49]

$$E_1 = \frac{\sigma_1}{\varepsilon_1} = \frac{E_x}{\cos^4\alpha - (E_x/E_y)\sin^4\alpha + (E_y/G_{xy})\sin^2\alpha\cos^2\alpha - (\nu_{xy}/2)\sin^2 2\alpha} \qquad (4\text{-}97)$$

where G_{xy} is the core shear modulus as if the core were loaded edgewise in shear only and ν_{xy} corresponds to the Poisson's ratio

$$\nu_{xy} = (\varepsilon_y/\varepsilon_x)_{\sigma_y = 0,\ \sigma_x \neq 0}$$

which is approximately equal to ν_x as previously noted in Case a. Equation 4-97 furnishes the relation of the core modulus E_1 in the direction α as a function of the core modulus E_x and E_y which have been estimated previously and G_{xy} which can also be predicted in a similar manner as E_x and E_y as an element, like the one shown in Figure 4-24 is loaded in pure shear. The assumption could be made that

the only wire that can carry any load is DC as the point D is displaced to D'. At the same time P moves to P' and the assumption is made that PP' = DD'.

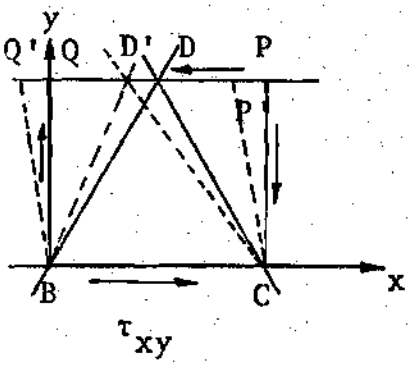

Figure 4-24. Displacement Model to Predict G_{xy}

Core Shear Modulus

The shear modulus is probably the most important property of a sandwich core. A very low modulus causes the core to have very large deformations and the whole concept of having a low weight structure with high inertia moment is lost, for the simple reason that the facings tend to behave like two independent members. In that case, the flexural rigidity D of the composite structure as presented in Eq. 4-73 has no meaning. Instead, the facings deform with respect to their own neutral axis.

The shear modulus is experimentally determined using the ASTM Standard test [50] as shown in Figure 4-25, either by applying a load in tension or in compression. The core

is bonded directly to 12.5mm thick steel plates.

The applied force F has a shear and a normal component which are given by

$$F_s = F \cos\alpha = Fa/(a^2+c^2)^{1/2} \qquad (4\text{-}98)$$

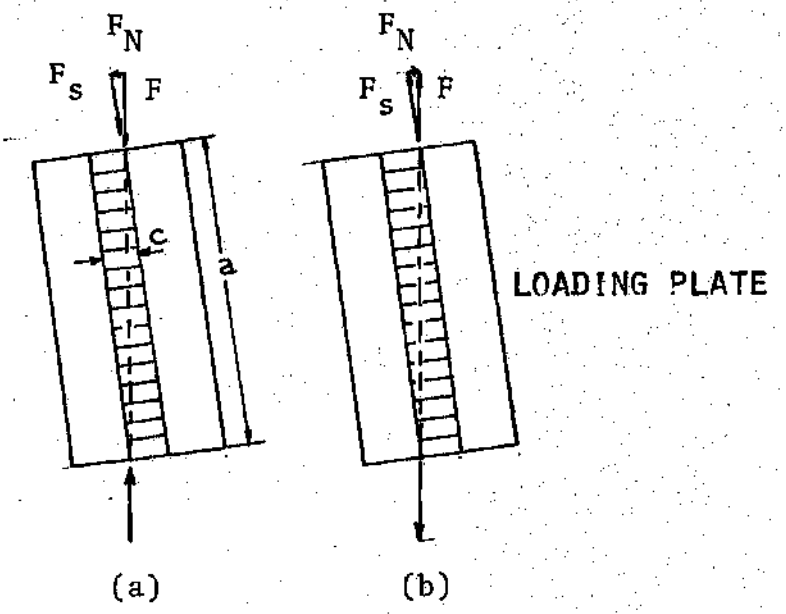

Figure 4-25. Core Under Shear.
(a) Compression Shear Test; (b) Tensile Shear Test.

$$F_N = F \sin\alpha$$

The structure as a whole has no applied external moments. The relative displacement of the shear plates can be exclusively considered due to F_s. As the core is firmly

bonded to heavy steel plates, it is reasonable to assume that the displacement v(h) in the direction of F_s of the top of each projection (see Figure 4-26b) respect to the bottom will be uniform for the entire specimen.

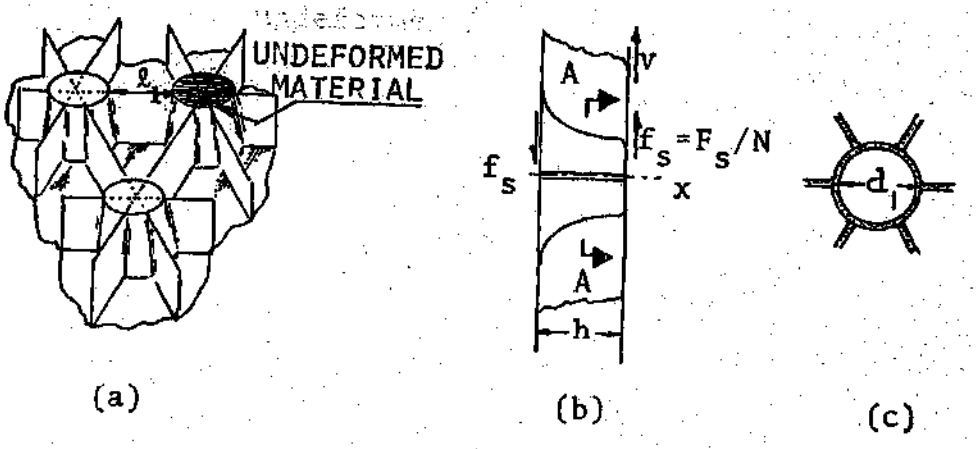

Figure 4-26. Core Geometry.
(a) Wire Reinforced Core; (b) Loaded Projection; (c) Cross Section A-A.

Also, due to the symmetry of the applied forces, the loading plates can be expected to remain parallel. The considerations justify the assumption that each projection is subjected to the same load situation, namely pure shear. The average shear τ' in a cross section such as A-A, Figure 4-26c, is

$$\tau' = F_s/AN = f_s/A \qquad (4\text{-}99)$$

where A is the cross section area/projection at a height x, N is the total number of projections in the plate, and

f_s is the shear force projection. The shear strain is given by

$$\gamma' = \tau'/G' \tag{4-100}$$

where G' corresponds to the shear modulus of the core material. Let us now define the core shear modulus [1], G_c as

$$G_c = \tau/\gamma \tag{4-101}$$

where τ is

$$\tau = F_s/\text{core area} = F_s/ab = f_s/A_o$$

where $A_o = ab/N$ is the area in the sandwich plane per projection and the average shear strain γ is given by

$$\gamma = v(c)/c = v(h)/h \tag{4-102}$$

where c is the thickness of the core, as shown in Figure 4-17 and h is the height of the projections as shown in Figure 4-26b. The displacement v in the y direction is related to γ' as follows

$$dv(x)/dx = \gamma'$$

or

$$v(h) = \int_o^h \gamma' dx = \frac{F_s}{G'N} \int_o^h \frac{dx}{A} \tag{4-103}$$

To proceed any further, it is necessary to formulate a relation between x and A(x). The variable A(x) proves to be a function of the metal forming parameters, such as pressure p, strain rate sensitivity factor m, and projection shape. However, if both the projection shape and height h, the sheet thickness t_o and the core material are known, as well as the forming conditions, it is possible to determine an empirical relation between A and x. In that case, A could be written as A(x) for a given t_o and h; therefore, v(h) in Eq. 4-103 becomes a known quantity and G_c can be determined from Eq. 4-101.

As G_c is directly related to A(x), it is of interest to find out the best A(x) function to maximize G_c for a given material and core density. Considering the wire reinforced core, let us assume a fixed projection height h, same stock thickness t_o, and a constant amount of undeformed material at the top of each projection. Under these conditions, and considering Eq. 4-101 and Eq. 4-103, the problem of finding an optimum G_c reduces to minimize the functional

$$J[A] = \int_o^h \frac{dx}{A} \qquad (4\text{-}102)$$

subject to the constraint:

$$V_p = \int_o^h A\,dx = (A_o t_o - A'_o t_o) \qquad (4\text{-}103)$$

where V_p is the volume of deformed material per projection,

$A_o t_o$ is the total volume of material per projection, and $A'_o t_o$ is the undeformed material.

Using the Lagrange multiplier λ, the extremization of the functional $J[A]$ is equivalent to finding a stationary value for the functional

$$J'[A,\lambda] = \int_o^h \frac{dx}{A} + \lambda \int_o^h A dx \qquad (4\text{-}104)$$

Euler's equation for the stationery condition of $J'[A,\lambda]$ is

$$\frac{\partial}{\partial A}\left(\frac{1}{A} + \lambda A\right) = -\frac{1}{A^2} + \lambda = 0 \qquad (4\text{-}105)$$

or $$A = \lambda^{-1/2} = \text{constant}$$

and from the constraint condition, A becomes

$$A = V_p/h \qquad (4\text{-}106)$$

Even if it might be impractical to generate the optimum area, Eq. 4-106 is quite enlightening for a practical consideration because now a given projection shape can be selected as a first approximation and depending on the material distribution Eq. 4-106 provides the necessary information to modify the projection so that a better area distribution and an improved G_c in consequence can be achieved.

Let us now consider a wire reinforced core with a given projection height h, initial sheet thickness t_o, a

given separation between projections ℓ_1, as illustrated in Figure 4-26, and let us assume that the projections are arranged in a hexagon pattern and have such shape that an optimum G_c can be obtained. Under these conditions, A_o is known and the cross sectional area A of the deformed material reduces to

$$A = (A_o - A_o')t_o/h \tag{4-107}$$

where

$$A_o = (d_1+\ell_1)^2\sqrt{3}/2$$

and

$$A_o' \approx \pi d_1^2/4$$

As the integration in Eq. 4-103 is executed, v(h) becomes

$$v(h) = \frac{f_s h}{G'A}$$

$$G_c = \frac{\tau h}{v(h)} = G' \frac{A}{A_o}$$

and

$$G_c = \frac{t_o}{h} G'(1 - \frac{A_o'}{A_o}) \tag{4-108}$$

It is interesting to analyze the significance of the terms in this final equation. The expression t_o/h is equivalent to ρ_c/ρ where ρ_c and ρ are the core and solid material densities. The term G' is the shear modulus of the solid material and $(1-A'_o/A_o)$ is the useful material per unit weight of the core that is subjected to the shear stress τ. The rest of the material, the one distributed on the top and bottom of projections may be considered ineffective under shear.

Significance of Core Mechanical Properties

It is specially meaningful from the economics standpoint and also from that of good design practice for us to study the load carrying capacity of sandwich beams under different load modes in terms of the core properties. Let us assume that there exists a composite structural sandwich fixed geometrical dimensions t, c, h, a, b and that we wish to assess the sandwich behavior in terms of core mechanical properties which would be the remaining independent variables.

Let us commence our analysis with the case of a simply supported beam subjected to a distributed load q(x), as indicated in Figure 4-27.

Using the ordinary beam bending theory, the maximum bending moment is related to the facing stress σ_f as

$$\sigma_f = \frac{MZ}{D} E_f \qquad (4\text{-}109)$$

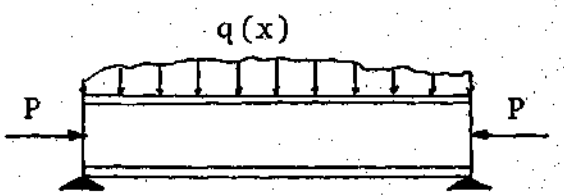

Figure 4-27. Simply Supported Sandwich Beam

where E_f is elastic modulus of the facing and D is the sandwich flexural rigidity given by

$$D = E_f \frac{bt^3}{6} + E_f \frac{btd^2}{2} + E_c \frac{bc^3}{12} \qquad (4\text{-}110)$$

The first and third terms of Eq. 4-110 add only less than 2 percent to D [15] and they can be disregarded if

$$(d/t)^2 > 33, \qquad (4\text{-}111)$$

and

$$6\left(\frac{E_f}{E_c}\frac{t}{c}\right)(d/c)^2 > 100 \qquad (4\text{-}112)$$

In such case, Eq. 4-109 can be written as

$$\sigma_f = \pm \frac{M E_f h/2}{E_f bt d^2/2} \qquad (4\text{-}113)$$

Should the failure of the beam occur at the facing, and as

long as the geometrical characteristics of the sandwich are kept constant, core basic properties are irrelevant in the determination of the maximum load that can be carried by a simply supported sandwich beam. However, in order to retain validity of Eq. 4-110, the beam theory requires that the sandwich exhibit one neutral axis only which is common to both core and facing. For this reason, the adhesive must possess good shear strength to maintain the whole sandwich as one single body with no sliding at the facing core interface.

If the failure mode is shearing of the core, the governing critical relation is

$$\tau = \frac{Q\Sigma(SE)}{Db} \qquad (4\text{-}114)$$

where Q is the shear load, S is the first moment of area respect to the neutral axis, and E is the elastic modulus for each area. The evaluation of $\Sigma(SE)$ at a distance z from the neutral axis is given by

$$\Sigma SE = E_f \frac{btd}{2} + E_c \frac{b}{2} \left(\frac{c}{2} - z\right)\left(\frac{c}{2} + z\right) \qquad (4\text{-}115)$$

If the condition in Eq. 4-112 is met, the only significant term in Eq. 4-115 is the first one. The shear stress of the core given in Eq. 4-114 would be simplified to an approximately constant value for the whole cross section equal to

$$\tau = Q/bd \qquad (4\text{-}116)$$

From equilibrium considerations, as shown in Figure 4-28, we have that

$$Q = -dM/dx \tag{4-117}$$

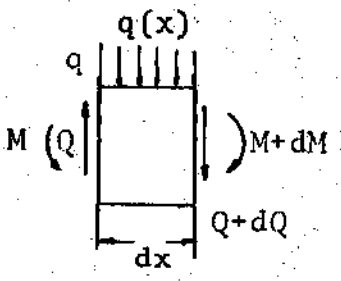

Figure 4-28. Equilibrium Diagram

Assuming two beams of equal geometry loaded in similar manner such that at any location x we have:

$$q_1(x) = kq_2(x) \tag{4-118}$$

where k is a constant factor, then the respective failure conditions are related by:

$$(\tau_1/\tau_2) = Q_1/Q_2 = \frac{\int dq_1}{k\int dq_1} = \frac{1}{k} \tag{4-119}$$

where τ_1 and τ_2 are the shear strength of the two cores. This indicates that if the failure mode of a beam is one of shearing of the core, the total load that can be carried by

a simply supported beam in any given loading fashion is directly proportional to the shear strength.

Continuing with the analysis concerning the significance of the core mechanical properties in a sandwich, it has been shown previously that for simply supported plate edgewise loaded, as shown in Figure 4-29, the maximum force per unit length that the plate can support is

$$N_x = \frac{-\pi^2 D_2}{b^2} k_1, \qquad (4\text{-}120)$$

where D_2 is the flexural rigidity of the sandwich, which is approximately equal to [15]

$$D_2 = Etd^2/2(1-\nu_f^2), \qquad (4\text{-}121)$$

and

$$k_1 = (mb/a + a/mb)^2/[1+\rho(m^2b^2/a^2+1)] \qquad (4\text{-}122)$$

and

$$\rho = \pi^2 E_f td/2(1-\nu_f^2)G_c b^2 \qquad (4\text{-}123)$$

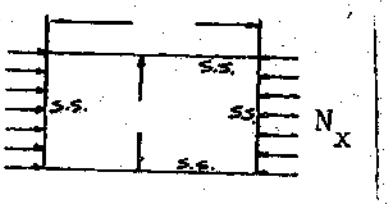

Figure 4-29. Edgewise Loaded Simply Supported Plate.

The analysis followed by Allen [15] indicates that when two sandwiches of identical facings and dimensions but different core material are compared, the ratio of forces reduces to

$$(N_x)_1/(N_x)_2 = (1+\rho_2 F)/(1+\rho_1 F) \qquad (4\text{-}124)$$

where $F = m^2b^2/a^2 + 1$.

Equations 4-123 and 4-124 illustrate that the effect of the shear modulus of rigidity of the core in the force ratio becomes more significant when weak cores are compared. For that case the force ratio approaches the modulus ratio, but it comes closer to unity when stronger cores are compared.

However, the buckling of the faces may not be the failure criteria for the simply supported sandwich, as compression failure of the facing may happen first at smaller loads. The core strength in the edgewise direction plays a role under these circumstances, but this is of minor importanct in practice because the loading capacity is much higher for the facing than for the core.

It has been determined so far that the characteristics of the core, namely shear modulus, shear strength, elastic modulus, do not always make a significant contribution to the loading capacity of the sandwich. The significance depends upon the type of loading and the boundary conditions of the structure. Whenever the core characteristics are immaterial, the most fortunate choice is the least expensive

cores. However, the internal stresses and the resisting bending moments that are developed upon loading are not always the governing factors for the selection of a given sandwich. The maximum deflection at selected location is at times the principal design criterion. There will be a correlation between the core mechanical properties and the sandwich deflection. The deflection can be thought as the combined result of a facing resisting bending moment and the shear stress applied at the core. Let us now consider an example that illustrates the deflection mechanism and the relevance of the core properties: a simply supported beam that is loaded axially by a force P and a distributed load q(x), as shown in Figure 4-30.

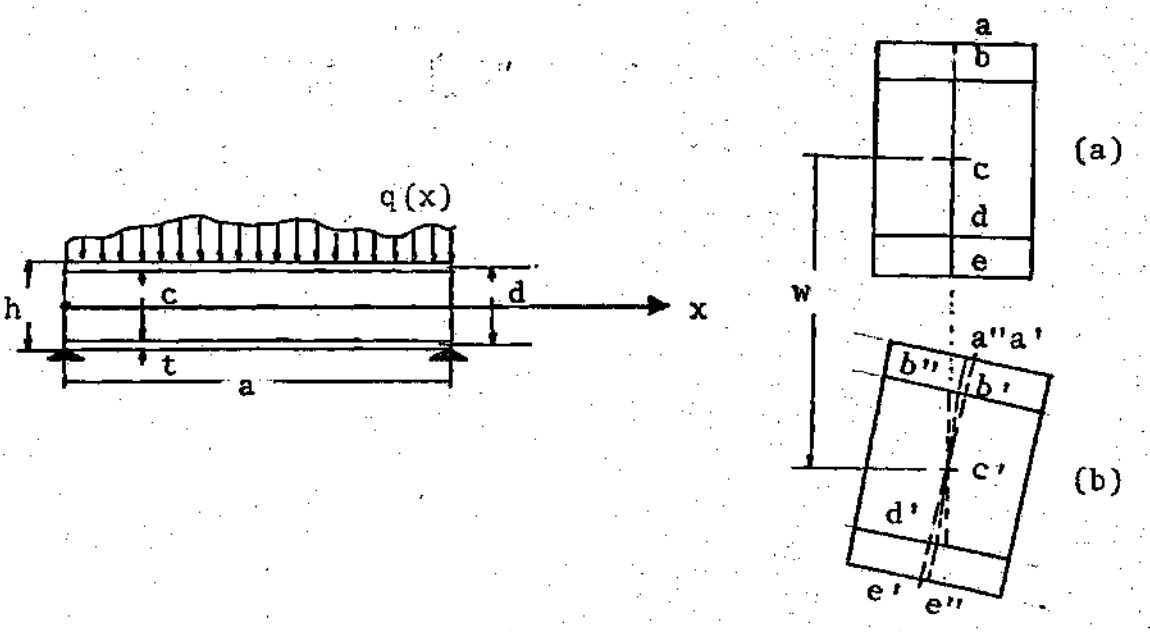

Figure 4-30. (a) Simply Supported Beam; (b) Unloaded; (c) Loaded.

A portion of a sandwich as it appears when not loaded is presented in Figure 4-30. Figure 4-30c shows how a material plane abcde takes a new position a"b"c'd"c" after deformation.

It is noteworthy to observe that this new surface does not coincide with the corresponding plane a'b'c'd'e' which would be the position to be assumed by the plane abcde if the core were infinitely rigid.

The shear strain γ of the core is represented in Figure 4-30c by the angle b"c'd'. If the angle oc'b" is identical by $\lambda dw/dx$, where oc' is in a vertical position, the shear strain can be written as

$$\gamma = (1-\lambda)dw/dx \qquad (4\text{-}125)$$

Under the assumption that there is no lateral movement of the point c in the neutral axis, the displacement u in the x direction of a point a distance z from the neutral axis can be put in terms of λ, dw/dx, and z. Furthermore, if for a given loading situation an approximate displacement function w can be anticipated, both the approximate strain energy of the beam U and the potential energy V of the load can be computed.

If a load q is selected such that:

$$q = q_n \sin n\pi \frac{x}{L}, \qquad (4\text{-}126)$$

an approximate solution for w could be given as

$$w = a_n \sin n\pi \frac{x}{L} \tag{4-127}$$

which satisfies the boundary conditions of $w(L) = w(0) = 0$. The strain energy of the beam U is stored in the form of strain energy due to core shearing, strain energy due to deformation of the facing as a membrane, and to a lesser extent, strain energy due to rotation of the facing around its own axis. From the standard formulation that relates displacement to strain, stress-strain to energy, and strain to stress, it can be shown that U is a known function of λ and a_n. Similarly, the potential energy of the loads is seen to be a function of a_n and can be estimated as [15]

$$V = \int_o^L q(x)w \, dx - \frac{P}{2} \int_o^L \left(\frac{dw}{dx}\right)^2 dx \tag{4-128}$$

As the equilibrium state corresponds to the condition that the total energy (U+V) is minimum, the following expressions result

$$\frac{\partial (U+V)}{\partial a_n} = 0 \tag{4-129}$$

$$\frac{\partial (U+V)}{\partial \lambda} = 0$$

Solving for λ and a_n in the set of Eq. 4-120 and 4-130, the following is obtained:

$$\lambda = (1 - \frac{t}{c} \xi n^2)/(1 + \xi n^2) \qquad (4\text{-}131)$$

where

$$\xi = \frac{\pi^2}{L^2} \frac{E}{G_c} c \frac{t}{c} \qquad (4\text{-}132)$$

and extending the above analysis, essentially due to Allen [15], a_n can be written as:

$$a_n = \frac{q_n}{n^2 \frac{\pi^2}{L^2} \{n^2 \frac{\pi^2}{L^2} Eb \frac{d^2 t}{2} (\frac{t^2}{1+n^2\xi} + \frac{t^2}{3d^2}) - p\}} \qquad (4\text{-}133)$$

From the Eqs. 4-131, 4-132 and 4-125 it can be seen that as the core modulus G_c increases, λ increases and the strain of the core is reduced. The effect of the shear modulus G_c on the deflection of the beam can also be appreciated from Eq. 4-133 and 4-127. In the absence of lateral load ($p = 0$), the expression in Eq. 4-133 can be approximated for low modulus cores as

$$a_n = \frac{q_n}{(\frac{n^2}{L^2})^2 Eb \frac{t^3}{6}} [1 - t^2/(1+n^2\xi) 3d^2] \qquad (4\text{-}134)$$

This equation suggests that the deflection of the beam $w = a_n \sin n\pi \frac{x}{L}$ can be considered as $w = (a'_n + a''_n) \sin n\pi \frac{x}{L}$ where the first coefficient a'_n is a dependent variable

of the sandwich dimensions but independent of the core properties. On the other hand, the second term a''_n includes the quantity ξ which is a function of the core shear modulus. As any loading q can always be interpreted as a combination of terms $q = \Sigma q_n \sin n\pi \frac{x}{L}$, the displacement w in general can be written as

$$w = w' + w''$$

where w" reflects the core properties and w' is independent of such properties. If attention is limited to the deflection of one point, the critical one, a list of values w' and w" can be compiled in a tabulated form as

$$w = w' + w'' = k_b \frac{PL^3}{D} + k_s \frac{PLC}{h^2 G_c b}$$

where the coefficients k_b and k_s are determined according to the nature of the load [48].

CHAPTER V

EXPERIMENTAL PROCEDURES AND RESULTS

The wire reinforced honeycomb (WRH) as a structural component in the sandwich construction has been considered in Chapter IV. References to general shape and appearance of the elements that form the WRH have been illustrated in Chapter I. The equipment and instrumentation for the making and testing of the WRH has already been discussed in Chapter III. This chapter starts by taking on the procedure followed in the manufacturing of the WRH. To assess the mechanical properties of the WRH, a series of tests were conducted following ASTM guidelines. The results concerning the compression shear test, tension shear tests, bending tests, buckling test, and the four edges simply supported buckling test are presented here.

Seeking a suitable process to join the vacuum formed polystyrene sheets together, heat welding was examined. Due to the quality of this bond, the adhesive saving and the short operational time, heat welding appeared to be very promising. Certain aspects of this bonding method, as well as the tensile test results to characterize the bond strength are presented in this chapter. Correlation between variables of industrial value such as forming time, pressure, and sheet thickness are also given in this section, as well

as the sheet thickness distribution after forming as a function of location.

The Plastic Wire Reinforced Honeycomb

The WRH can be made from either superplastic metal or polymeric materials. The construction of the WRH using High Impact Polystyrene sheets is explained below. The process can be reduced to the following steps: (1) cutting the sheets to size, (2) surface preparation, (3) vacuum or pressure forming, (4) bonding semicore sheets and wires, (5) cutting excess material, (6) bonding the semicore to the facings or to the loading plates, and (7) bonding the semicores together to make a sandwich.

The cores were made from polystyrene sheets 0.5mm, 0.75mm, and 1.00mm thick (0.020in, 0.030 in, and 0.040 in). The 120cm x 240cm sheets were cut into 40cm x 35cm (16 in. x 14 in.) rectangular pieces which were later cleaned either with isopropyl alcohol or aliphatic naphtha so that they were oil and dust free. Proper conditioning of the surfaces proved to be very important for a good bond. To make a semicore (two formed sheets plus wire), one of the cleaned pieces is placed in the steel holding frame of the vacuum forming machine. The polystyrene is brought to the forming temperature between 176 °C (350 °F) and 193 °C (380 °F), as it is kept at a distance of about 15cm (6 in.) away from the heating coil for some time, between 45 and 80

seconds, depending on the sheet's thickness. The heating time proved to be a very important control parameter in the reduction of the number of flaws during the forming operation, as illustrated in Figure 5-1.

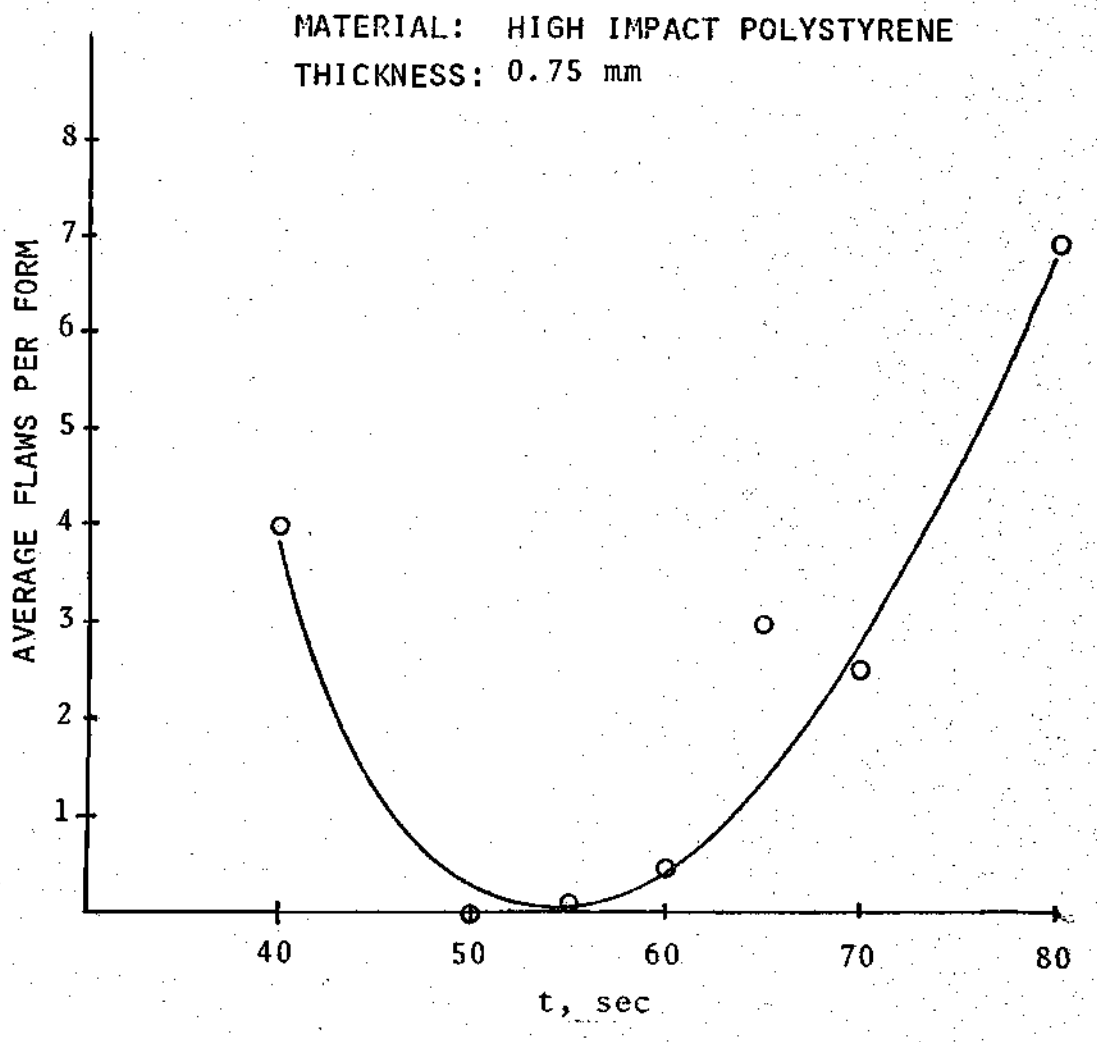

Figure 5-1. Number of Flaws per Vacuum Formed Sheet as a Function of Heating Time.

Once the sheet is heated up to the correct temperature, vacuum forming will take place, as illustrated in Figure 3-1, Chapter III. Some of the excess material is removed from the first formed sheet, so that a wire mesh can be placed on top of the form, as shown schematically in Figure 5-2.

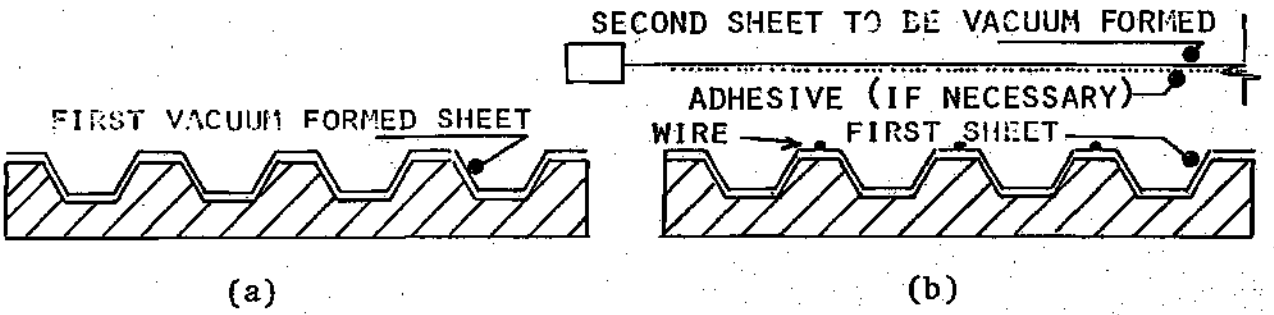

Figure 5-2. Core Forming.
(a) First Sheet is Vacuum Formed;
(b) Second Sheet With or Without Adhesive is Ready to be Formed.

The preliminary forms were made using 0.125mm (0.005 in.) plain carbon steel wires; but the idea was dropped in favor of Kevlar 49 which has a tensile strength of 1.3 MPa (500,000 lb/in^2), about twice the tensile strength of the steel wires. As the Kevlar comes in a yarn, it lies essentially flat on top of the projections and the height of all the webs will be approximately the same. The Kevlar also proved to be much better to work with and much

easier to cut than the steel wires. Nylon fibers were also tried. They could be easily cut; however, the diameter of the fiber, 0.3mm, was such that webs were formed at three different levels. Once the wire mesh is prepared, a series of 1mm holes, one every 30 cm^2 of core, is punched in the first form to ensure proper air evacuation as the second sheet is formed on top of the first one and the wire mesh. The two plastic sheets and the Kevlar can be bonded together if an adequate adhesive is sprayed on both sheets, as illustrated in Figure 5-2b. The adhesive must be such that it is not flammable and curing is not completed while the second sheet is being heated. Spray Adhesive 7 met the conditions specified hereto; however, its cohesive strength was not fully satisfactory. Keeping industrial production in mind, several attempts to heat weld the sheets during the second vacuum forming operation were made; however, the vacuum forming machine did not prove to have the capability to maintain the first form sufficiently hot without its losing shape.

Still another attempt to heat weld the two plastic sheets with the Kevlar embedded was made but only after vacuum forming. In this case the sheets were formed with no adhesive, they were placed in the furnace for a total of 6 minutes. For the first two minutes the sheets were heated inside the die which was kept at 176 °C (350 °F). The two sheets were then brought into intimate contact as a

pressure of 138 KPa (20 psi) was applied to the upper surface of the forms. The semicores bonded in this way proved to have superior mechanical properties than the adhesively bonded ones; however, as shown in Appendix C, some of these semicores had minor defects, in that the second sheet was not touching completely the first one at certain locations. They were thus not heat welded properly. In fact, the second forms were many times ruptured by the air pressure in the vicinity of a flaw. Thus the hot air escaped continuously, and the two sheets were separated and cooled down to a temperature below the heat welding range. For this reason it was felt that the sheets should be brought into intimate contact not by air pressure but by applying a force F at the bottom of the semicore. This, it was also felt might take place as the components are placed between the forming die and the heat welding fixture, as illustrated in Figure 5-3.

Depending on the test to be carried out, the semicores were bonded to 0.3mm (0.012 in.) 2024 T3 aluminum alloy sheet or to a 6mm steel plate. The surface of both the plastic and metals were prepared as specified in the Appendix D, following reference [20].

To complete the specimens, two sets of semicore-facing or semicore-loading plate were bonded together, as schematically shown in Figure 5-4.

Modified epoxy (1), toluene (2), and room temperature

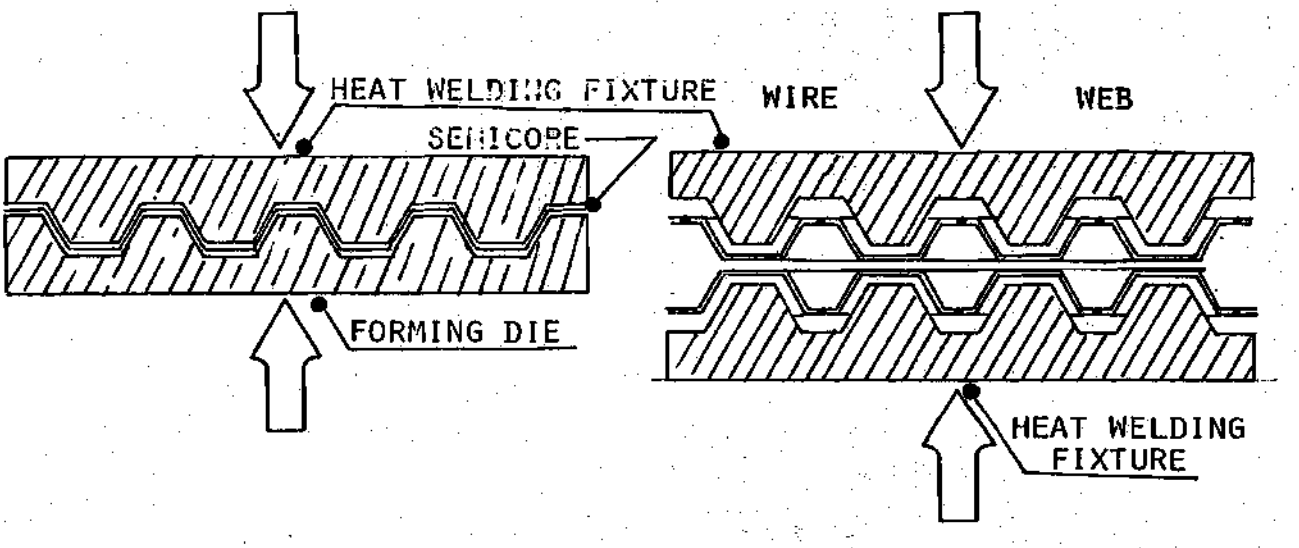

Figure 5-3. Heat Welding Steps.
(a) Heat Welding a Semicore; (b) Heat Welding a Core.

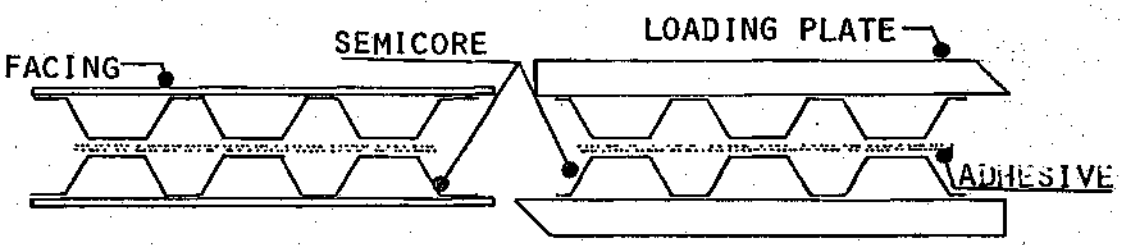

Figure 5-4. Core Bonding.
(a) Final Bonding of a Sandwich Specimen;
(b) Preparation of Core for Shear Testing.

curing epoxy (3) were tried for the last bonding operation, following industrial recommendations and reference [20]. The curing of the first adhesive, however, could not be fully attained because of the polystyrene cores would have been distorted by the end of the process, if a minimum temperature of 280 °F for 20 minutes as recommended for the curing would have been used. Toluene, the second adhesive, was very convenient to work with; however, as it had a liquid consistency and as the mating surfaces were not fully parallel, only a small percentage of the area was bonded. The third adhesive provided a good degree of filing, it was quite rigid with good cohesion, but was very fragile and gave poor adhesion.

Heat welding may be used to bond two semicores together using the fixture illustrated schematically in Figure 5-3b. This technique may prove to be rather convenient and may be of commercial value. The semicores would be placed on the fixture, inside the furnace at a temperature of 176 °C (350 °F). A force F would be applied by the furnace power screw. The welding should take place in a few seconds [21].

The Zn-22Al Wire Reinforced Honeycomb (WRH)

The metallic WRH were made from eutectoid superplastic Zn-22Al sheets having a thickness of either 0.075mm (0.003in) or 0.125mm, and an average size of 15cm x 20cm. The sheets

were cleaned with aliphatic naphtha and with acetone and dried out in the furnace. A first sheet is preheated for 5 minutes at 265 °C (520 °F) and then pressure formed, as described in Chapter III in the section describing the Pressure Forming Furnace. The time for the forming process to reach completion was a function of the applied pressure as illustrated in Figure 5-5.

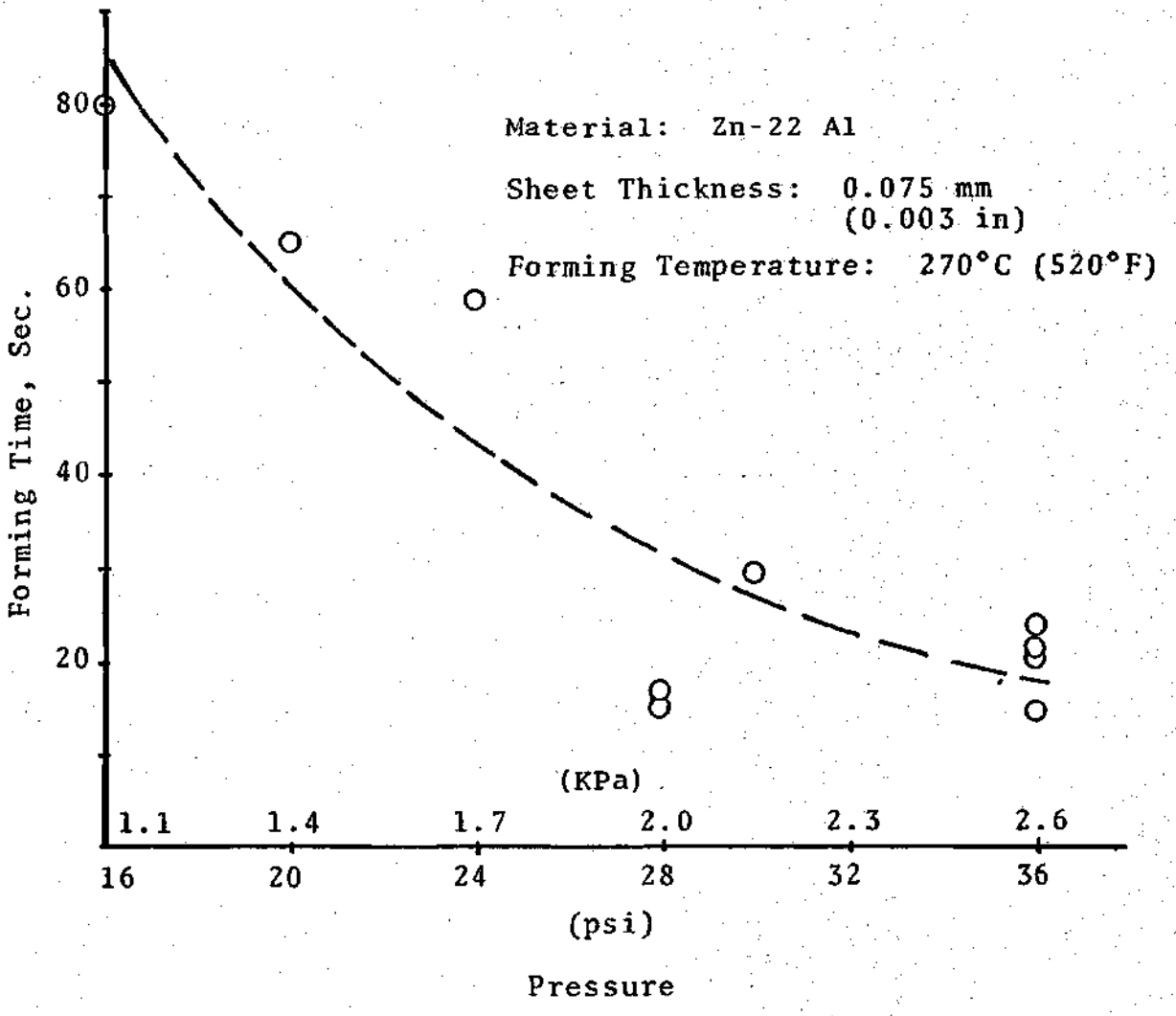

Figure 5-5. Forming Time vs. Applied Pressure in Core Forming.

As the first sheet is formed and removed from the die, the wire mesh is woven on the die boundary frame and on top of the first form. The frame is again put in the furnace for 10 minutes so that it is brought back to the forming temperature. In the meantime, a film of modified epoxy AFEPOXY 1, 0.075mm thick, is made to adhere to the second sheet to be formed. As the die is removed from the furnace, the evacuating holes are punched, the second sheet is placed on top of the wire mesh and the hot die is put back in the furnace in an average time of two minutes. The second sheet is heated for 5 minutes and pressure formed between 30-50 psi. The formation of the second sheet takes somewhat longer than the first one, as indicated in the tabulation given in Appendix C. This occurs since the second sheet has a larger thickness reduction. The combination of furnace temperature and forming time is such that the adhesive is fully cured at the end of the forming process. Some of the semicores were bonded to the facings or to the loading plates with AFEPOXY 2 which is a conventional structural adhesive used in sandwich construction. Some of the cores were treated to remove only the oil from the bonding surface, as it is the standard practice. In an attempt to improve the adhesive wetting action, some cores were etched slightly with the same solution used for the facings. Further details of the Zn-22Al sandwich core preparations are given in Appendix D.

The Shear Test

The shear test is a basic requirement in characterizing the behavior of a light weight structure, as the shear strength and the modulus of rigidity G_c of the core may be limiting factors in a particular loading situation. The relevant features of the loading apparatus were reported in Chapter III and illustrations of the apparatus appear in Figures 3-8 and 3-9. Both polystyrene and Zn-22Al cores were tested under shear. Tensile and compressive loading testing were conducted.

Figure 5-6 represents the behavior of the High Impact Polystyrene core subjected to shear under the action of a tensile load. The sheets were 0.508mm (0.020 in.) thick, and they were bonded with Spray Adhesive 7 during the vacuum forming process. Adhesive AFEPOXY 2, cured for 10 minutes at 138 °C (280 °F) was used to bond the core to itself and to the loading plates. After several attempts, it was determined that 10 minutes was the longest possible time the adhesive could be cured without the core losing its shape. The maximum load supported by the structure was 8,900 N (2,000 lbs). The cross section under shear was 124 cm^2 (3.5 in. x 5.5 in.). The failure mode of the specimen was cohesive failure of the AFEPOXY 2 adhesive at the core-loading plate interface. There was a considerable amount of sliding at the bonded areas and some sliding at the grips. Considering that there are four sheets per core,

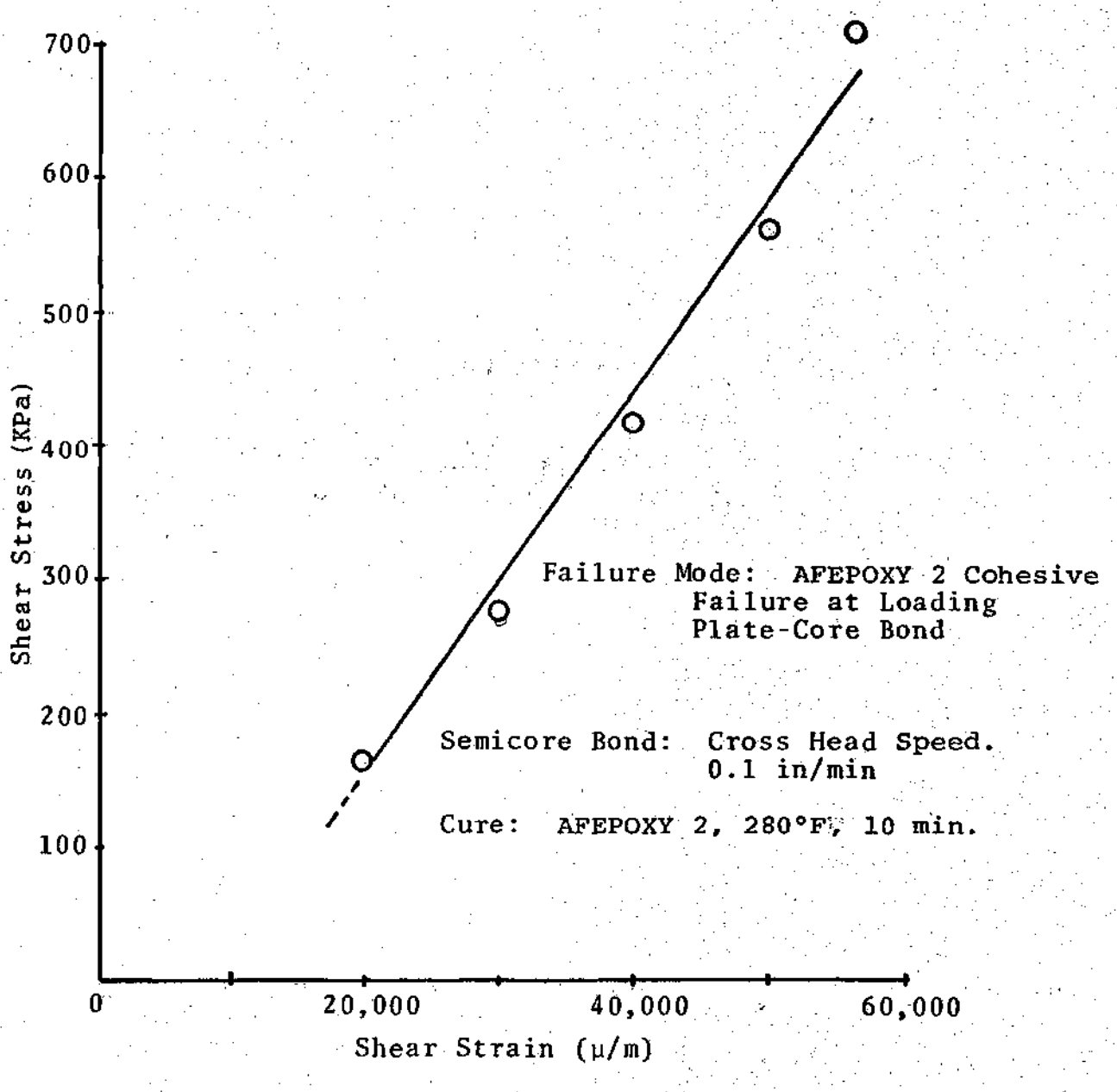

Figure 5-6. Shear Stress vs. Shear Strain of a Sandwich with a WRH Polystyrene Core.

the density of the core can be estimated as

$$\text{Density} = \frac{4\rho t\cancel{A}}{c\cancel{A}} \qquad (5\text{-}1)$$

where ρ is the plastic density = 0.768 gr/cm^3; (61.2 lb/ft^3)

t is the sheet thickness, and

c is the core height = 12.7mm (0.5 in.)

thus Density = 0.123 gr/cm^3 = (9.8 lbs/ft^3)

The apparent shear strength of the core can be taken from Figure 5-6 as 700 KPa (102 lb/in^2), and the ratio of shear strength in (lb/in^2) to density in (lbs/ft^3) is about 10.0; however, since the failure happened to be in the adhesive, it can be inferred that the core is capable of supporting higher loads.

For the subsequent experiments, the bonding procedure was modified. The semicores were bonded together with toluene and again AFEPOXY 2, at 138 °C (280 °F) and a 10 minute cure, was used for bonding the loading plates to the core. The specimens were tested in shear under a compressive load, and the results are illustrated in Figure 5-7.

The cross head velocity was 1.27 mm/min (0.05 in/min). Again the adhesive AFEPOXY 2 had a cohesive failure, but at a lower stress level than in the previous cases. Also, as the mating surfaces of the semicore were not completely parallel, only about 15% of the surface was actually bonded by the toluene. As a consistent failure of the adhesive was taking place, a decision was made to use room temperature

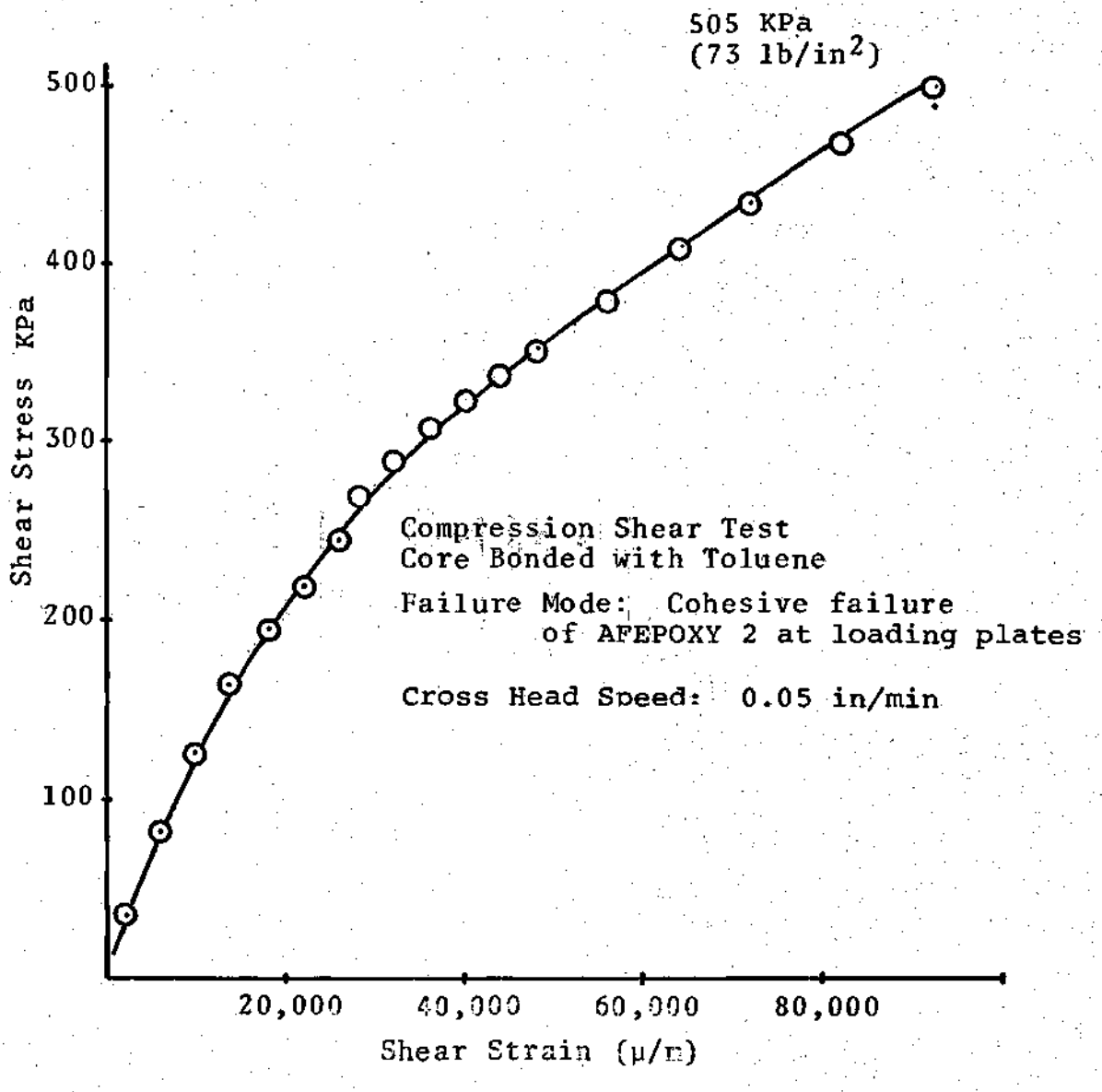

Figure 5-7. Shear Stress vs. Shear Strain of Sandwich with WRH Polystyrene Core.

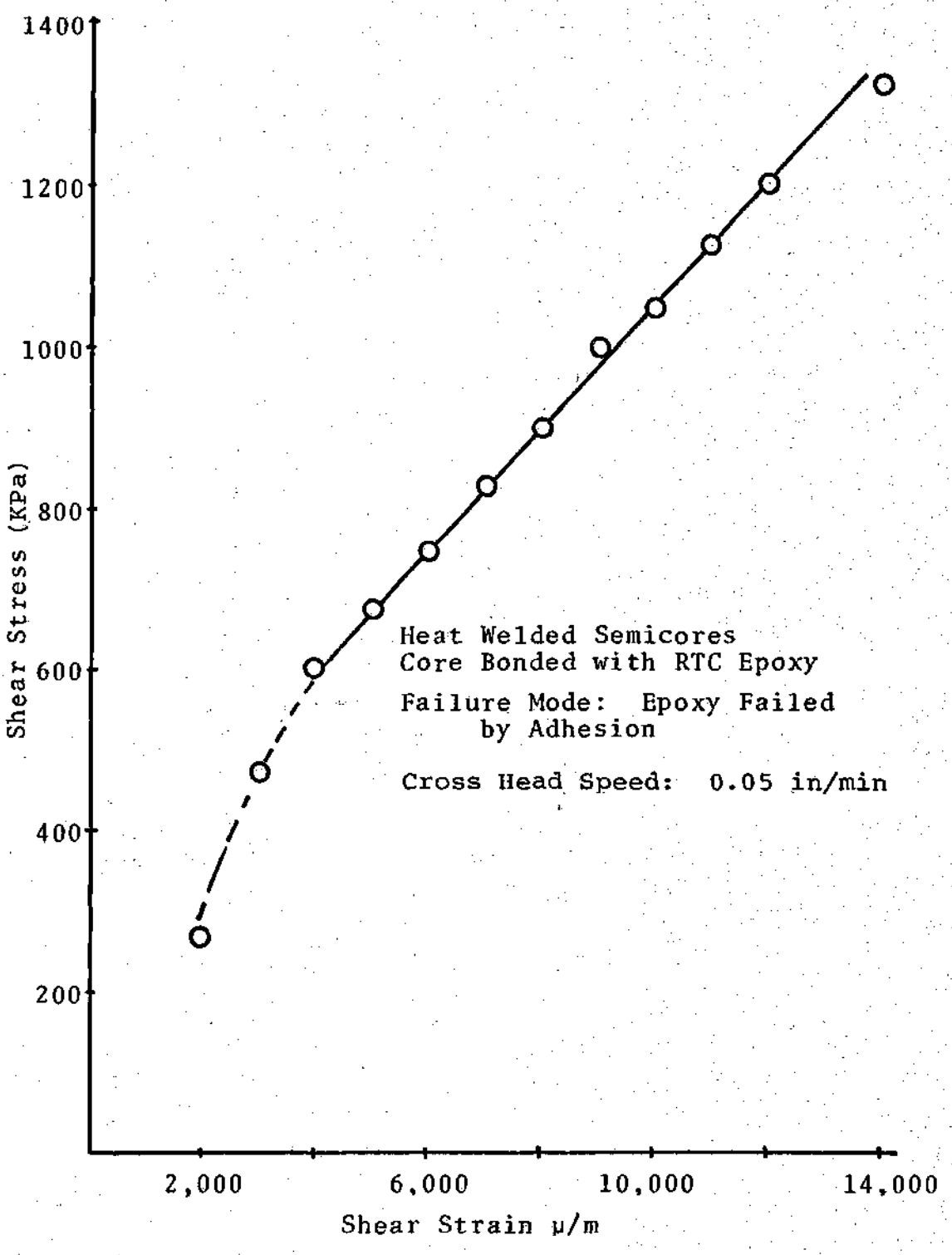

Figure 5-8. Shear Stress vs. Shear Strain of a Sandwich with a WRH Polystyrene Core.

curing epoxy to bond the semicores together and the loading plates. The results are presented in Figure 5-8. The crosshead movement was 1.27 mm/min (0.05 in/min). The two 0.76mm thick sheets that form the semicore were bonded together not with adhesive but by heat welding during 6 minutes at 176 °C and a pressure of 138 KPa (20 psi). There is a marked improvement in both the shear strength and the rigidity of the core prepared as mentioned above, as they are compared against the results of the previous experiments. A tensile shear strength of 1400 KPa (206 lb/in^2) was obtained. This represents a shear strength (lb/in^2) to density ratio (lb/ft^3) of 14.0. But once again the adhesive joining the semicores together failed. However, the heat welded semicores exhibit much higher strength than those bonded with Spray Adhesive 7 with the significant economic advantage that no adhesive is used in the manufacturing of the core. To further improve the mechanical properties of the Polystyrene WRH core, in relation to the heat welded semicore, it is evident that attempts should also be made to heat weld the core-core interface. For this reason, a die has been designed and construction is in progress. The basic components of this die are two slotted heat welding elements, as illustrated in Figure 5-9, which are fastened by bolts to the base plates. The die is heated in the furnace at 176 °C (350 °F), then a vacuum formed semicore is placed on each slotted element. The semicores are

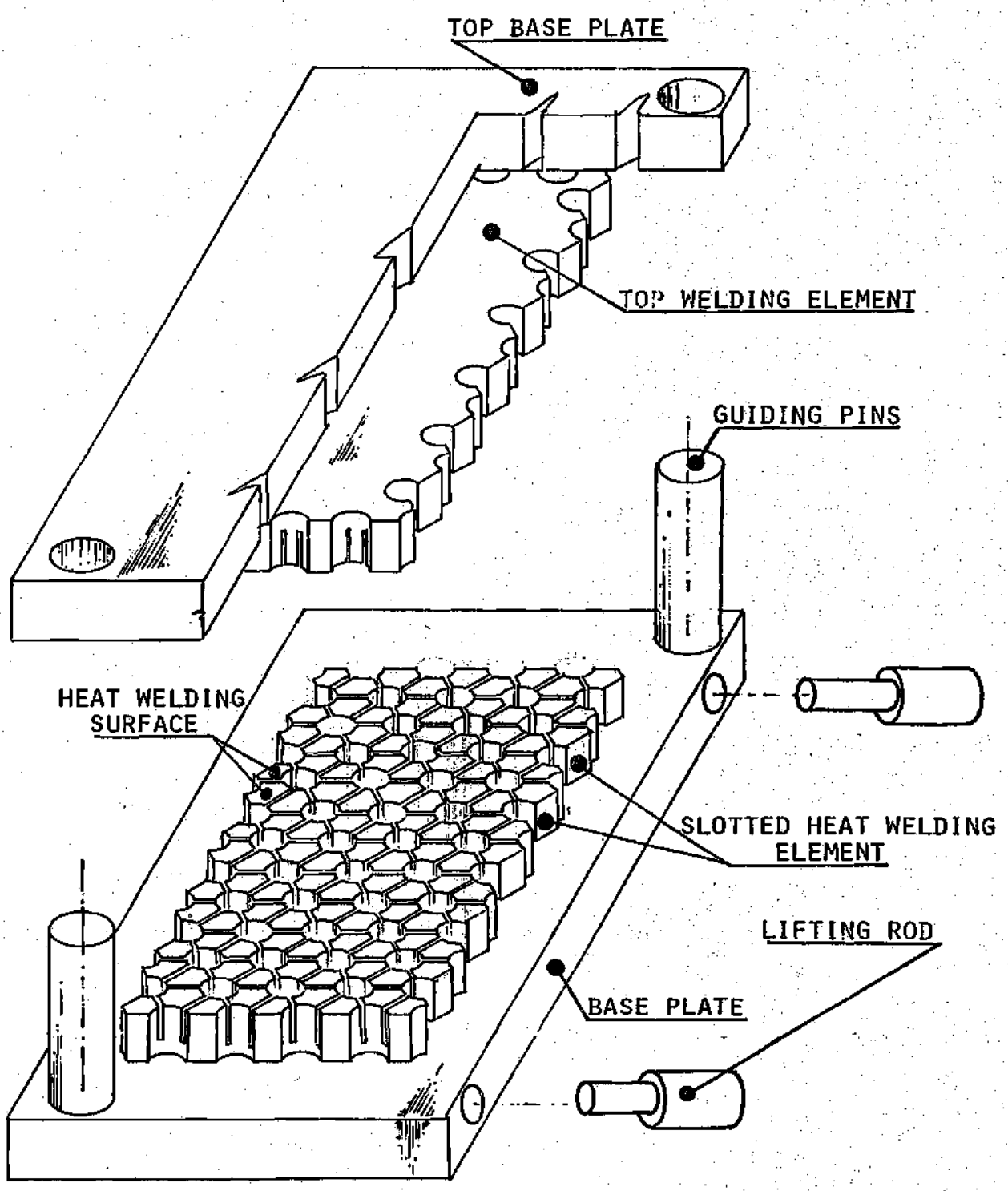

Figure 5-9. Heat Welding Die

brought closer together as the top base plates slide over the guiding pins. The semicores are kept under pressure for an appropriate time by the action of the mechanical press inside the furnace. The die is removed from the furnace and the semicores are quickly taken out as steel lifting rods with plastic handles are inserted in the base plates.

Turning to the tests concerning the Zn-22Al cores, Figure 5-10 illustrates the results of shear test of such a core under tensile load. The adhesive AFEPOXY 2 was cured at 121 °C (250 °F) for one hour as suggested by the manufacturer. The load was applied with a cross head velocity of 5.08 mm/min (0.2 in/min). The AFEPOXY 2 adhesive had a cohesive failure, and there was a very large slippage between the loading plates and the semicores, as can be observed in the Figure 5-10. The core did not really fail; only there was a sign of plastic deformation at the lower border of the core and this was due to stress concentration at the very end of the testing process. The shear strength and the modulus of rigidity computed from Figure 5-10 could not be very significant because of the excessive strain at the bonding lines which is irrelevant to the deformation of the core itself. Figures 5-11 and 5-12 represent typical tensile shear test curves for the Zn-22Al core and for heat welded polystyrene cores.

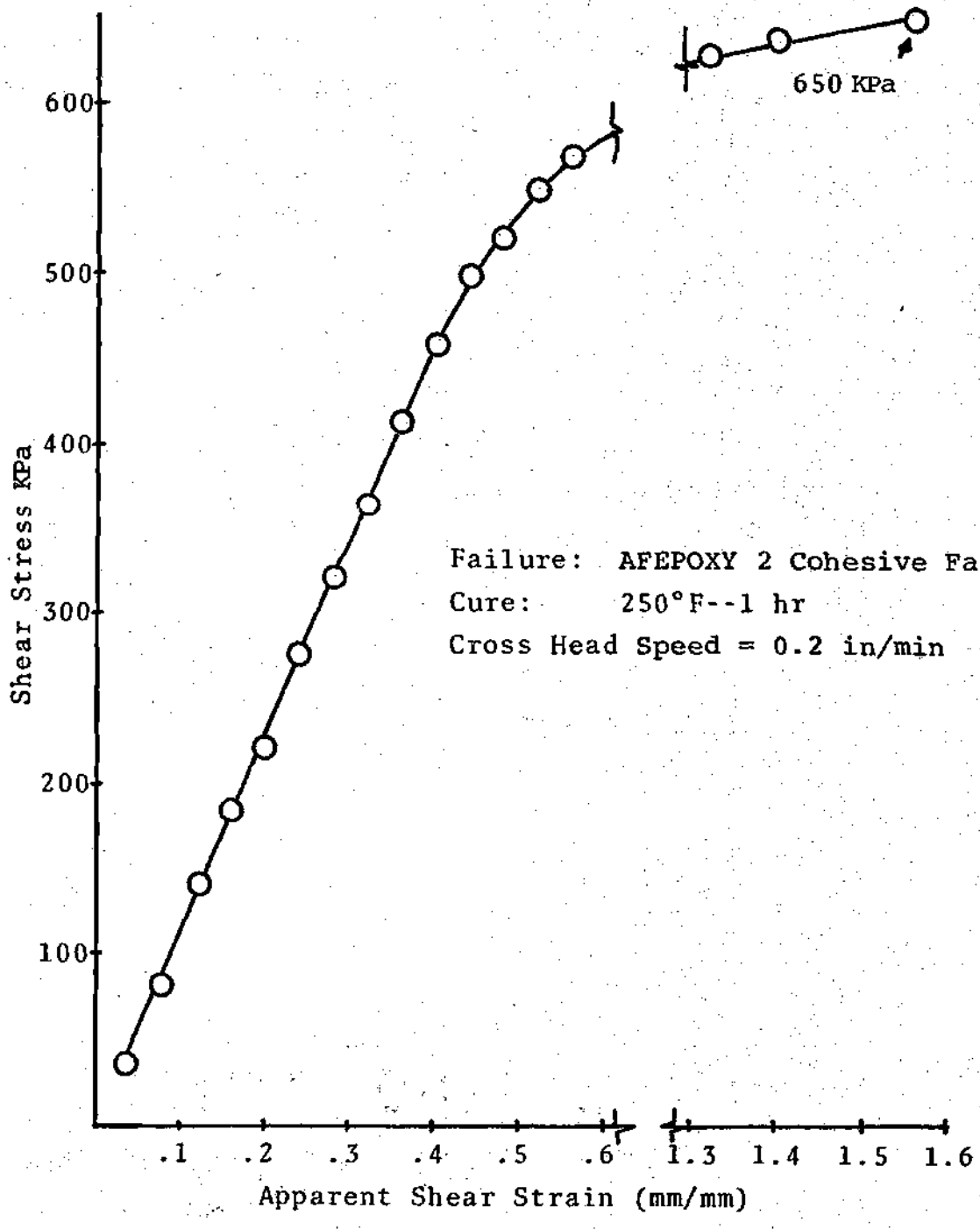

Figure 5-10. Shear Stress vs. Apparent Shear Strain of a Sandwich with a WRH Zn-22Al Core.

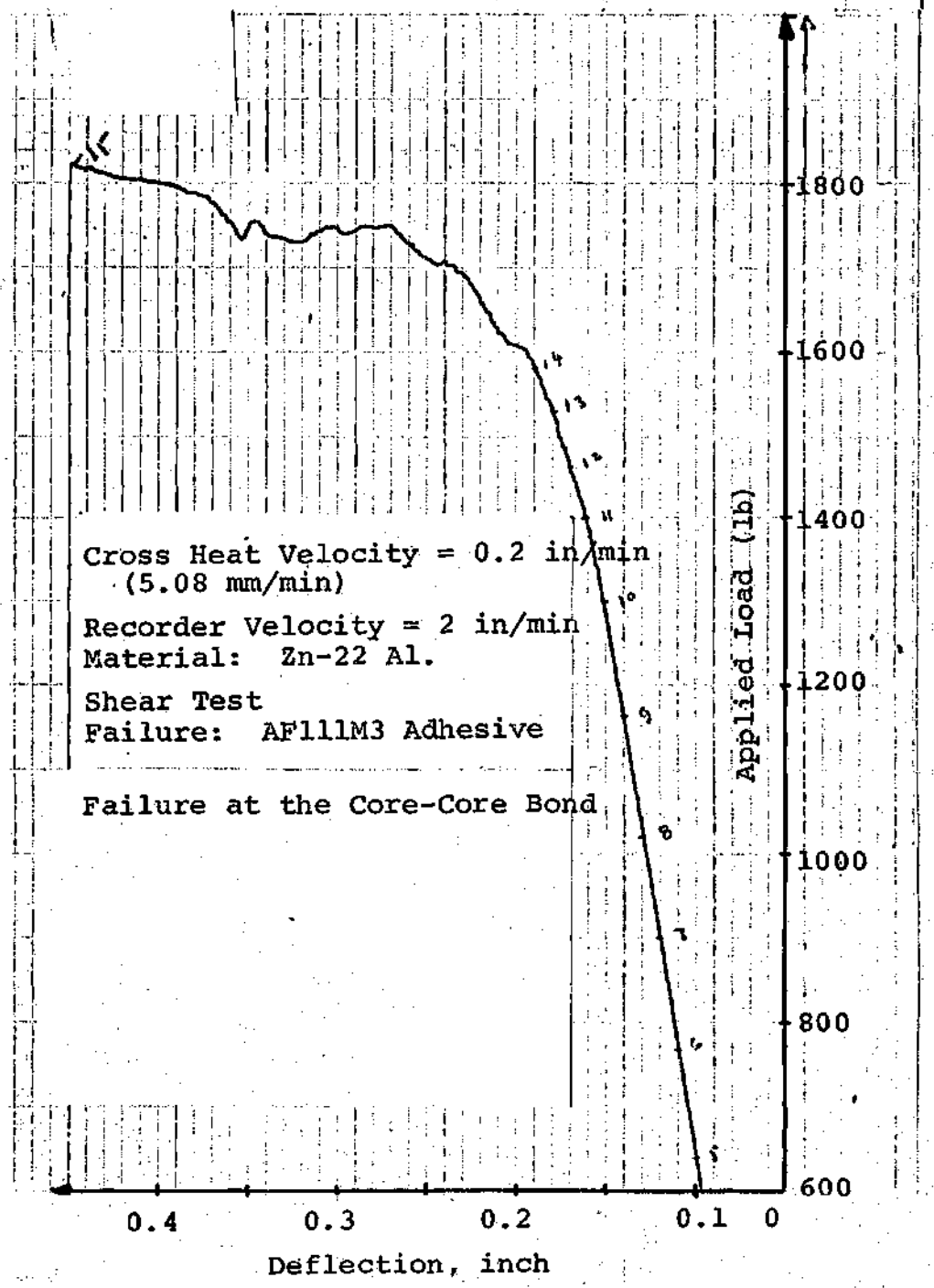

Figure 5-11. Upper Portion of a Tensile Shear Tests in a Sandwich with WRH Zn-22Al Core.

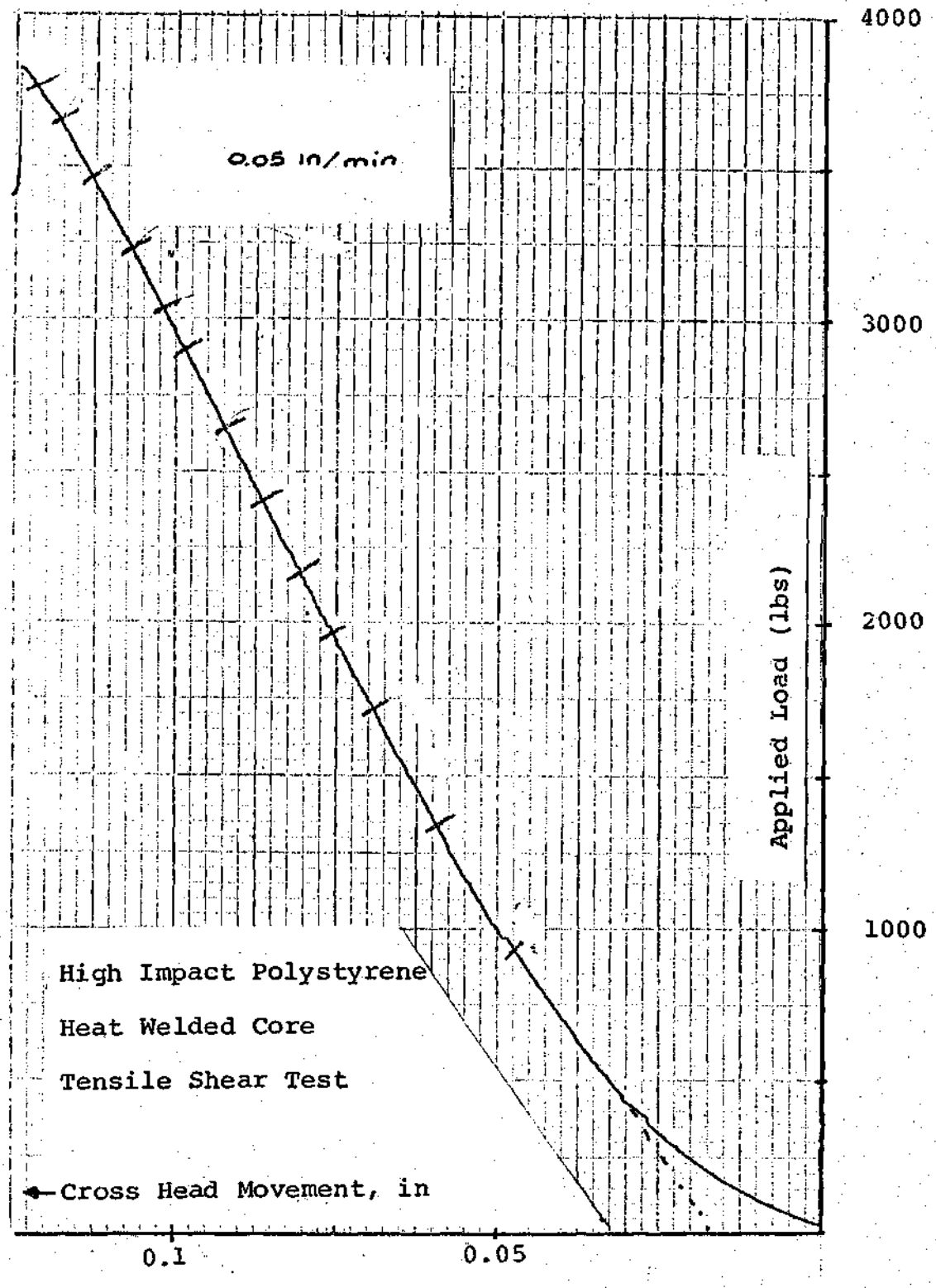

Figure 5-12. Typical Tensile Shear Test

Heat Welding Variables

In the process of manufacturing the heat welded plastic cores, it was necessary to determine for how long and at what temperature the semicores should be heated. For this purpose a series of flat specimens about 166mm x 25.4m (6.5 in. x 1 in.) were heated in the furnace in a temperature range between 94 °C (200 °F) and 176 °C (350 °F), at a pressure of 1.4 KPa (20 psi), for different time intervals. The specimens that were heated between 94 °C and 149 °C did not heat weld even after 20 minutes of heating. However, the specimens that were heated at 163 °C and 176 °C were bonded in less than two minutes. The specimens were cleaned with isopropyl alcohol, but some were cleaned and intentionally covered with a very thin film of oil. These oily specimens did not bond at all, indicating quite clearly that surface cleaning for heat welding is a mandatory requirement. A preliminary set of specimens was prepared and samples subjected to tension testing. It was seen that failure in the cross section occurred, indicating that the bond was stronger than the base material, see Figure 5-13a. This problem was solved by increasing the cross sectional area of the specimens and reducing the shear bonding area, as indicated in Figure 5-13b. The results of the new tests are presented in Figure 5-14 for 163 °C and in Figure 5-15 for 176 °C. It was observed in both cases that if the specimens were left too long in the furnace, the shear

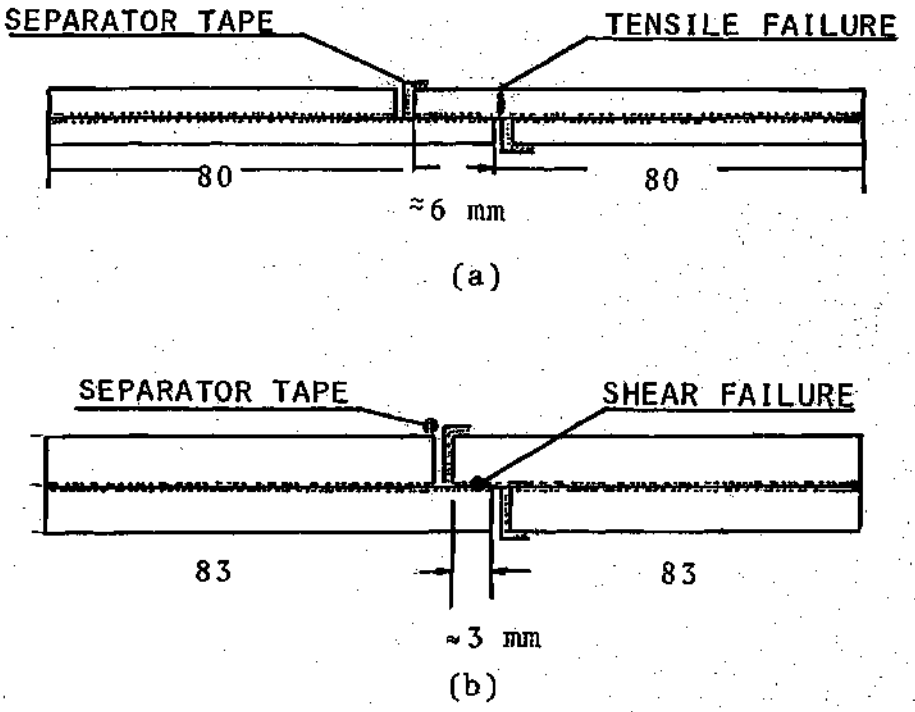

Figure 5-13. Heat Welded Specimens.
(a) Flat Heat Welded Specimen Having a Tensile
(b) Shear Failure on the Heat Welded Zone.

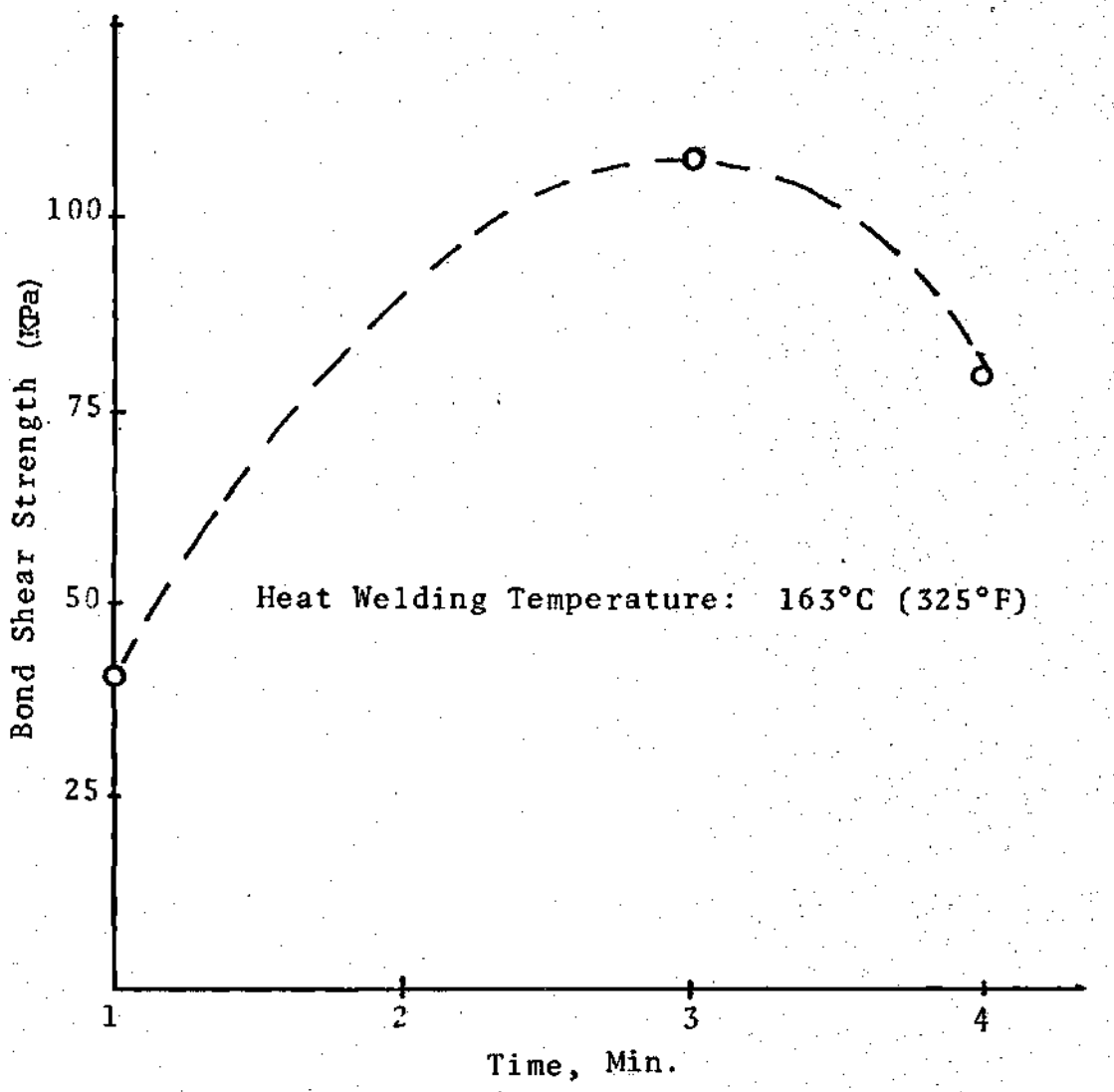

Figure 5-14. Bond Shear Strength vs. Heat Welding Time.

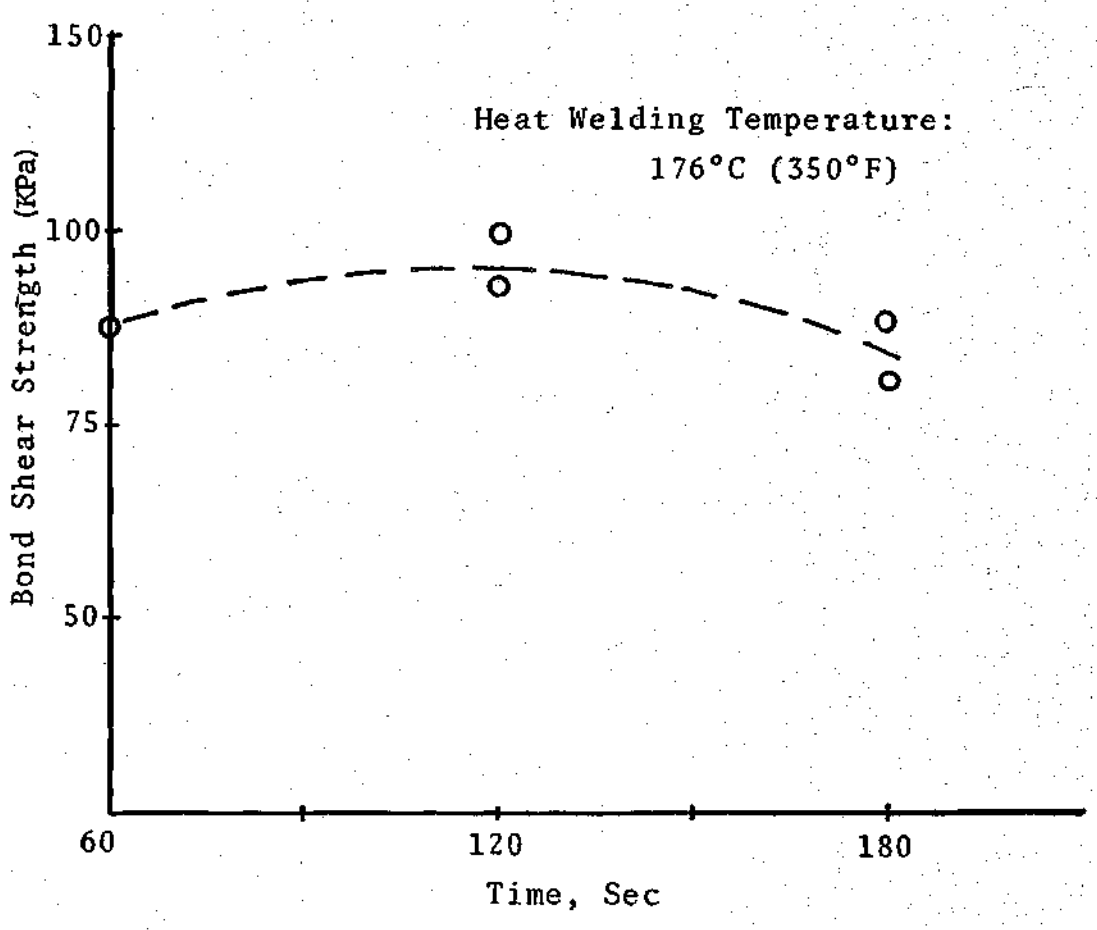

Figure 5-15. Shear Strength of Bond vs. Heat Welding Time.

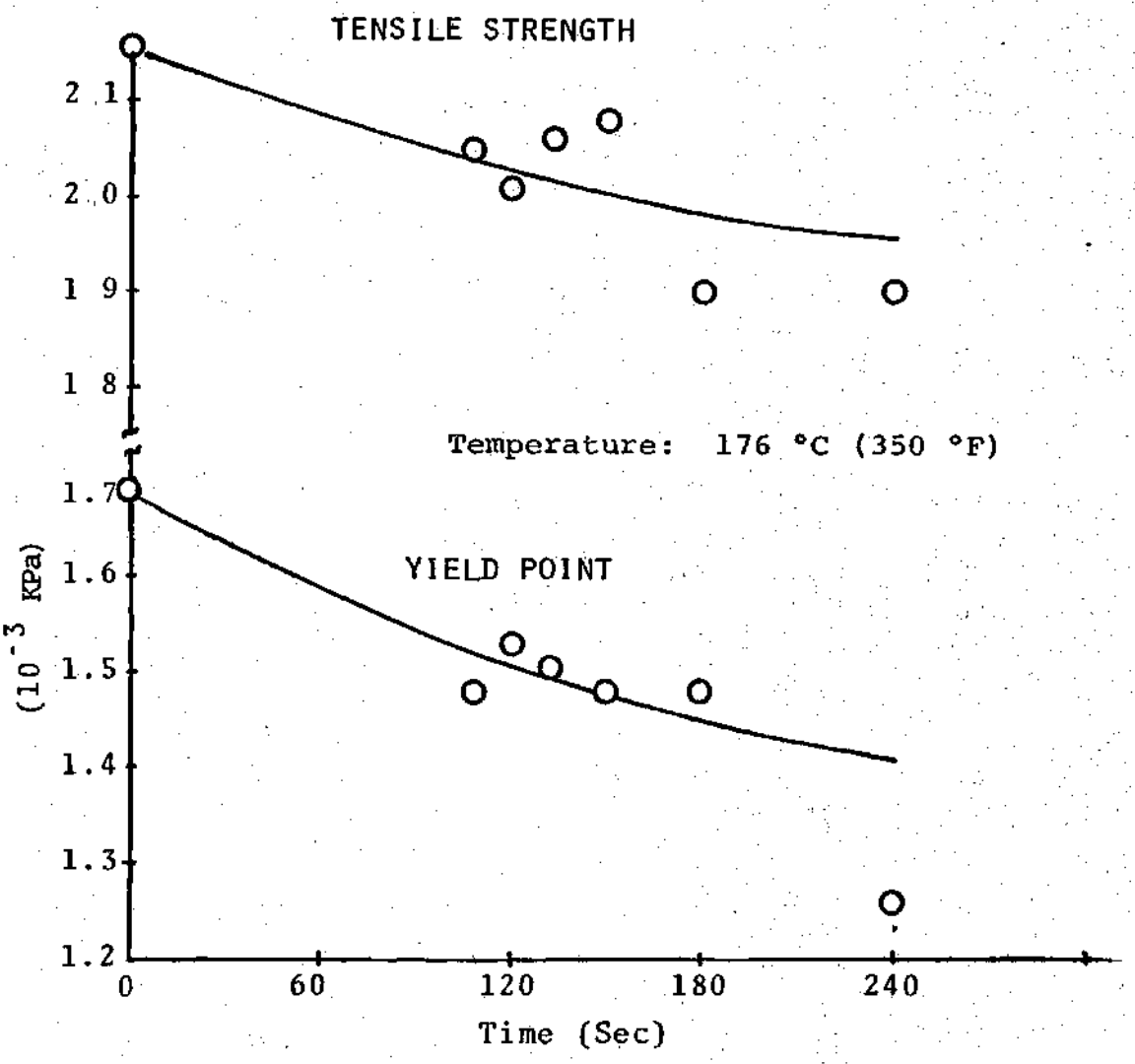

Figure 5-16. Tensile Strength and Yield Point of High Impact Polystyrene as a Function of Heating Time.

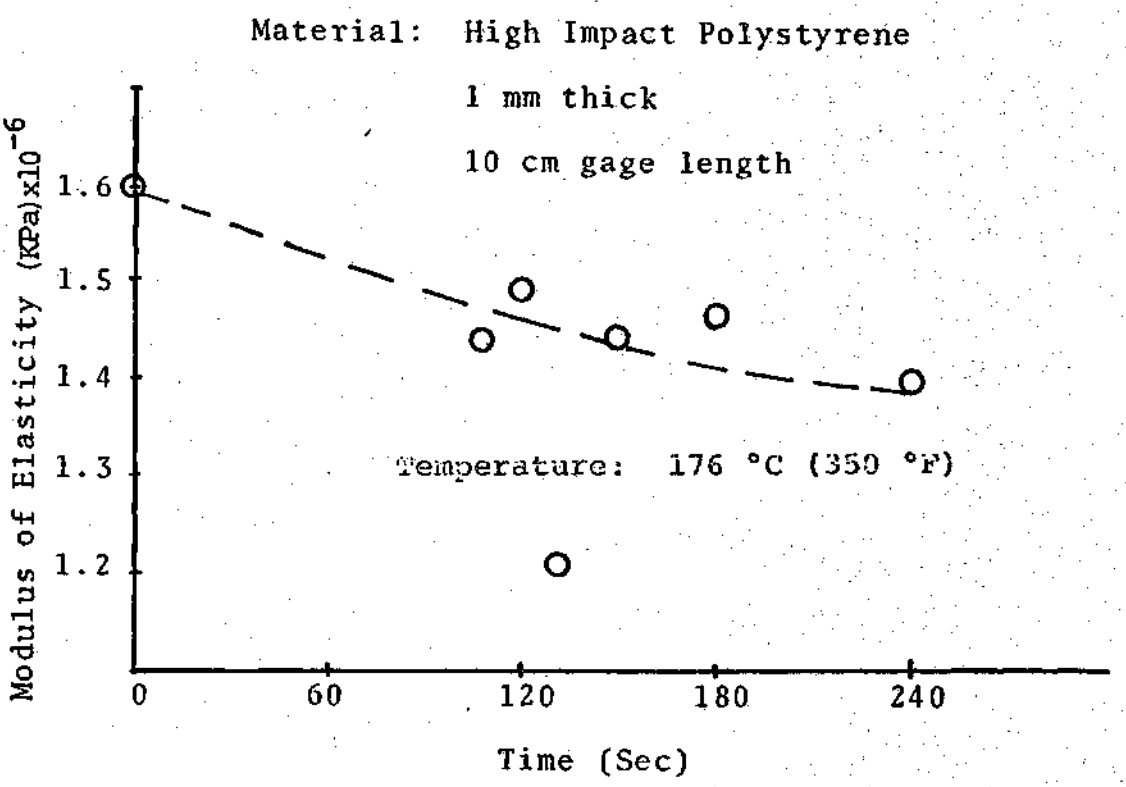

Figure 5-17. Modulus of Elasticity of High Impact Polystyrene as a Function of Heating Time.

strength of the bond had a tendency to diminish. To corroborate this phenomenon, a series of tensile test specimens were prepared, 10cm gage length 1mm thick, and about 12.5mm in width. The specimens were heated in the furnace at 163 °C (325 °F) for different time intervals. It was found that the tensile strength, the yield point, and the modulus of elasticity of the high impact polystyrene dropped continuously as a function of heating time, as illustrated in Figures 5-16 and 5-17. It may be inferred from these tensile tests that the reason why the heat welding shear strength dropped if the specimens were for too long in the furnace may be linked to material degradation effects as a result of annealing.

The Four Point Bending Test

The behavior of a beam subjected to pure bending gives an indication of the elastic modulus of the core in the L direction. The bending apparatus was described in Chapter III. The load was applied as indicated in Figure 5-18.

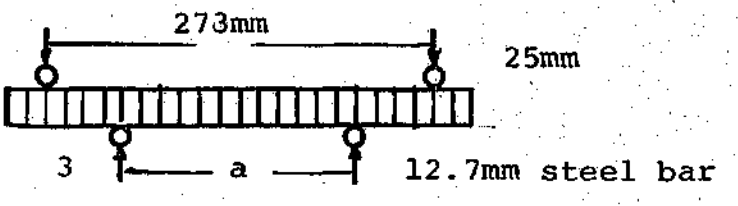

Figure 5-18. Four Point Bending Test.

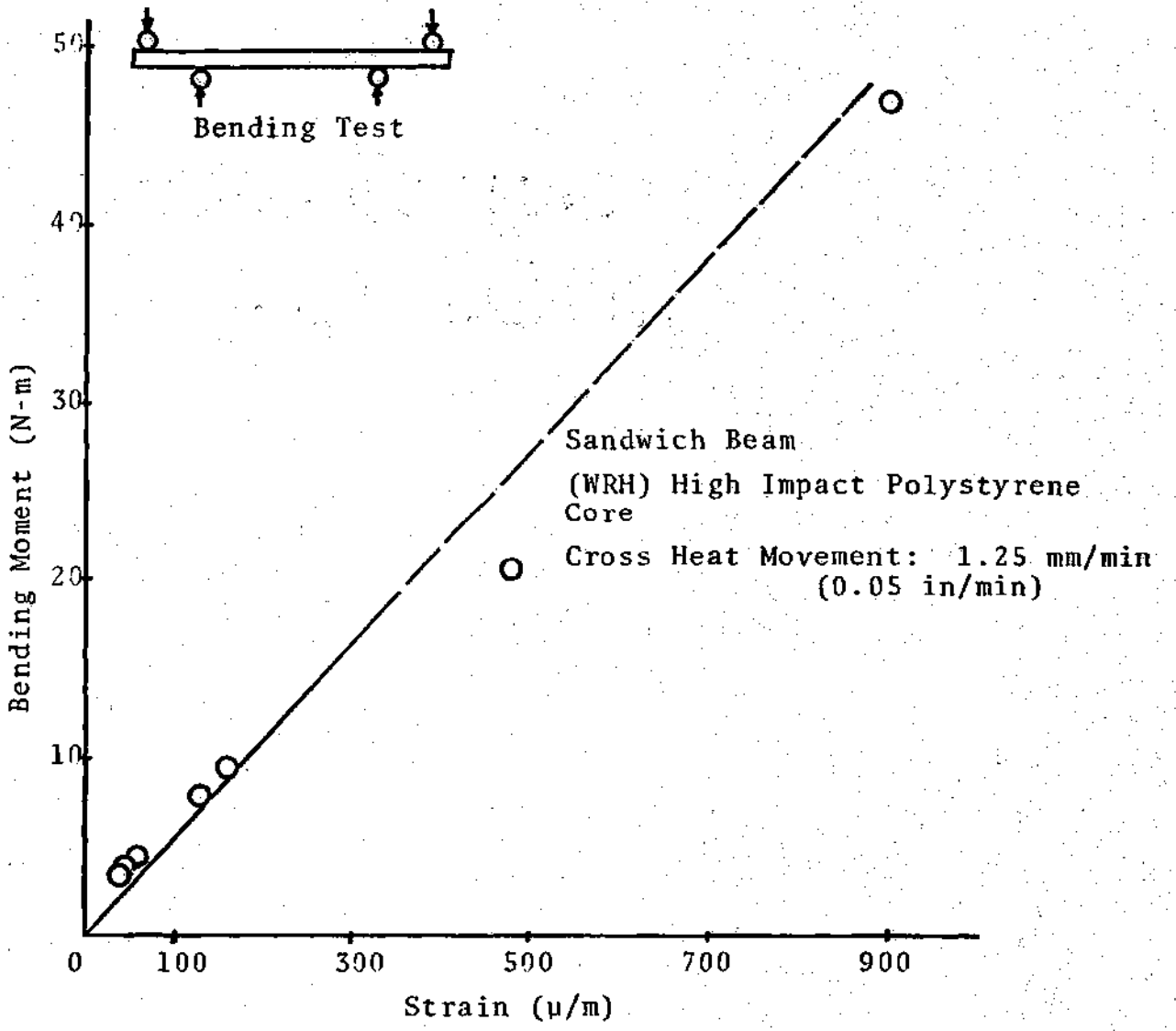

Figure 5-19. Sandwich Beam Behavior Under Pure Bending

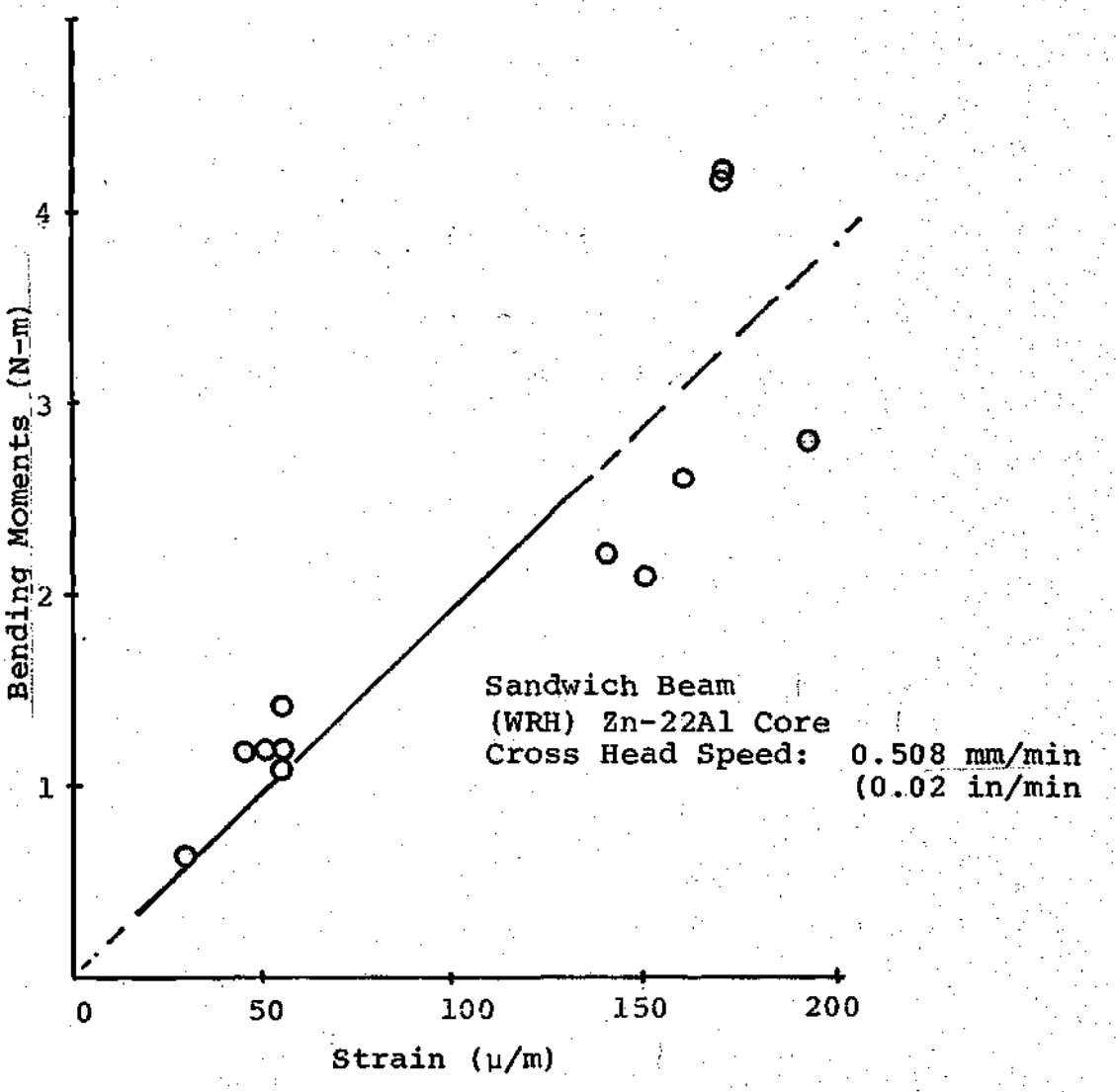

Figure 5-20. Sandwich Beam Behavior Under Pure Bending.

The distance "a" was varied from test to test. The beams were made by bonding two sandwiches with RTC Epoxy. Strain gages were mounted in the central portion of the top facing. The Zn-22Al cores were bonded to the facing with AFEPOXY 2 and plastic cores were bonded with RTC Epoxy. The Zn-22Al cores were tested at a cross head velocity of 0.508 mm/min (0.02 in/min) and the plastic cores were tested at 1.25 mm/min (0.05 in/min). The loading bars at the top of the beam were separated a fixed distance of 273mm (10.75 in) and each bar was about 44mm (1.75 in) from the free ends, according to ASTM Specifications. The beams were 89mm wide (3.5 in). To reduce stress concentration, the loading bars were covered with a double coated adhesive foam, 0.80mm thick (1/32 in). Figures 5-19 and 5-20 are the test results for High Impact Polystyrene cores and Zn-22Al core respectively. The flexural rigidity D of the core can be determined by combining Eq. 4-109 and the results in Figures 5-19 and 5-20. The height c for the Zn-22Al core is 7mm (.276 in) and for the polystyrene core is 12.7mm. The facing thickness is 0.305mm (0.012 in) and its modulus E is 6.9×10^7 KPa (10^7 psi). Eq. 4-109 can be written as $D = Z\ \Delta M/\Delta\varepsilon$, where $Z = c + t$ and $\Delta M/\Delta\varepsilon$ can be taken from Figure 5-19 or 5-20. Computing the value of D, it is found that

$$D_{poly} = 295 \text{ N-m}^2 \; ; \quad (10^5 \text{ lb/in}^2)$$

$$D_{Zn-22Al} = 61 \text{ N-m}^2 \; ; \quad (21{,}000 \text{ lb/in}^2)$$

Using Eq. 4-110, the modulus E_c of the cores are computed as

$$E_c(\text{Poly}) = 6.89 \times 10^6 \text{ KPa}; \; (10^6 \text{ lb/in}^2)$$

$$E_c(\text{Zn-22Al}) = 4.35 \times 10^6 \text{ KPa}; \; (630{,}000 \text{ lb/in}^2)$$

The Two Edge Simply Supported Buckling Test

The behavior of a simply supported sandwich under compression, loaded as indicated in Figure 5-21, is a function of the modulus of rigidity of the core. For this reason, a series of light beams with a Zn-22Al core were tested under buckling.

Figure 5-21. Two Edge Simply Supported Buckling Test.

The experimental apparatus was described in Chapter III. The Zn-22Al sandwich beams were prepared using

adhesive AFEPOXY 2. To avoid major stress concentrations, the loading ends of the sandwich were filled with RTC Epoxy and covered with a double coated adhesive foam. One strain gage was mounted on the center of each side of the sandwich, not only to record the deformation, but also to help in the alignment of the sandwich, i.e., to even load the facings. The average strain recorded by the two strain gages at the beginning of the test may be used to determined the modulus of elasticity of the core in the direction of the load. The test results are given in Figure 5-22. The even distribution of the load turned out to be somewhat difficult. In all cases a buckling failure took place as a result of the adhesive failure. The maximum load P that can be carried by the beam is related to G as follows [15].

$$1/P = 1/P_E + 1/AG \qquad (5\text{-}2)$$

where P_E is the load that could be carried by the sandwich assuming infinite shear modulus and is given by

$$P_E = \frac{2_D}{L} = \frac{2}{L^2} E_f \, bt \, \frac{d^2}{2}$$

Also, A in Eq. 5-2 is given by

$$A = d^2 b/c$$

The tests variables have the following average values

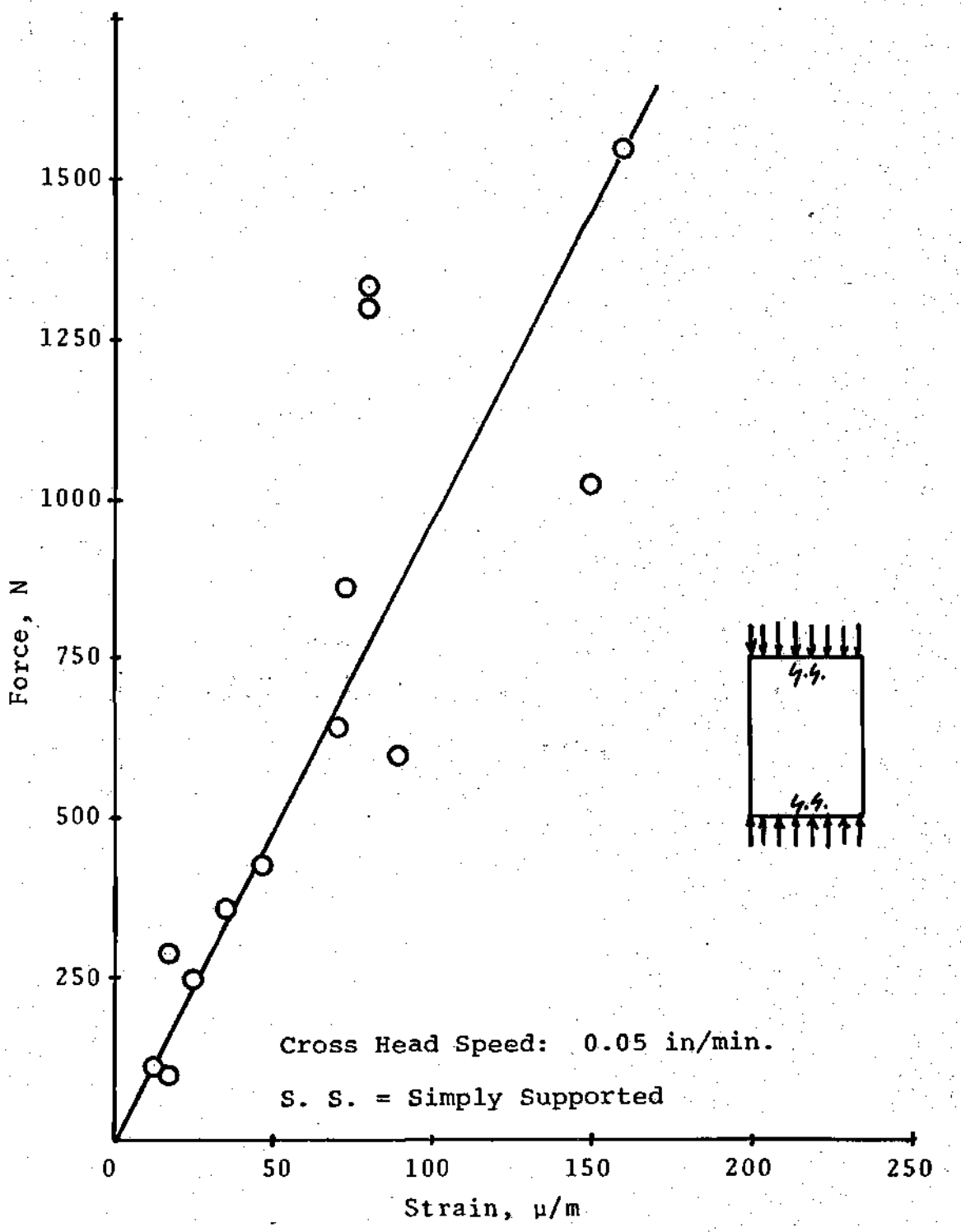

Figure 5-22. Buckling Force vs. Strain in a Sandwich Beam with a WRH Zn-22Al Core.

$E_f = 6.80 \times 10^7$ KPa (107 psi)

b = 0.080 m (3.5 in)

t = 0.0003 m (0.012 in)

d = 0.0073 m (0.288 in)

c = 0.007 m (0.276 in)

L = 0.1397 m (5.5 in)

P = 3830 n (860 lbs)

Replacing these values in Eq. 5-2, it is found that the core shear modulus is:

$$G_{c(Zn-22Al)} = 6760 \text{ KPa}, \quad (980 \text{ lb/in}^2)$$

The Four Edge Simply Supported Buckling Test

As the two edge simply supported buckling test proved to be difficult to align, which is in agreement with reference [16], p. 157, it was thought that a better way to determine the core G and E modulus could be by performing the four edge simply supported test. The modulus G is related to the maximum compressive load N_x per unit width, as shown in Eq. 4-70, and the modulus E can be computed from the force-average strain relation. The sandwiches were supported on both facings along two vertical lines 8.9cm (3.5 in) apart and along two horizontal lines 14cm (5.5 in) apart. They were supported in such a way that they were free to move in the vertical and horizontal direction under the sole action of the compressive load. The polystyrene

core was bonded with toluene at its mid plane and bonded with RTC Epoxy to the facings. Strain gages were mounted at the center of each facing. The loading ends were prepared with epoxy and covered with double coated polyurethane foam to reduce stress concentration. The results are given in Figure 5-23 for the Zn-22Al core and in Figure 5-24 for the polystyrene. The balance of forces in the direction of the applied load furnishes the relation below from which E_c can be computed directly,

$$\Delta P = \Delta\varepsilon(E_f A_f + E_c A_c) \qquad (5\text{-}3)$$

where ΔP and $\Delta\varepsilon$ can be taken from the Figure 5-23 and Figure 5-24, and A_f and A_c are the cross section of the facing, and the core. Using Eq. 5-3 and considering that the height of the Zn-22Al and the polystyrene cores are 6.3mm (0.250 in) and 12.7mm (0.5 in), it is found that

$$E_{c(Zn\text{-}22Al)} = 2.27 \times 10^6 \text{ KPa} = (330{,}000 \text{ lb/in}^2)$$

$$E_{c(poly)} = .793 \times 10^6 \text{ KPa} = (115{,}000 \text{ lb/in}^2)$$

The failure mode in all cases was the same. The cores were not affected apparently by the load; but the facings appeared to fail by wrinkling which results from a combined effect of the compressible load P and the normal stresses acting on the facings as a reaction by the core, as shown in Figure 5-25 [15].

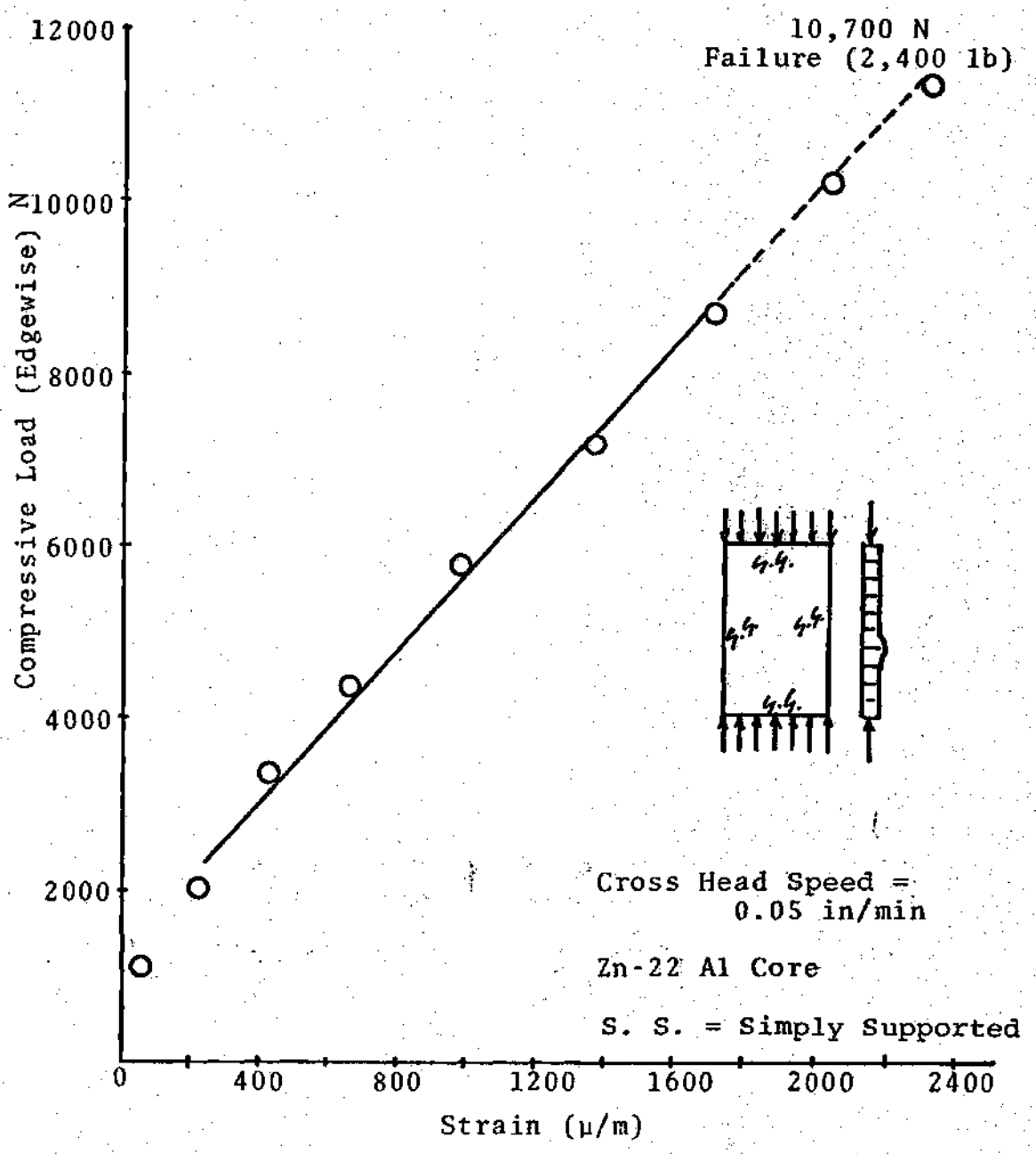

Figure 5-23a. Simply Supported Sandwich Beam Loaded Edgewise.

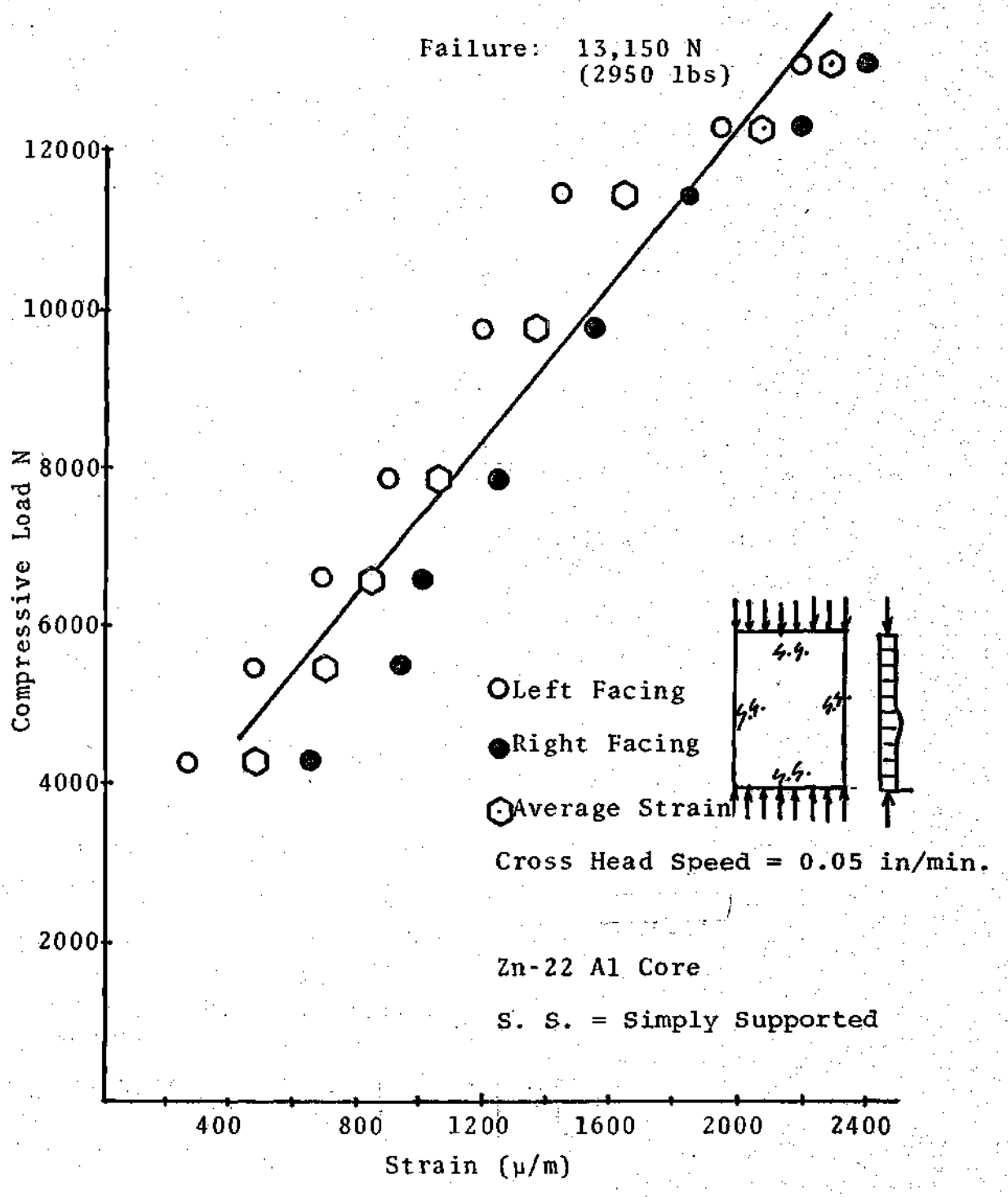

Figure 5-23b. Four Edge Simply Supported Sandwich Beam Loaded Edgewise.

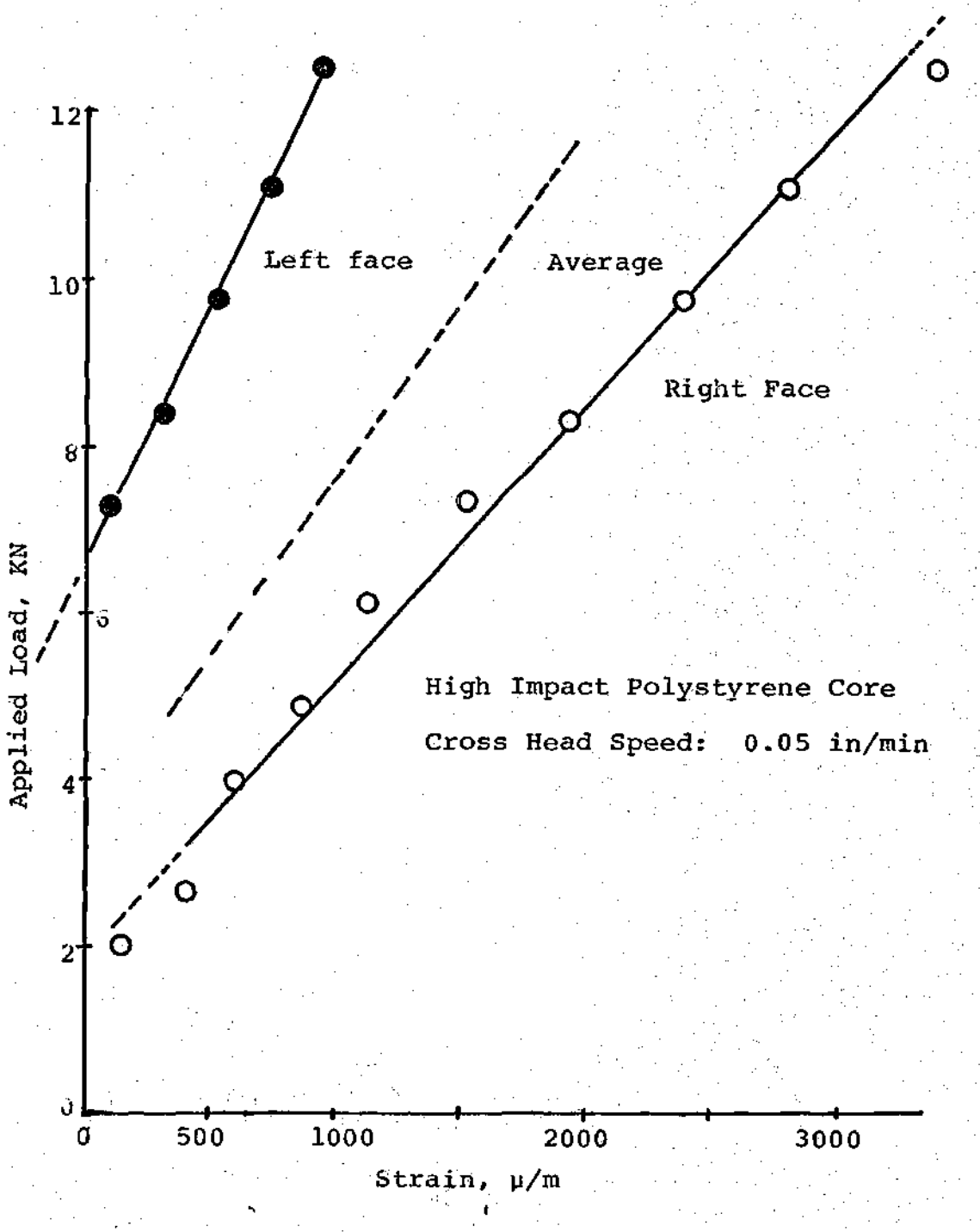

Figure 5-24. Four Edge Simply Supported Buckling Test Loading Edgewise for HIP Core.

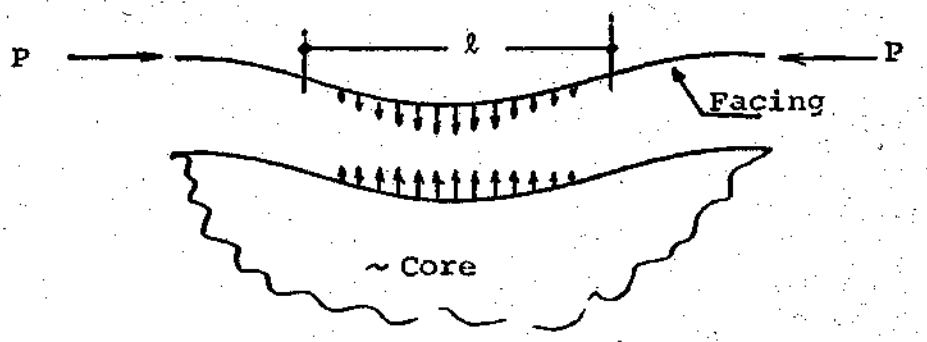

Figure 5-25. Wrinkling of a Sandwich Testing Under Compressive Load.

The relation between P, D, E_c is given by Allen as

$$\frac{P\pi^2}{\ell^2} = \frac{D\pi^4}{\ell^4} = ab/\ell \qquad (5\text{-}4)$$

where $a = 2\pi E_c/(3-\nu_c)(1+\nu_c)$

and $D = E_f bt3/12$

However, considering that the average ℓ for the Zn-22Al core was about 18 mm (0.7 in) and for the polystyrene core was 25.4mm (1.0 in), and taking the failure loads given in Figures 5-23 and 5-24, the values of E_c are estimated as

$$E_{c(Zn\text{-}22Al)} = 34,500 \text{ KPa} = (5,000 \text{ lb/in}^2)$$

$$E_{c(poly)} = 28,000 \text{ KPa} = (4,000 \text{ lb/in}^2)$$

As these later values of E_c are no where near to the former values which were determined in a direct manner, it

can be reasonably assumed that the failure occurred because the adhesive bonding of the core to the facings was stressed under tension to its limit, and the adhesive either had cohesive failure as in the Zn-22Al cores or adhesion failure as in the polystyrene cores. Under these circumstances, the failure criterion expressed in Eq. 5-4 does not apply and it can be safely inferred that the WRH cores are capable of withstanding much higher loads than what the four edge simply supported test revealed.

Core Thickness Distribution

The wire reinforced honeycomb (WRH) core mechanical properties are greatly influenced by the way the material flows in a vacuum on pressure forming process. The shape of the projections inserted in the die base to form the cores, see Figure 3-2, the properties of the sheets at the forming temperature, the strain rate and the distribution of the reinforcing wires are all contributing factors in the material flow process. A flow study for strain rate sensitive materials was presented in Chapter IV, where two distinctive problems were considered: (a) friction free flow around the wires and (b) restricted flow around the projections. Attention was called then to the perhaps critical degree of thinning that may take place at the end of a forming process in a restricted flow case, as compared to the fairly uniform thickness distribution that ideally

happens in a friction-free flow around the wires. The analysis of the material flow in a WRH core is quite involved from a geometrical standpoint; however, the way the material is redistributed in such structures should bear some resemblance to the theoretical distribution presented in Chapter IV. For this reason, the thickness of both High Impact Polystyrene and Zn-22Al sheets formed with or without wires were examined following different paths and examined according to the predictions. Strips of material about 1mm wide were cut in all cases, and the strips thickness was measured at 1mm intervals, as shown below. Paths 1, 2, 2*, and 3 correspond to sheets formed without wires, and paths 4, 4*, and 5 have the wires embedded. The path 5 correspond to a core with a square pattern and 13mm high cylindrical projecting. The results are presented in Figures 5-27, 5-28, 5-29, 5-30, and 5-31. Figure 5-27 represents the thickness ratio w/wo of High Impact Polystyrene sheets, 0.762mm thick (0.030 in), as they are formed in the die illustrated in Figure 3-2, having truncated cone projections 6.25mm high inserted. It is interesting to observe that the thickness of the sheets reduces continuously from the top of the die to the bottom. This effect is more pronounced in the portion of the sheet that is formed against the flat vertical boundary of the die, where a critical thinning tends to take place during the last stage of the forming process.

No change in thickness was observed at the flat top

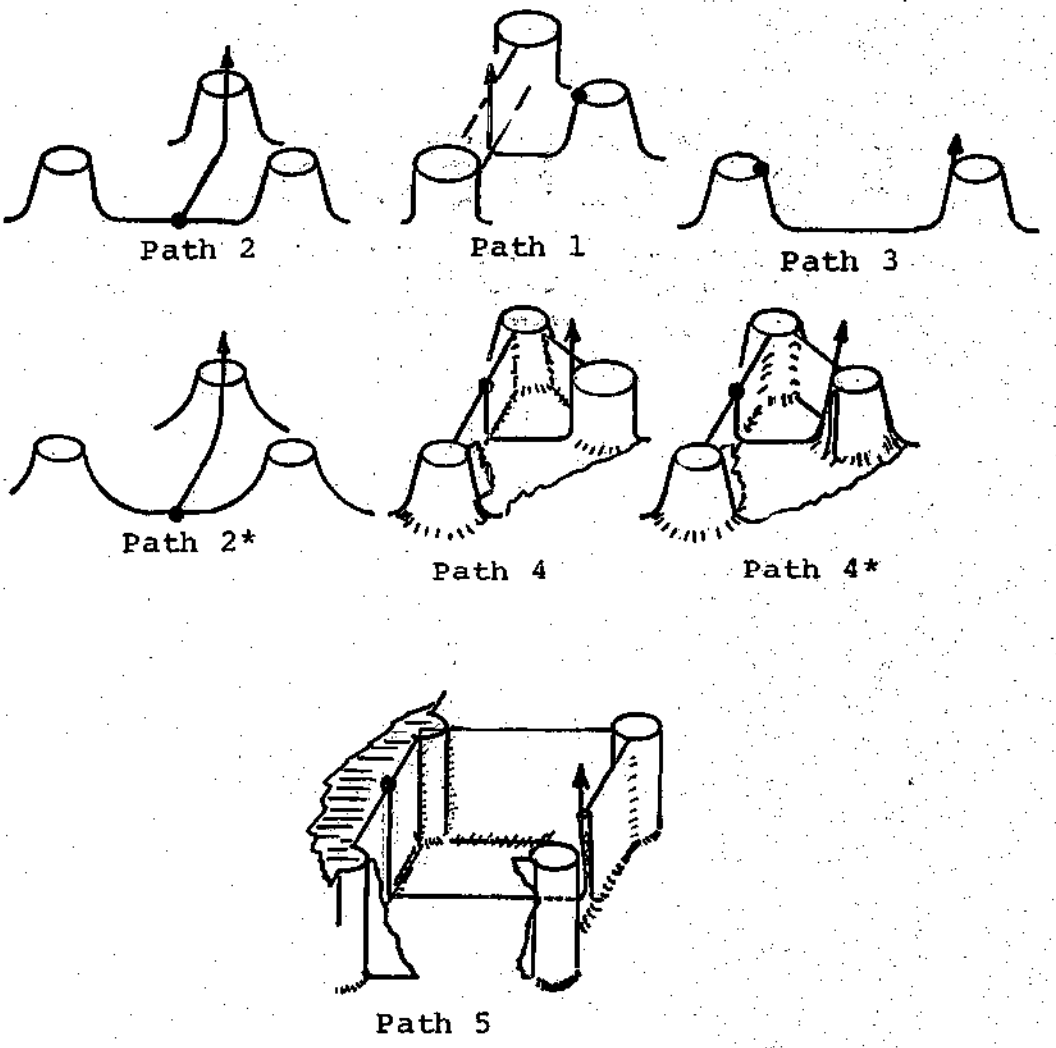

Figure 5-26. Several Cross Sections of WRH Cores.

of the projections in any of the cases studied; however, the flat bottoms of the forms seemed to have a maximum thickness where the material first touches the die bottom. The thickness is slightly reduced at both sides of the maximum and the reduction is more pronounced at the vicinity of the projections. Figure 5-28 illustrates the thickness distribution of High Impact Polystyrene sheets as they are formed with a mesh of wires embedded in a triangular fashion. Again the material is thicker at the top of the projections than at the bottom. However, it is interesting to observe that the material that drapes around the wires in a friction-less flow manner seems to be more uniformly distributed. This effect, perhaps, can be better observed in Figure 5-29 corresponding to High Impact Polystyrene cores 12.5mm high formed around a mesh of wires in a square pattern. The same trend is again observed in Figure 5-31, where the thickness ratio w/wo for Zn-22Al cores with wires in a triangular fashion is presented.

Attention is called to the fact that the flow behavior around the conical projections for the Zn-22Al sheet with and without wires embedded seem to be completely the opposite. Thinning tends to occur at the top of the forms without wires, Figure 5-30, and at the bottom of the forms with wires, Figure 5-31. This apparently opposing behavior can be exploited to control the thickness at will. Therefore, it appears possible at least for the Zn-22Al cores, to approach

best configuration for optimum core shear modulus; that is, a configuration with uniform cross section, as demonstrated in Chapter IV.

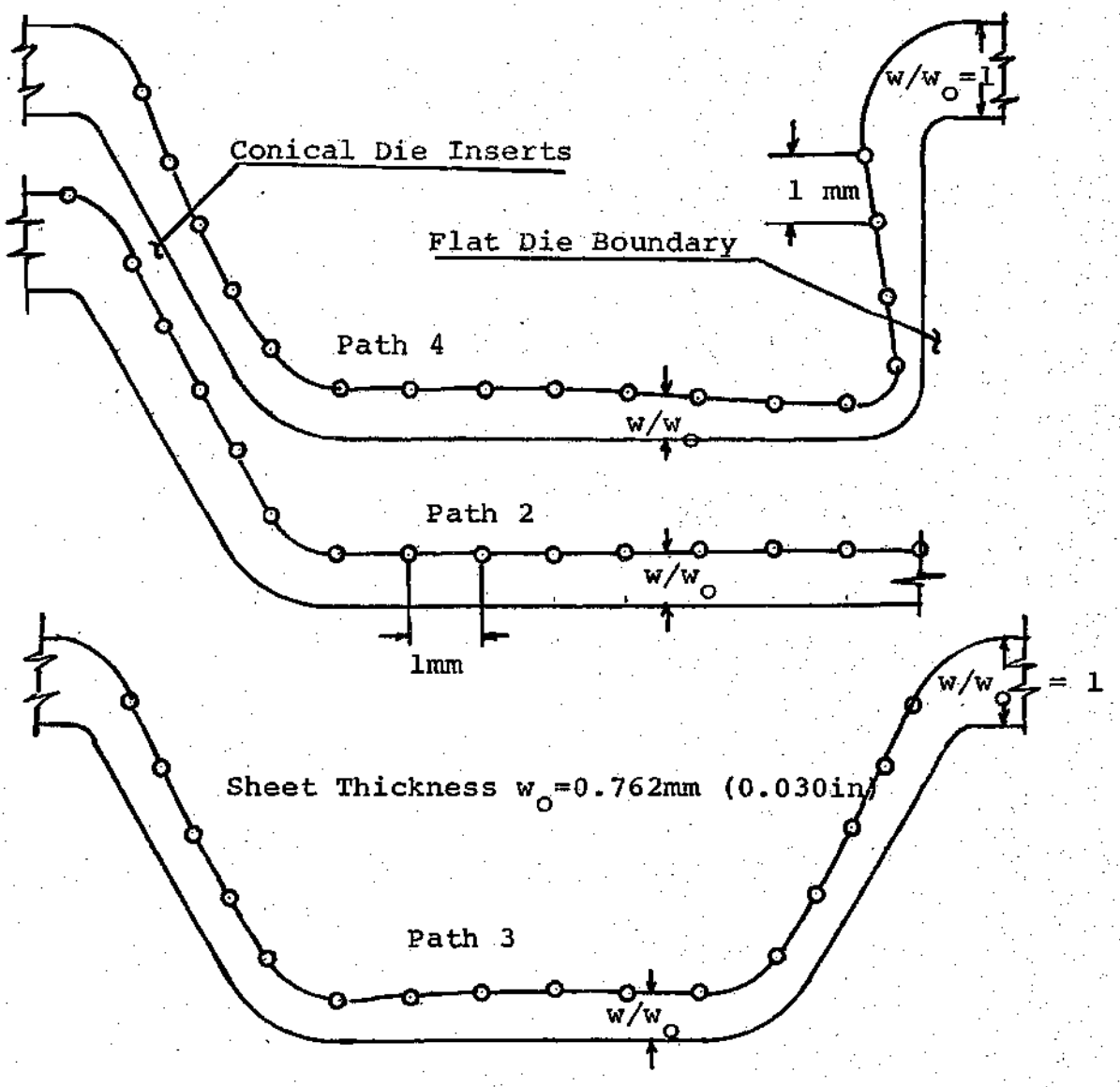

Figure 5-27. Thickness Distribution Ratio w/w_o in High Impact Polystyrene Forms with no Wires.

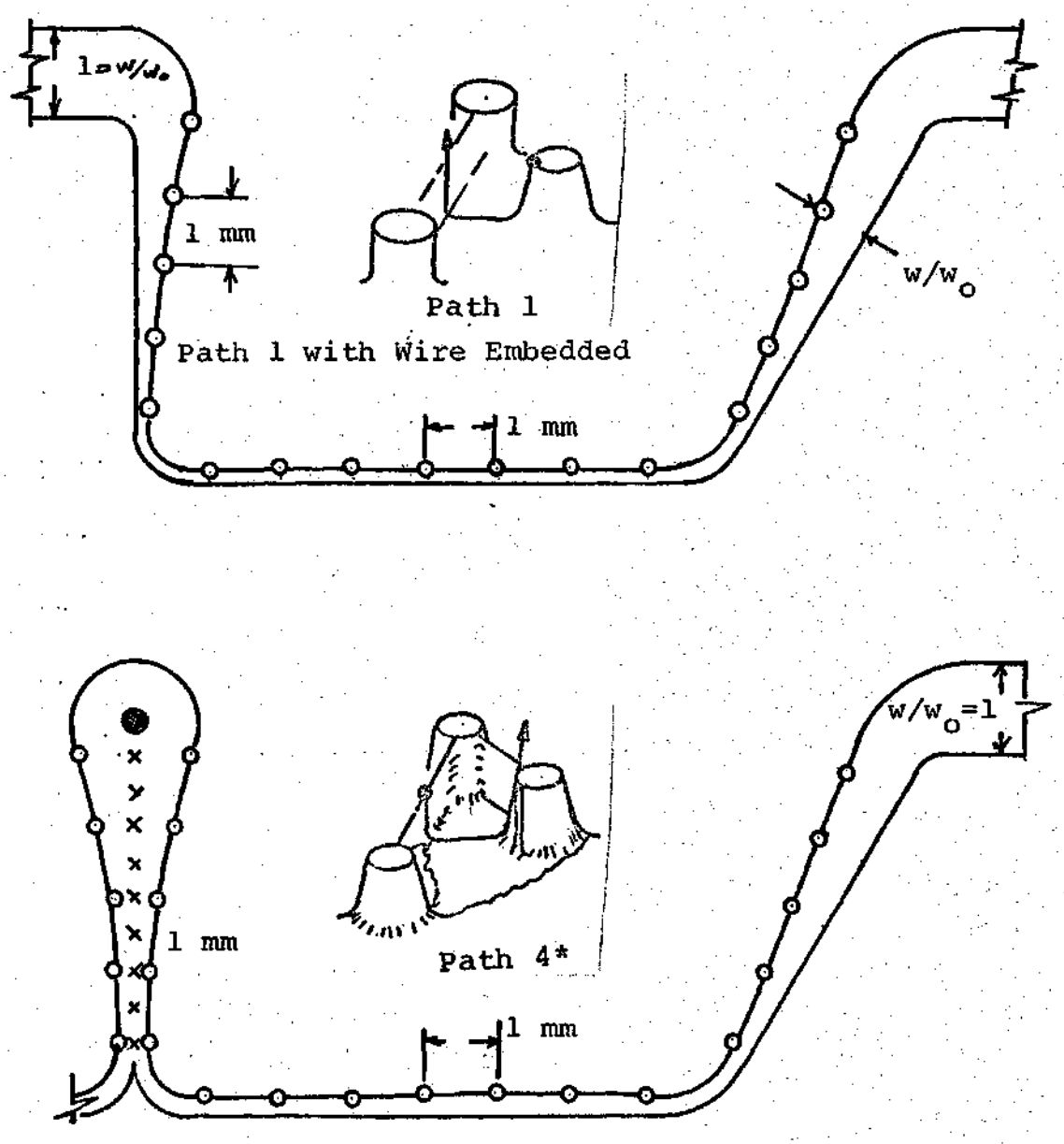

Figure 5-28. Thickness Distribution Ratio w/wo of High Impact Polystyrene in WRH Cores Along Paths 1 and 4*.

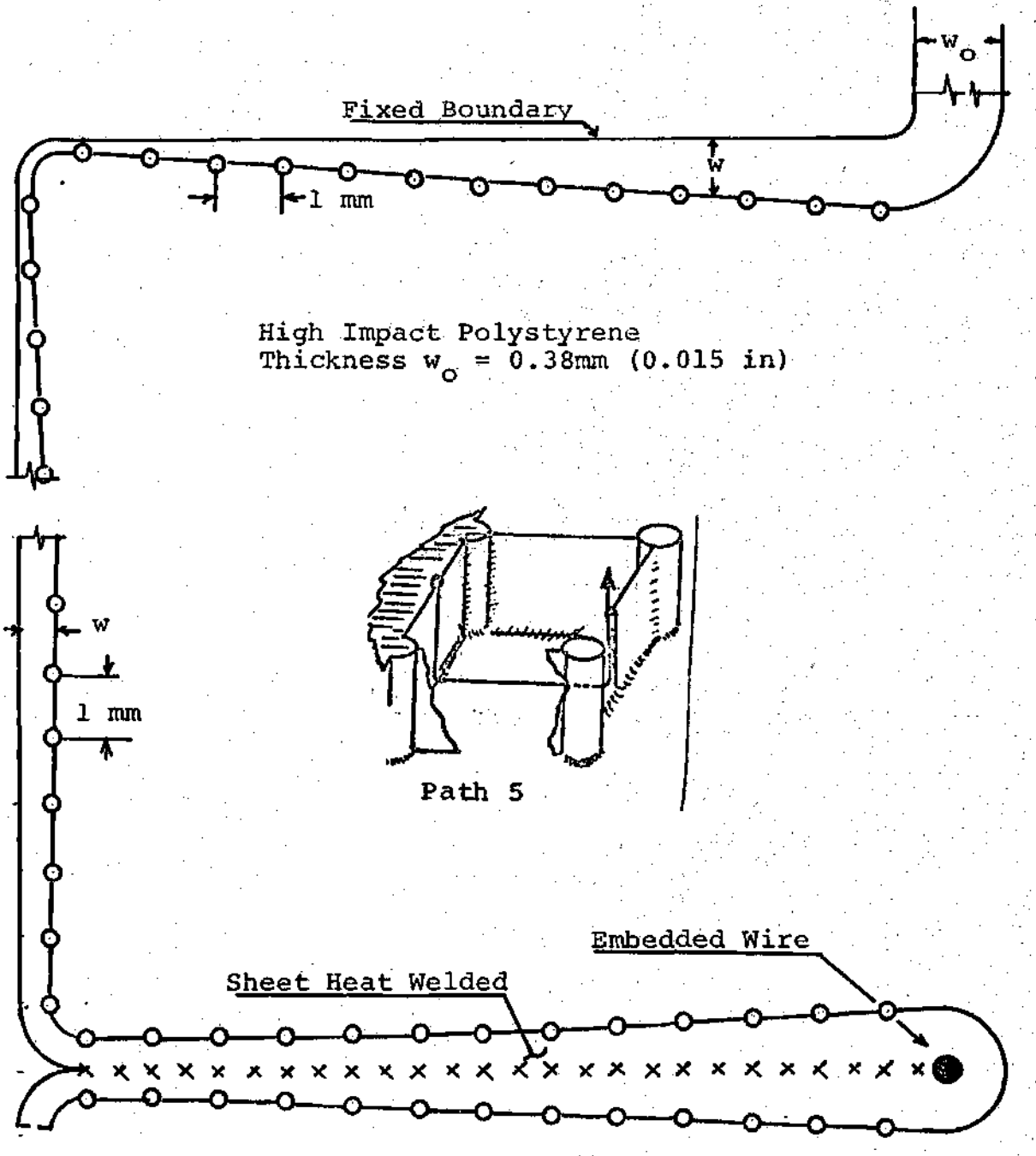

Figure 5-29. Thickness Distribution of a High Impact Polystyrene Formed in a Square Pattern with Wires Embedded.

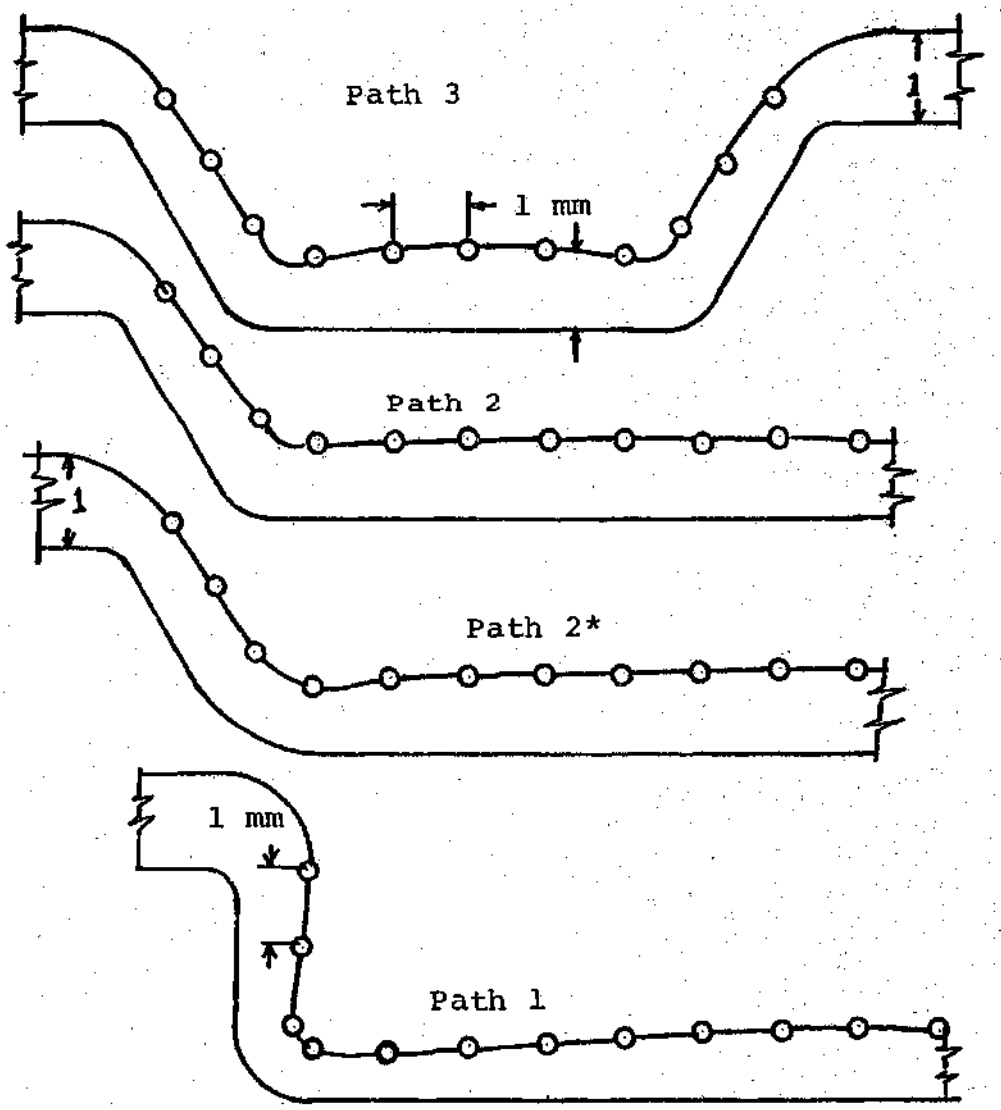

Figure 5-30. Thickness Distribution of a Zn-22Al Sheets Pressure Formed with No Wires Embedded.

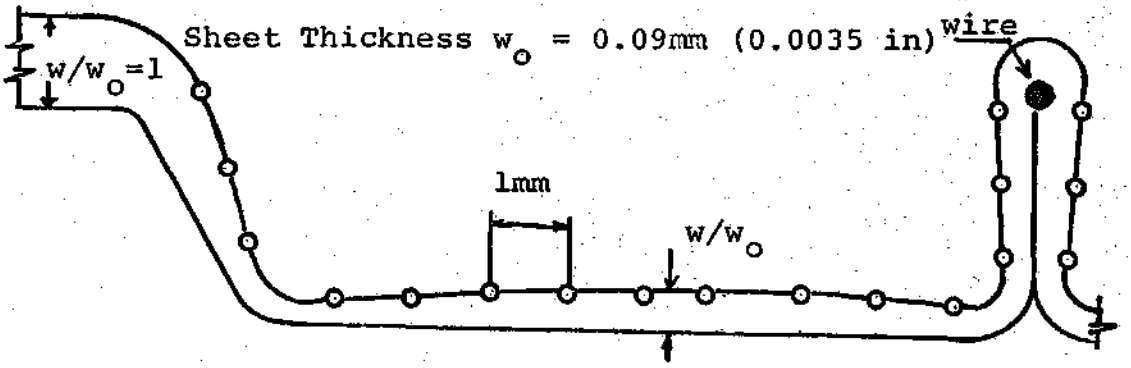

Figure 5-31. Thickness Ratio w/wo Distribution for Zn-22Al. Sheets Formed with Wires Embedded in a Triangular Pattern.

CHAPTER VI

ANALYSIS OF DATA AND DISCUSSION

A preliminary discussion of the experimental results has already been introduced in the previous chapter in an effort to point out the relevant characteristics of the WRH cores. Comparison of the results with the theoretical predictions and discussion of discrepancies will be presented in the current chapter.

Vacuum Forming Variables

In order to properly vacuum form the High Impact Polystyrene sheets, it was necessary to find the optimum value of the forming parameters. The results were presented in Figure 5-1, Chapter V. The evidence indicates that for a fixed separation between the heating coil and the sheet, and a fixed power consumption, the heating time is the variable to control. It is shown in Figure 5-1 that for a separation of 15 cms, the 0.76 mm thick polystyrene sheets should be heated for about 50 seconds for best results. Under these conditions the thickness distribution is quite uniform, and it can be inferred that the material is very much strain rate sensitive. If the heating time is too long, the material seems to be less strain rate sensitive, the thickness distribution is very poor and degradation of material

properties as well as porosity becomes a concern. On the other hand, if the sheet is not heated sufficiently, cracking at the most stressed areas may take place, the vacuum can not be sustained, and no forming is possible.

The Pressure Forming Variables

Pressure, forming time, and temperature are the most relevant parameters in the forming process from the economic standpoint. Figure 5-5 illustrates the relation between forming time and pressure for a fixed temperature of 270°C and sheet thickness of 0.075 mm. The curve for the Zn-22Al alloy seems to confirm the validity of Equation 4-52; that is,

$$(p_1/p_2)^{1/m} = t_2/t_1 \qquad (4\text{-}52)$$

The experimental value for m obtained from Figure 5-5 gives

$$m = 0.58 \qquad (6\text{-}1)$$

which is 20 percent higher than the m found in the literature [29]. It should be pointed out at this point that as the superplastic sheets are very thin, they may be very sensitive to temperature variations of the fluid applying the pressure. This perhaps can account for the slight difference between the m as reported here compared to other values found elsewhere.

The Shear Test

The object of the shear test is to determine both the shear strength of the core τ_{max} and the modules of rigidity G_c.

A formulation to predict the value of G_c was presented in Chapter IV,

$$G_c = \frac{t_o}{c} G'(1-A_o'/A_o) \qquad (4\text{-}108)$$

where t_o is the total thickness of solid material ($4w_o$) needed to make the core. A_o' and A_o are given by

$$A_o' = \pi d_1^{\,2}/4$$

$$A_o = (d_1 + \ell_1)^2 \cdot \sqrt{3/2}$$

For the above quantities, we will take the following values for the Zn-22Al alloy cores (see Figure 5-25).

w_o = 0.0762 mm (0.003 in)

c = 7.0 mm (0.276 in)

G' = 21 x 10^6 KPa (4.5 x 10^6 lb/in^2)

A_o'/A_o = 0.19

Substituting these values in Eq. 4-108, we obtain:

$$G_{c(Zn\text{-}22Al)} = 1.1 \times 10^6 \text{ KPa} = 158{,}000 \text{ lb/in}^2 \qquad (6\text{-}2)$$

For the core variables for the polystyrene, we will take the following values:

$w_o = 0.762$ mm (0.030 in)

$c = 12.7$ mm (.5 in)

$G' = 590{,}000$ KN/m^2 (86,000 lb/in^2)

$A_o'/A_o = 0.19$

and using Eq. 4-108

$$G_{c(poly)} \approx 115{,}000 \text{ KPa} = (17{,}000 \text{ psi}) \qquad (6\text{-}3)$$

A similar expression can be ascribed to predict the shear strength of the core τ_c and can be written as

$$\tau_c = \tau_s A_s/A \qquad (6\text{-}4)$$

where τ_s represents the shear strength of the solid material, A_s is the solid cross section area of the core, and A is the total area of the core ($A = b \cdot L$). If a constant cross

section A_s is assumed and considering that the material located on the flat top and bottom of the core, which amounts to 15 percent of the total core material, offers little resistance to shear, A_s can be written as

$$A_s \simeq 4(0.85\, w_o)\frac{A}{C} \tag{6-5}$$

and

$$\tau_c = \tau_s \frac{4(.85\, w_o)}{c} \tag{6-6}$$

where w_o is the initial thickness of each of the four sheets making the core. Using the maximum shear failure criteria for both Zn-22Al and polystyrene, τ_s can be estimated as

$$\tau_{s(Zn\text{-}22Al)} = 104{,}000 \text{ KPa} = 15{,}000 \text{ psi} \tag{6-7}$$

and

$$\tau_{s(poly)} = 21{,}000 \text{ KPa} = 3050 \text{ psi}$$

Then

$$\tau_{c(Zn\text{-}22Al)} = 380 \text{ KPa} = (550 \text{ psi}) \tag{6-8}$$

$$\tau_{c(poly)} = 2150 \text{ KPa} = (310 \text{ psi})$$

Let us examine now the results of the shear tests for both High Impact Polystyrene (HIP) and Zn-22Al cores on the light of the predicted values for G_c and τ_c. Figure 5-6 gives an apparent tensile shear strength of the HIP cores of 700 KPa, which is only 35 percent of the estimated value; however, the failure occurred at the core-loading plate interface. A substantial relative motion at such interface was recorded and translated into a shear strain; but this does not represent a deformation of the core itself. This now explains why the experimental value for G_c = 15,000 KPa is quite low compared against the estimate given in Eq. 6-3.

The value for the apparent τ_c when the core bond is made with toluene is 505 KPa (73 psi) and G_c is about 20,000 KPa, see Figure 5-7. Once more both quantities τ_c and G_c are reported below expectation; however, the failure was again a cohesive failure of the adhesive at the core-loading plate interface. At this point the trend of the experiments indicated that improvement of the adhesive was necessary. In this report, the semicores (two sheets with wires embedded) were not adhesively bonded but heat welded and RTC epoxy was used for the core-core and core-loading plates bond. The test results, see Figure 5-8, represent quite an improvement. The apparent shear stress τ_c was increased to 1400 KPa

$$\tau_{c(poly)} = 1400 \text{ KPa, } (206 \text{ psi}) \qquad (6\text{-}9)$$

and

$$G_{c(poly)} = 100{,}000 \text{ KN/m}^2, \text{ (14,500 psi)} \qquad (6\text{-}10)$$

The failure was a sudden adhesion failure of the RTC Epoxy at the core-core interface, with no indication of slippage. It is quite interesting to observe that the value of G_c obtained experimentally falls short of the expected value by only 15 percent. The shear strength is still about 30 percent below the estimates given in Eq. 6-8; however, the failure mode indicates that the shear strength can still be further improved as better adhesives become available. This experiment was nevertheless quite enlightening and convincing that the best shear strength, τ_c, and modulus of rigidity G_c for the polystyrene cores are found with heat welded cores. These, of course, are the least expensive of the types considered and can be readily welded during the vacuum forming process in a production line using the heat already present in the sheets at that stage. As the results of the heat welded cores were quite encouraging, it was thought that one of the next logical tasks to be carried out in future work would be using heat welding not only to join the two sheets forming the semicores, but also to join two semicores as indicated in Figure 5-3b. No problems are anticipated here as the process is frequently used to bond plastics [21]. More importantly, the shear strength of the core should

certainly be improved further. Referring to the Zn-22Al cores, the results of τ_c and G_c fall below the expectation, which is a reflection of the consistent adhesive failure, as can be observed in Figure 5-9. However, considering the good thickness distribution as evidenced in Figures 5-29 and 5-30, there is plenty of room for improvement of the WRH Zn-22Al core properties as soon as an adequate adhesive is found. Let us now make a comparison of the actual data gathered with the heat welded High Impact Polystyrene cores against some of the conventional honeycomb materials on the market. All the properties are referred to a core density of 0.123 gr/cm^3 (9.8 lb/ft^3), the actual density of the WRH cores tested, and linearity of the properties with respect to the core density has also been assumed. It can be observed in Figure 6-1 that the heat welded WRH cores and the non-metallic commercial honeycombs have comparable shear strength; but the WRH core has a clear improvement prospect if the semicore-semicore bond is also performed by heat welding.

Equally interesting is the comparison of the modulus of rigidity G_c presented in Figure 6-2. The only core material exhibiting slightly better rigidity than the WRH core is the Kraft paper; but the WRH appears to be a better choice on considering other factors such as shear strength, decay, weather resistance, and density range [3].

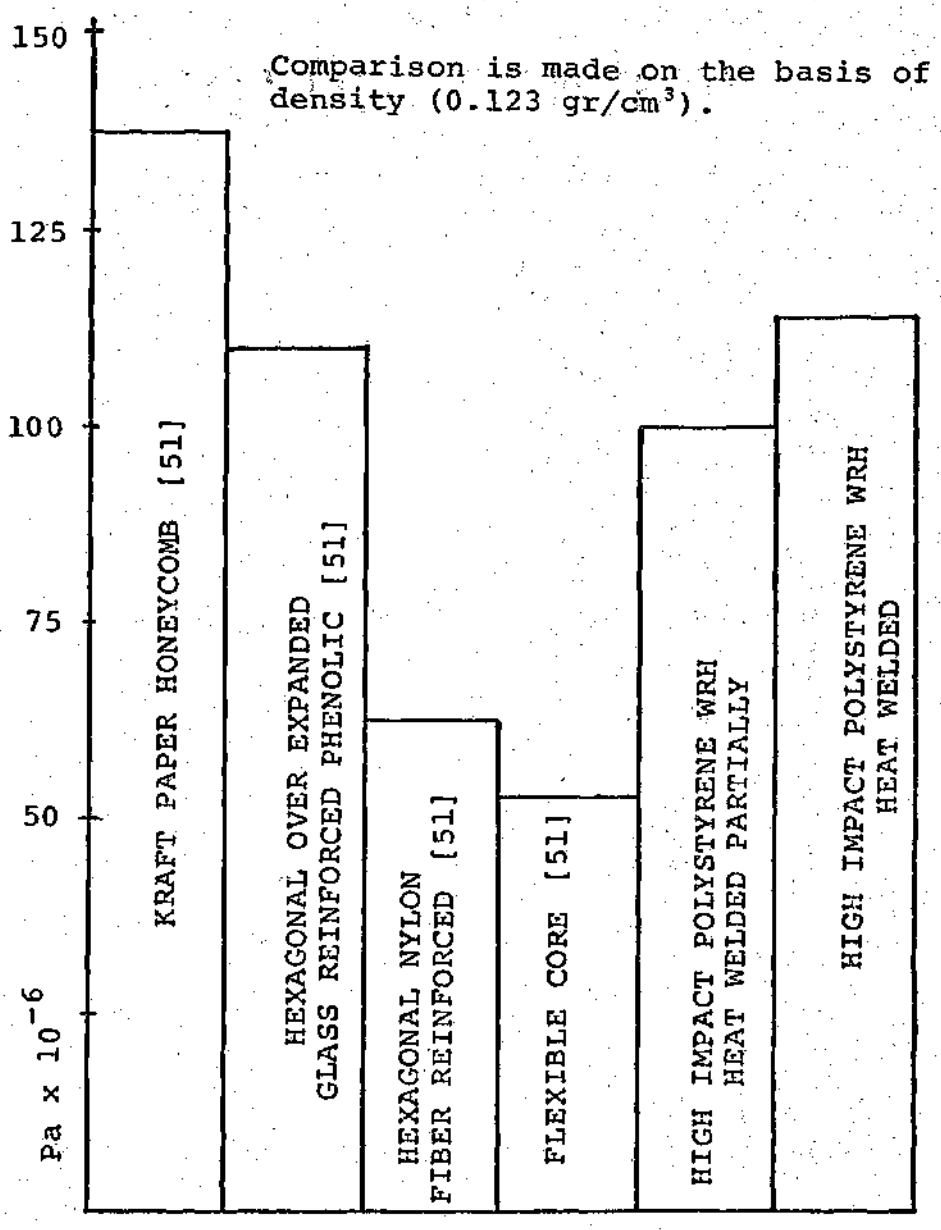

Figure 6-1. Shear Modulus for Non-Metallic Cores.

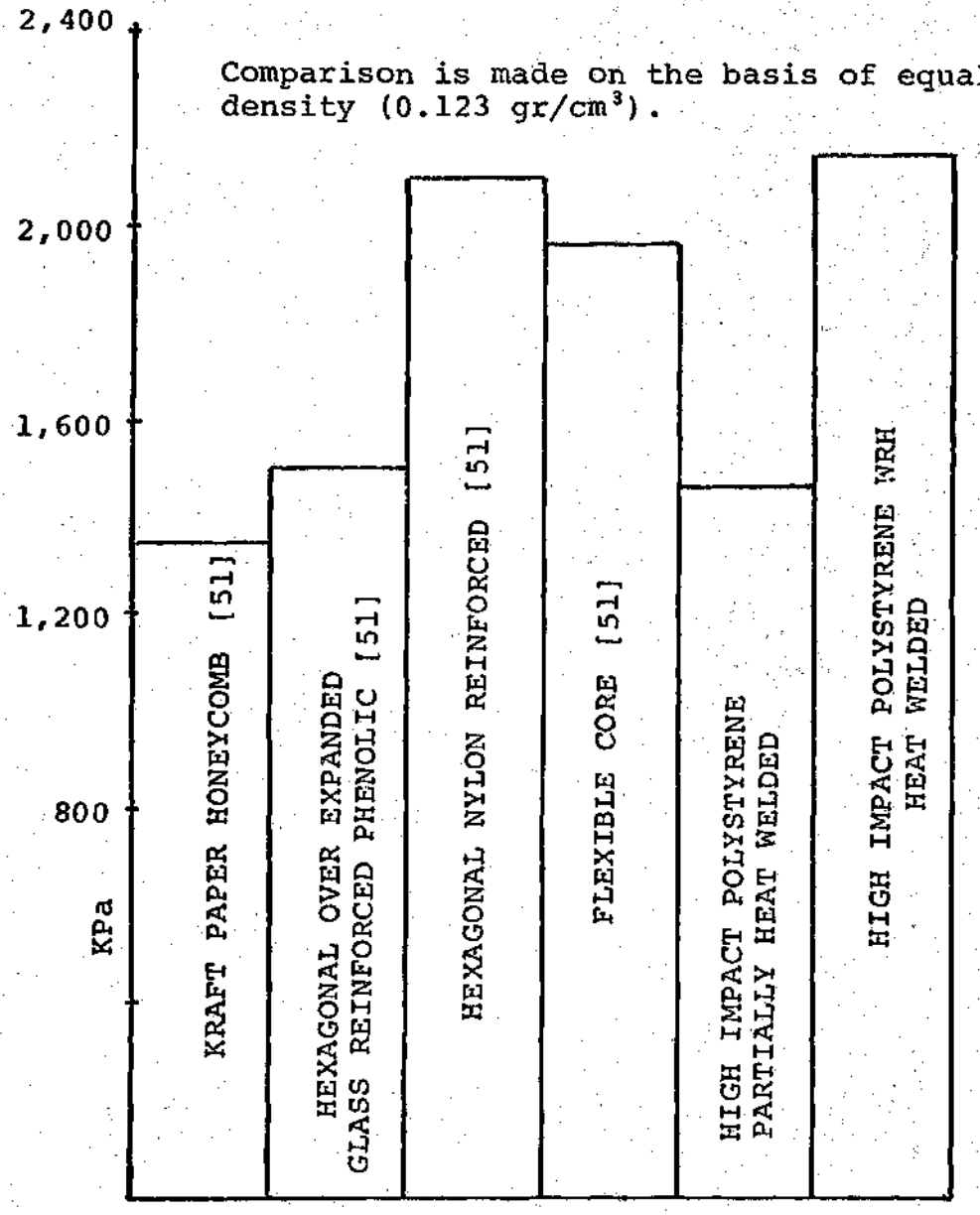

Figure 6-2. Shear Strength for Non-Metallic Cores.

The Four Point Bending Test

The intention of this test was to determine if the core modulus E_c had significant influence in the coefficient D, which normally is evaluated solely on the characteristics of the facings, as presented in Chapter IV. In order to have an approximate reference for E_c, let us estimate its value using Eq. 4-92, assuming that

$$E_w = E_{Kevlar} = 131 \times 10^6 \text{ KN/m}^2 \qquad (19 \times 10^6 \text{ psi})$$

$$E_{s(Zn\text{-}22Al)} = E_s = 82 \times 10^6 \text{ KN/m}^2 \qquad (12 \times 10^6 \text{ psi})$$

$$E_{s(poly)} = 1.6 \times 10^6 \text{ KN/m}^2 \qquad (230{,}000 \text{ psi})$$

$$A_w = 0.02 \text{ mm}^2 \qquad (0.00005 \text{ in}^2)$$

Inserting these values in Eq. 4-92, it is estimated that

$$E_{c(Zn\text{-}22Al)} = 3.7 \times 10^6 \text{ KN/m}^2 \qquad (540{,}000 \text{ psi})$$

$$E_{c(poly)} = 420{,}000 \text{ KN/m}^2 \qquad (61{,}000 \text{ psi})$$

The experimental values for E_c were determined in Chapter V based on the results presented in Figure 5-18 and 5-19. The experimental value for the Zn-22Al cores is 15% better than the estimated value shown above. The High Impact Polystyrene

results seem to be much higher than the predictions and this perhaps may be attributed to the combined effect of the flat portion of the polystyrene and the wires that are far from the neutral axis and also to the fact that a continuous layer of good adhesive was used in the core-facing interface. The recorded charts from the Instron universal testing machine, relating the displacement of the cross head to the applied force, exhibited an early yield point when the plastic cores were tested, and this is in agreement with the solid polystyrene behavior in the tensile tests that were conducted. This may be taken as an indication that the core modulus E_c may have a real contribution to the sandwich construction performance under bending; therefore, the flexural rigidity D may in fact be significantly affected by E_c.

The Two Edge Simply Supported Buckling Test

This test was only carried out with the Zn-22Al. The purpose of the test was to obtain another experimental expression for the modulus of rigidity G_c and to compare it against the data obtained in the shear test. The results of the test are presented in Figure 5-21. As the failure occurred at the core-facing interface, displacement discontinuities may have developed at the interface and the net result was that the members comprising the sandwich beam were only partially joined. The experience from the shear tests confirms this observation. In consequence, the value derived

for G_c from Eq. 5-2 and Figure 5-21 may not be very significant.

The Four Edges Simply Supported Test

With this test it was possible to make a direct measurement of E_c taking into account the average strain reading as a function of the applied force in the first portion of the loading. Using Eq. 5-3 and Figure 5-22 and 5-23, it was possible to determine E_c, and the experimental value of E_c for both Zn-22Al and High Impact Polystyrene cores were in the range of the predicted value using Eq. 4-92.

As to the failure mode, it is quite evident that the maximum load was limited by localized adhesive failure at the core-facing interface, as has been argued in Chapter V on the basis of the results derived from Eq. 5-4.

Core Thickness Distribution

As previously pointed out, the thickness distribution of the formed sheets is a dominant factor that determines both the shear strength τ_c and the modulus of rigidity G_c of the wire reinforced honeycomb (WRH) core. In the discussion that follows, an attempt is made to explain why the material flows in the various patterns illustrated in Chapter V.

An important observation was made in the previous chapter referring to the completely different material distribution around the surface of revolution projections for

the Zn-22Al sheets, depending if they were formed with or without wires embedded. The explanation for the thinning at the top of the truncated cones when no wires are used seems to be given by Eq. 4-34 and Eq. 4-43. In fact, if attention is concentrated on one single projection, it will be seen that it is surrounded by six more projections which are arranged as indicated in Figure 6-3.

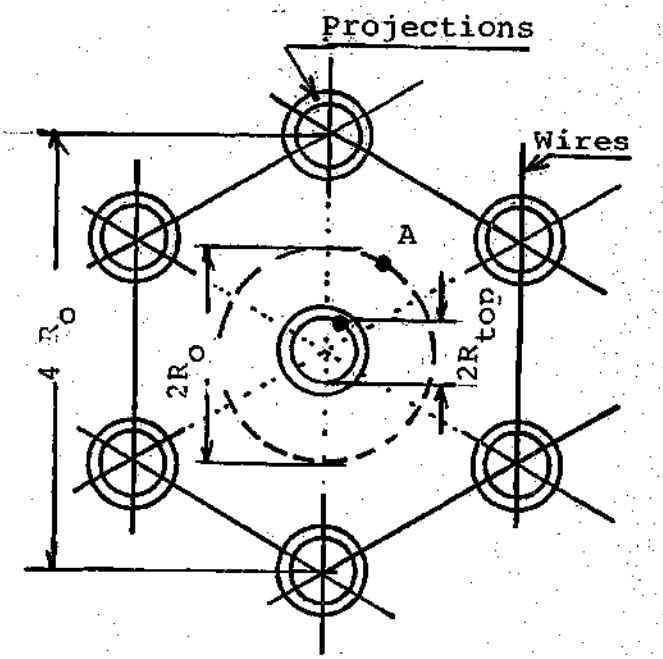

Figure 6-3. Projection Arrangement in the WRH Core

If the sheets are formed with no wires, it can be assumed that the effective amount of material been formed around the central projection is a circle of radius R_o = 8 mm, and the radius at the top of the projection is R_{top} = 4 mm. If

Eq. 4-43 is used to compare the thinning taking place at points A and B in Figure 6-3 when the sheet still has uniform thickness w_o, a thinning ratio $\dot{w}_B/\dot{w}_A = 3.2$ results. As the process continues, thinning at location B tends to be accentuated because $w_B < w_A$ at any other time.

However, when the wires are placed on top of the projections, the material closer to the top of the projections takes a curvature with a smaller radius than the material further away from the projection top, as the pressure is applied. This point is illustrated in Figure 6-4 where two small elements AA and BB are considered.

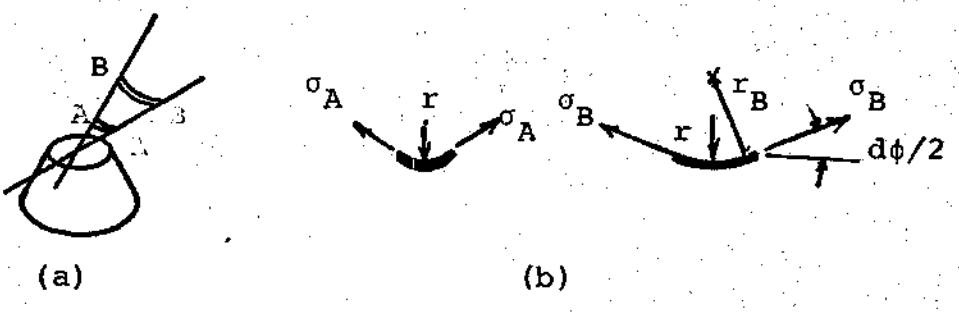

Figure 6-4. Internal Stresses in the Forming Process
(a) Portion of a Sheet in the Forming Process
(b) Force Balance of Small Elements

Since the curvature of the sheet in the radial direction is negligible, the pressure p is only balanced by the tangential stress σ. Considering the radius of curvature r_A and r_B ($r_A < r_B$), and the stress-strain rate relation for the superplastic materials, the following expressions result.

$$pr_A = \sigma_A$$

$$pr_B = \sigma_B$$

and

$$(\sigma_A/\sigma_B) = (r_A/r_B) = (\dot{\varepsilon}_A/\dot{\varepsilon}_B)^m \qquad (6\text{-}11)$$

Considering now the incompressibility condition, Eq. 4-40 can be approximately written as

$$(\dot{\varepsilon}_A/\dot{\varepsilon}_B) = [(\partial w/\partial t)/w]_A/[(\partial w/\partial t)/w]_B \qquad (6\text{-}12)$$

Combining 6-12 and 6-11, it is found that:

$$(r_A/r_B)^{1/m}(w_A/w_B) = dw_A/dw_B \qquad (6\text{-}13)$$

But as soon as the material at A and B take a slight deformation, it is evident from the boundary conditions that $r_A < r_B$ and it can be inferred from Eq. 6-13 that $dw_A/dw_B < 1$. This is in complete agreement with the results presented in Figure 5-30 and Figure 5-27 for both polystyrene and Zn-22Al sheets.

The optimization of the WRH core properties perhaps can be achieved by taking full advantage of the way in which the material actually flows. It has been established that

the thickness distribution in the webs of the polystyrene core with the square pattern, see Figure 5-25, is more uniform than in the webs of the core in wires in a triangular fashion on top of the conical projections, as indicated in Figure 5-27. However, if the ratio A_p/A_{web} is examined for both cases, where A_p is the area around the projections, it is found that the core with the conical projections and wires in a triangular fashion has a higher ratio A_p/A_{web}. This suggests that a considerable amount of material that supposedly should go to the webs is pulled toward the projections if the ratio A_p/A_{web} is too big. This discussion has a practical interpretation in the sense that polygonal projections, having wires going across the vertices probably approximate the form ideal, whilst the larger the angle α between the wires and the sides of the polygon, the better the flow at the webs. This immediately leads to only one choice, i.e., square pyramids. Along the same line of thought, it is observed that the material seems to have better thickness distribution around projections with large inclination, as can be seen in Figure 5-27, path 1; therefore, the projections should ideally be square pyramids with highly inclined walls. Another fact is that as the thinning at the top can be balanced by the presence of the wires, a very small top can be permitted. In this way more material is available for the projection walls and the webs. Finally, to balance the tendency of the material to thin down at the

bottom of the projections and webs, wider projections base should be used, reducing again the flat bottom material which does not contribute to the shear strength of the core. The arrangement of the structures could be as indicated in Figure 6-5a. To further improve the strength, the flat bottom in Figure 6-5a can be reduced more by placing another projection there without wires on its top or by putting two sets of wires that cross each other at 90° as shown in dotted lines in Figure 6-5a.

Another apparent alternative which would reduce the bottom surface would be to use Hexagonal Pyramids, as shown in Figure 6-5b. However, the webs would not be as uniform as in Figure 6-5a because the angle $\alpha = 120° < 135°$.

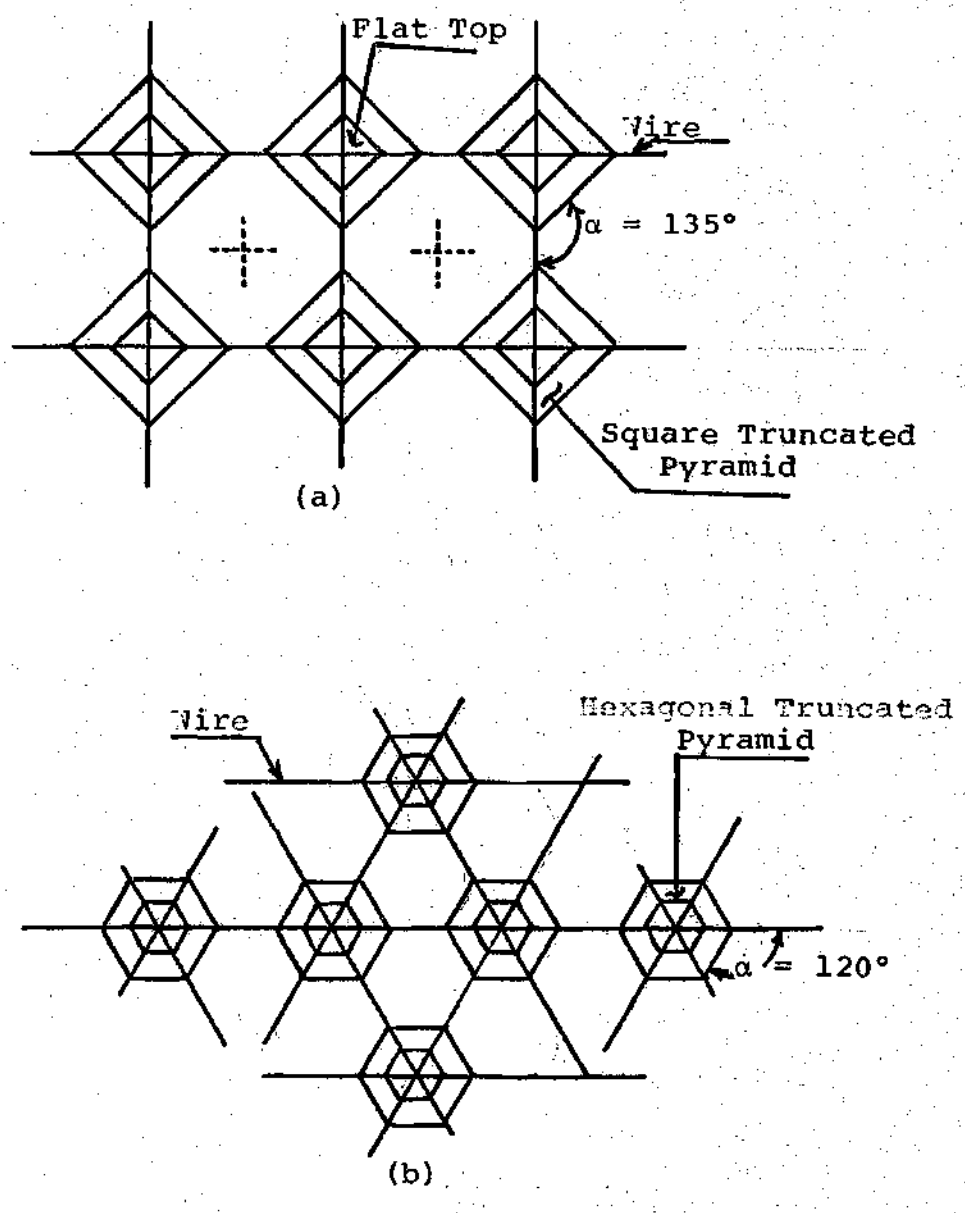

Figure 6-5. (a) Octagon WRH Core with Square Truncated Pyramid.
(b) WRH Core with Hexagonal Truncated Pyramid.

CHAPTER VII

CONCLUSIONS AND RECOMMENDATIONS

The determination of the mechanical properties of wire reinforced honeycomb (WRH) cores, their manufacturing feasibility and their further improvement have been both theoretically and experimentally investigated. Two and three dimensional analyses for both restricted and friction-free pressure and vacuum forming processes have been presented, and experimental evidence provided confirming that friction free flow permits more uniform thickness distribution. In view of the importance of production time in any industrial process, a theoretical analysis was also presented relating sheet thickness to forming time for a constant pressure. The experimental results confirm the flow analysis for the Zn-22Al core, for a strain rate sensitivity factor of $m = 0.58$. In the forming of the Zn-22Al sheets without wires, a thinning tendency at the top of the projections was reported and seemed to be due to stress concentration, which again is in agreement with the theory presented.

Formulations for predicting the shear strength τ_c, the modulus of rigidity G_c, as well as E_c of the WRH cores were developed. Due to persistant adhesive failure at the core-facing bond, the experimental results of τ_c and G_c are very

conservative and they do not truly represent the actual properties of the core; however, the results of the High Impact Polystyrene came close to the predictions. Although the wires did not contribute directly to the shear strength or the G_c in the tested specimens, they do have a definite influence when the core thickness is increased as several elemental layers are put together. The wires also have a definite effect on E_c; an effect of the order of 30 percent for the polystyrene, for only a negligible increase in weight. Furhtermore, they are essential for the proper material distribution, far from the neutral axis to enhance the flexural rigidity D of the sandwich construction.

As the shear strength and the modulus of rigidity of the core are the most important mechanical properties, the theoretical analysis was extended to this topic and it was further determined that the optimum core configuration is the one possessing uniform cross section in a plane parallel to the facings. This theoretical conclusion leads to important practical considerations in the search for adequate projections shape and arrangements.

In an effort to underline the significance of the core mechanical properties, a nondimensional analysis was carried out to compare the load carrying capacity of two geometrically similar sandwich beams subjected to proportional loading conditions but having differing core shear strengths and moduli of rigidity. Also, as an extension of Allen's

analysis, a derivation has been developed to clearly show that the displacement w for a sandwich beam subjected to a load P under various boundary conditions can be separated into one component w' that depends on the facing properties and another component w" that depends on the modulus of rigidity of the core.

The experimental results clearly indicate that, under the action of heat and pressure, it is possible to shape superplastic Zn-22Al and High Impact Polystyrene sheets into complex shells having reinforcing wires embedded and with different configurations resembling honeycombs, and further that such shells can be used in sandwich construction. If the plastic shells are heat welded, both the shear strength and the modulus of rigidity can be significantly improved. A definite advantage is seen in that cell buckling may not become a dominant factor in the WRH for thicker cores, in contrast to the drastic detrimental effect that buckling has in the shear strength of the conventional honeycomb in the thicker core range.

To determine the mechanical properties of the WRH cores, compression and tensile shear, four point bending, two edge and four edge simply supported buckling tests were carried out. The shear test of the heat welded polystyrene gave the best apparent τ_c. The other shear tests had the inconvenience of large relative displacements at the core-facing interface. As the Zn-22Al cores exhibit

very good material distribution, the mechanical properties should be remarkably improved in proportion to the quality of the adhesive; although the theoretical calculations of the shear strength indicates that the Zn-22Al cores are not as effective as the aluminum honeycomb, primarily because the Zn-22Al is about twice as heavy as the aluminum alloys used for the honeycomb.

To gather more information in the search for a core with optimum τ_c and G_c, the thickness distribution of the WRH cores was experimentally determined along a number of basic paths. The sheets with the wires embedded seemed to present the best material distribution in terms of strength and rigidity, as opposed to the sheets formed without wires. This suggests that when an industrial process is set up, a better option would involve using wire reinforced sheets alone. As an alternative, wire reinforced sheets in combination with thinner gage without wires embedded can also be used. Based on the experimental thickness distribution results, it has been suggested that regular square or hexagonal pyramids with small upper surface and wider base interconnected with webs with the reinforcing wires embedded, may prove to be the best forms of projections in terms of optimum τ_c and G_c.

The following recommendations are made regarding future research in the area of the WRH cores.

1. As heat welded plastic cores, in contrast to those adhesive bonded, give better results in terms of shear strength and modulus of rigidity, new research should concentrate on completely heat welded cores, using adhesive only at the core-loading plates interface.

2. As the sheets formed with the wires embedded give the best material distribution, the heat welding experiments should include (a) the testing of cores made only with sheets and wires embedded, and (b) cores with sheets formed with wires embedded, in combination with thinner gage sheets formed without wires.

3. In the optimization procedure of projection configuration and arrangement, special consideration should be given to the square and hexagonal pyramids with highly inclined walls and reinforcing wires. Magnitude of fillet radii required should be carefully studied, however, because of stress concentration.

4. Further research, industrially oriented, using other plastic materials as well as pertaining to the heat welded WRH cores is highly recommended.

5. Further research is also desirable using adhesives with superior quality and also with appropriate temperature curing ranges; so that the Zn-22Al WRH cores can develop their full shear strength.

6. The technique of pressure or vacuum forming with wires embedded may not only be applicable in the manufacturing of light weight sandwich construction. Research could be made to evaluate this new forming technique for various industrial items using thicker plastic sheets in combination with inexpensive dies, as opposed to plastic injection molding.

7. The WRH cores manufacturing technique is quite appropriate for (a) inserting metallic columns into the core to enhance the shear strength and (b) for developing cores with a cylindrical or more general central surface for special requirements (i.e. shaped panels).

8. In the present work, two and three dimensional analyses of the forming of strain rate sensitive materials was advanced. Further experimental work corresponding to the mathematical model should obviously be carried out to support this analysis.

9. The influence that the angle between the wires and the projections has upon the web thickness distribution also requires further theoretical and experimental analysis.

APPENDIX A

CORE MECHANICAL TEST DATA

Compression Shear

Tensile Shear

Four Point Bending

Two Edge Simply Supported Buckling

Four Edge Simply Supported Buckling

Table 1. Compression Shear Test

Material: Sandwich Construction with Polystyrene Core
Semi Core Bonding: Toluene ($C_6H_5CH_3$)
Internal Semicore Bonding: Spray Adhesive 7
Loading Plate Bonding: AFEPOXY 2
Shearing Area: 8.9 cm x 14 cm (3.5 in x 5.5 in)

Number	Load lbs	Load N	Shear Stress KPa	Deflection in x 10^{-4}	Shear Strain μ/m
1	100	445	35	5	2,000
2	225	1,000	81	15	6,000
3	350	1,560	126	25	10,000
4	450	2,000	161	35	14,000
5	540	2,400	193	45	18,000
6	610	2,700	217	55	22,000
7	680	3,025	243	65	26,000
8	750	3,350	270	75	28,000
9	800	3,550	290	85	32,000
10	850	3,800	306	95	36,000
11	900	4,000	322	105	40,000
12	940	4,200	340	115	44,000
13	975	4,350	350	125	48,000
14	1,020	4,550	365	135	52,000
15	1,050	4,700	380	145	56,000
17	1,125	5,000	400	165	64,000
19	1,175	5,250	425	185	72,000
23	1,300	5,800	470	225	72,000
28	1,400	6,250*	505	275	

*Cohesive failure of adhesive at the core-plate bond.

Table 2. Compression Shear Tests

Heat Welded High Impact Polystyrene Cores
Sheet thickness: 0.762 mm (0.030 in)

Reading	Deflection (mm)	Shear Strain (mm/mm)	Force (lbs)	Stress lbs/in^2	Stress KPa
1	0.0254	0.002	925	48	331
2	0.0381	0.0003	1,350	68	468
3	0.0508	0.004	1,725	87	600
4	0.0635	0.005	1,960	98	675
5	0.0762	0.006	2,160	108	744
6	0.089	0.007	2,400	120	827
7	0.101	0.008	2,650	132	910
8	0.1143	0.009	2,900	145	1,000
9	0.127	0.010	3,050	152	1,047
10	0.1397	0.011	3,250	162	1,116
11	0.1524	0.012	3,500	175	1,206
12	0.1651	0.013	3,650	182	1,254
13	0.1780	0.014	3,850*	193	1,330

*Core bonded with RTC Epoxy. Epoxy failed by adhesion.

Table 3. Tensile Shear Test

Material: Sandwich Construction with Polystyrene Core
Adhesive: Spray Adhesive 7
AFEPOXY 2-(280 °F, 10 min cure)
Test: 2-4/27
Cross Head Speed: 0.1 in/min/

Number	Load lb	Load N	Shear Stress KPa	Deflection mm	Shear Strain μ/m
1	440	1,960	160	0.254	20,000
2	760	3,340	270	0.381	30,000
3	1,160	5,160	415	0.508	40,000
4	1,600	7,100	570	0.635	50,000
5	2,000	*8,900	720	0.720	56,000

*Cohesive Failure of Adhesive at the Core-Loading Plate Bond.

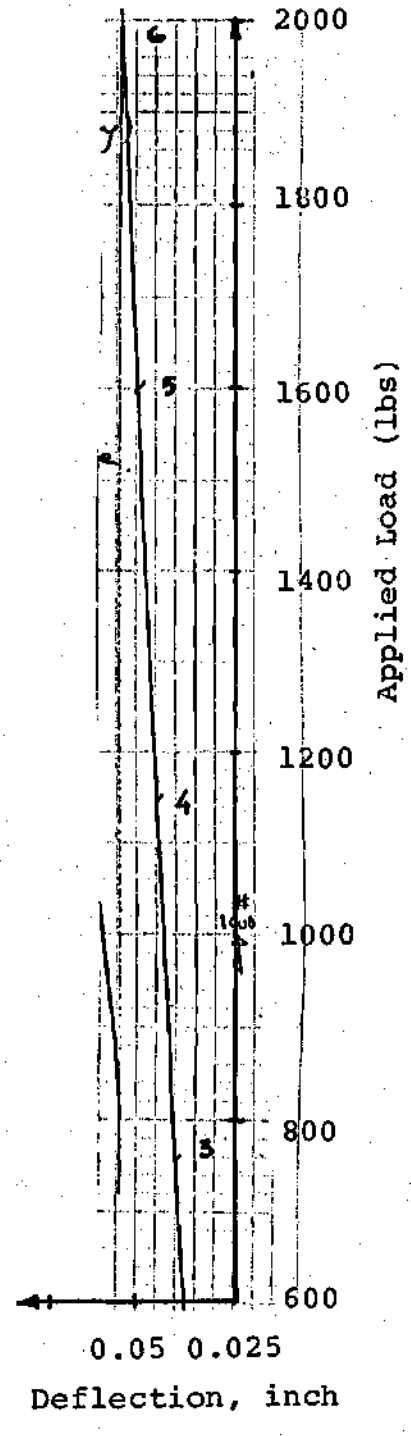

Cross Head Speed = 0.1 in/min
(2.54 mm/min)

Recorder Speed = 2 in/min

Material: High Impact
Polystyrene Core
(0.030 in sheets)

Figure A-1. Upper Portion of Tensile Shear Tests Graph in a Sandwich with WRH High Impact Polystyrene.

Table 4. Tensile Shear Test - 2-5/6

Material: Sandwich Construction with Zn-22Al WRH Core
Adhesive: AFEPOXY 2 (250°F - 1 hr. Cure)
Cross Head Speed: 0.2 in/min

Number	Load lbs	Load N	Shear Stress KPa	Deflection mm	Shear Strain mm/mm
1	125	555	45	.254	0.04
2	230	1,025	83	.508	0.08
3	400	1,780	143	.762	0.12
4	520	2,300	185	1.016	0.16
5	640	2,850	230	1.27	0.20
6	775	3,450	278	1.524	0.24
7	900	4,000	322	1.778	0.28
8	1,020	4,540	365	2.032	0.32
9	1,160	5,160	415	2.286	0.36
10	1,300	5,790	462	2.54	0.40
11	1,400	6,230	501	2.794	0.44
12	1,640	6,500	523	3.048	0.48
13	1,530	6,800	550	3.302	0.52
14	1,580	7,050	570	3.556	0.56
15	1,820	8,100	650	9.9	1.56

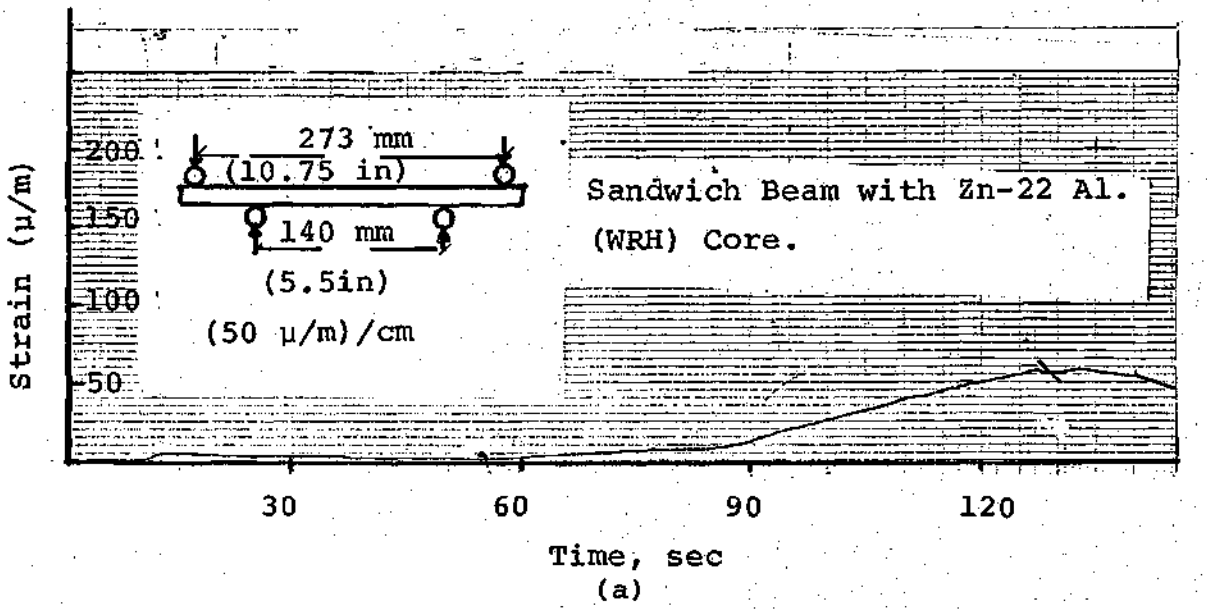

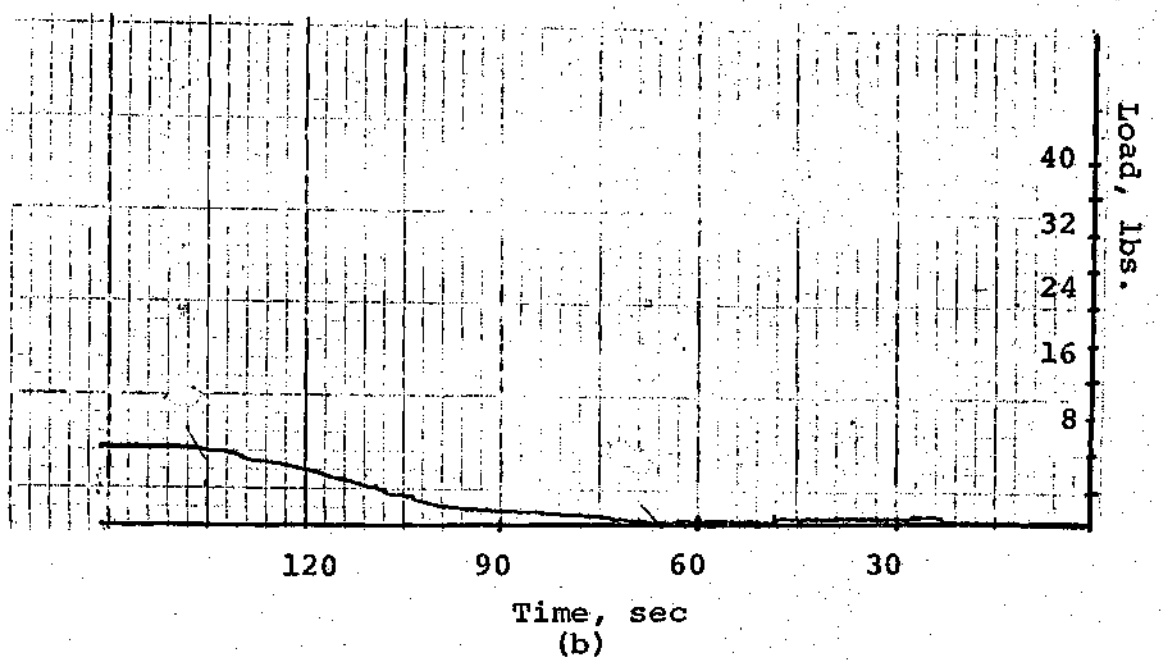

Figure A-2. Bending Test Characteristic Curve
(a) Strain Gage Reading vs. Time
(b) Applied Load vs. Time

Table 5. Beam Subjected to Pure Bending.

High Impact Polystyrene Core
Cross Head Speed: 1.25 mm/min (0.05 in/min)

Test	Force N	Distance (e) m, (in)	Moment N-m, (in-lb)	Strain μ/m
1-	51	0.07143 (2-13/16 in)	3.64 (32.3 in-lb)	40
2-	55.6	"	3.97 (35.15)	50
3-	60.1	"	4.29 (38.7)	60
4-	102	"	7.29 (64.68)	132
5-	128	"	9.14 (80.85)	178
6-	294	"	21.2 (185.62)	480
7-	636	"	45.43 (402.2)	900

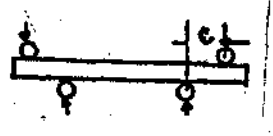

Table 6. Bending Test of Sandwich Beams With WRM Zn-22 Al Core.

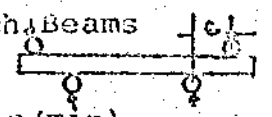

Cross Head Speed: 0.508 mm/min (0.02 in/min)

Test	F N (lb)	Distance (e) m (in)	Moment N-m (in-lb)	ε μ/m
1-	35.6 (8)	.073 (2.825)	2.6 23	160
2-	15.8 (3.5)	.0857 3.375	1.4 12	55
3-	31.1 (7)	0.066 2.625	2.1 18.5	150
4-	40 (9)	0.066 2.875	2.7 26	185
5-	15.8 (3.5)	0.073 2.875	1.2 10.1	51
6-	8.9 (2)	0.073 2.875	.65 5.75	30
7-	17.8 (4)	0.066 2.625	1.2 8.75	55
8-	15.8 (3.5)	0.08 3.125	1.26 11	55
9-	33.4 (7.5)	0.066 2.625	2.2 19.7	140
10-	51.2 (11.5)	0.08 3.125	4.1 36	170
11-	51.2 (11.5)	0.08 3.125	4.1 36	175
12-	15.8 (3.5)	0.073 2.875	1.2 10.1	45
13-	15.8 (3.5)	0.066 2.625	1.1 9.2	55

Table 7. Buckling Test Data

Test	Force N (lb)	Strain μ/m
1-	290 (65)	17
2-	1,300 (292)	80
3-	1,335 (300)	80
4-	1,024 (230)	150
5-	600 (135)	90
6-	1,544 (347)	160
7-	3,800 (860)	370
8-	356 (80)	35
9-	89 (20)	16
10-	111 (25)	13
11-	245 (55)	25
12-	423 (95)	47
13-	645 (145)	70
14-	868 (195)	73

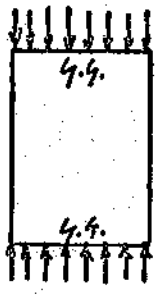

Zn-22Al. Core, Simply Supported at the Loaded Ends.
Cross Head Speed: 0.05 in/min

Table 8
Four Edge Simply Supported Sandwich Beam
with WRH Zn-22Al Core

Edge Wise Load
Cross Head Speed: 1.27 mm/min (0.05 in/min)

Test	Load lbs	Load N	Strain μ/m	Stress KN/m^2
1	250	1,112	75	627
2	450	2,000	237	1,129
3	780	3,470	425	1,960
4	975	4,338	675	2,450
5	1,275	5,673	1,000	3,200
6	1,675	7,200	1,375	4,075
7	1,950	8,700	-	4,900
8	2,275	10,200	-	5,750
9	2,400	10,700	-	6,040

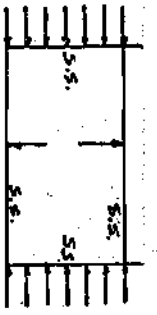

Table 9. Four Edge Simply Supported Sandwich Beam with Zn-22 Al Core Loaded Edge Wise

Test	Load lbs	Load N	Strain Gage Face One μ/m	Strain Gage Face Two μ/m
1	175	780	50	No Reading
2	300	1,335	175	"
3	500	2,225	325	"
4	525	2,340	325	"
5	750	3,340	525	75
6	950	4,230	700	275
7	1,225	5,450	950	475
8	1,475	6,600	1,000	700
9	1,760	7,840	1,250	900
10	2,200	9,800	1,550	1,200
11	2,625	11,725	1,850	1,450
12	2,750	12,240	2,200	1,950
13	2,950	*13,150	2,400	2,200

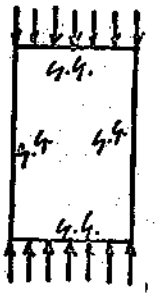

*Cohesive failure of adhesive AFEPOXY 2 caused buckling of face one.

Table 10.

Four Edges Simply Supported Buckling Test

Core: High Impact Polystyrene Core, bonded with Toluene
Core – Facing Bond: RCT Epoxy
Cross Head Speed = 1.27 mm/min (0.05 in/min

Test	Load lbs	Load N	Strain Gage 1 μ/m	Strain Gage 2 μ/m
1	450	2,000	150	No reading
2	600	2,670	420	"
3	900	4,000	600	"
4	1,100	4,900	850	"
5	1,375	6,120	1,150	"
6	1,650	7,350	1,550	100
7	1,875	8,350	1,950	300
8	2,200	9,800	2,400	525
9	2,500	11,125	2,800	750
10	2,800	12,475	3,400*	950

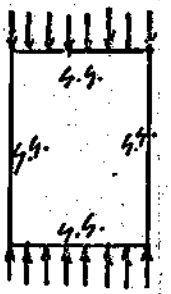

Failure of RTC Epoxy by adhesion.

APPENDIX B

CORE THICKNESS DISTRIBUTION DATA

High Impact Polystyrene Without Reinforcing Wires

High Impact Polystyrene with Reinforcing Wires in Triangular Pattern

High Impact Polystyrene with Reinforcing Wires in Square Pattern

Zn-22Al Without Reinforcing Wires

Zn-22Al with Reinforcing Wires

Table 11
Thickness Distribution Ratio w/w_o in High Impact Polystyrene Forms Without Reinforcing Wires

Distance mm	Thickness Ratio w/w_o mm/mm Path 2	Path 3	Path 1
1	57	0.58	0.63
2	58	0.50	0.53
3	57	0.47	0.43
4	57	0.45	0.36
5	57	0.45	0.29
6	57	0.47	0.33
7	57	0.50	0.36
8	55	0.53	0.42
9	55	0.53	0.47
10	52	0.50	0.52
11	53	0.47	0.52
12	54	0.44	0.50
13	60	0.45	0.50
14	63	0.47	0.43
15		0.50	0.43
16		0.59	0.45
17			0.50
18			0.63

w_o is initial thickness
w is the thickness at a particular location after forming.

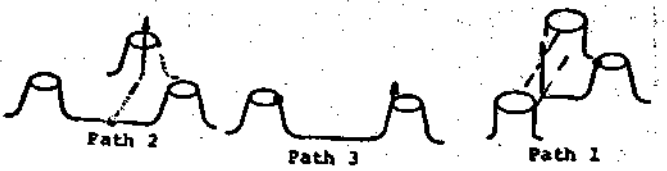

Table 12.

Thickness Distribution Ratio w/w_o for the High Impact Polystyrene Forming with the Reinforcing Wires.

Distance mm	Thickness Ratio w/w_o Path 1 mm/mm	Path 4 mm/mm	Path 4* mm/mm
1	0.63	0.63	0.65
2	0.42	0.43	0.43
3	0.33	0.24	0.25
4	0.24	0.17	0.17
5	0.15	0.15	0.17
6	0.1	0.17	0.19
7	0.13	0.18	0.18
8	0.13	0.19	0.19
9	0.15	0.21	0.20
10	0.14	0.21	0.22
11	0.13	0.20	0.22
12	0.13	0.17	0.21
13	0.19	0.15	0.20
14	0.28	0.13	0.28
15	0.39	0.13	0.37
16	0.54	0.20	0.47
17	0.78	0.32	0.50
18		0.46	0.77
19		0.57	
20		0.64	

w_o is the initial thickness of the sheet
w is the thickness at a particular location after forming.

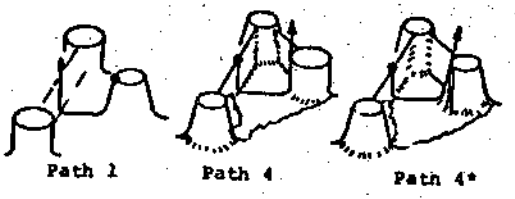

Table 13.

Thickness Distribution w of High Impact Polystyrene Formed in a square Pattern with Embedded Wires.
Path 5

Distance From Top mm	Thickness mm	Distance From Top mm	Thickness mm
1	0.22	25	0.13
2	0.22	26	0.14
3	0.2	27	0.14
4	0.18	28	0.14
5	0.165	29	0.13
6	0.15	30	0.12
7	0.14	31	0.12
8	0.13	32	0.12
9	0.118	32	0.11
10	0.1	33	0.105
11	0.08	34	0.1
12	0.06	35	0.1
13	0.03	36	0.1
14	0.03	37	0.1
15	0.06	38	0.1
16	0.07	39	0.11
17	0.08	40	0.12
18	0.09	41	0.13
19	0.10	42	0.14
20	0.11	43	0.15
21	0.12	44	0.16
22	0.12		
23	0.12		
24	0.12		

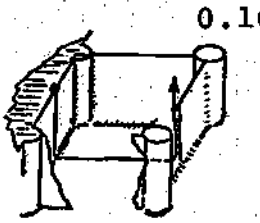

Table 14.

Thickness Distribution Ratio w/w_o in Zn-22Al Forms w/o the Reinforcing Wires.

Distance mm	Thickness ratio w/w_o, mm/mm			
	Path 1	Path 2	Path 3	Path 2*
1	0.68	0.84	0.55	0.86
2	0.77	0.81	0.62	0.85
3	0.73	0.79	0.67	0.81
4	0.69	0.81	0.74	0.81
5	0.64	0.81	0.79	0.81
6	0.61	0.81	0.81	0.78
7	0.57	0.80	0.78	0.79
8	0.52	0.76	0.69	0.69
9	0.57	0.74	0.62	0.69
10	0.61	0.62	0.55	0.69
11	0.69	0.58		0.63
12	0.75			

*Sheet formed 80% only

w_o is the initial thickness of the sheet

w is the thickness at a particular location.

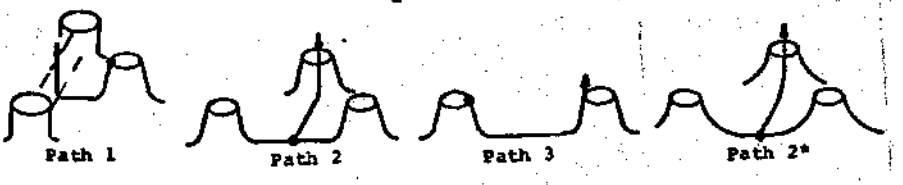

Table 15.
Thickness Distribution Ratio w/w_o of Zn-22Al Sheets Formed with Wires Embedded in Triangular Pattern*

Path 4* Distance From Cone Top mm	Thickness Ratio
0	1.
1	.7
2	.5
3	.35
4	.28
5	.31
6	.34
7	.37
8	.4
9	.4
10	.4
11	.4
12	.32
13	.37
14	.42


Path 4*

*Sheet Thickness w_o = 0.080mm (0.0035 in)

APPENDIX C

SHEET PROPERTIES AND FORMING CONDITIONS

Comparison of Heat Welded HIP Cores Against Conventional Cores

Flaws as a Function of Forming Time

Mechanical Properties of High Impact Polystyrene as a Function of Heating Time

Heat Welding Flat Polystyrene Specimens for Shear Tests.

Heat Welding of Semicores Observations

Relations Between Sheet Thickness and Forming Time of Zn-22Al

Table 16.

Comparison of Heat Welded High Impact Polystyrene Cores Properties Against Some of the Conventional Cores in the w Direction.*

Core Designation	Shear Strength KPa (psi)	Shear Modulus KPa (psi)
Kraft-Paper Honeycomb	1331 (193)	135,000 (19,600)
Hexagonal Nylon Fiber Reinforced	2100 (306)	65,500 (9,500)
Hexagonal Over Expanded Glass Reinforced Phenotic Honeycomb	1500 (220)	110,000 (16,000)
Flexible Core	1930 (280)	55,000 (8,000)
High Impact Polystyrene WRH Core Partially Heat Welded	1420 (206)	100,000 (14,500)
Improved High Impact Poly. WRH Core Heat Welded	2140 (310)	117,000 (17,000)

*The properties are estimated at a core density of 0.123 gr/cm^3, and linearity between properties and core density has been assumed.

Table 17. Characterization of the Vacuum Forming of the 0.75 mm High Impact Polystyrene with Wires Embedded

Number	Flaws	Heating Time (sec)	Observations
1-7/28/76	2	80	Well formed, adequate evacuation
2-7/28/76	2	60	Well formed, adequate evacuation
3-7/28/76	3	65	Light air draft
4-7/28/76	0	65	Perfect
5-7/28/76	BAD	40	Ventilation holes not punched
6-7/28/76	5	65	Possible long heat effect
7-7/28/76	0	55	Perfect
8-7/28/76	0	55	Perfect
9-7/28/76	0	55	Perfect
10-7/28/76	0	55	Perfect
11-7/28/76	0	55	Perfect
12-7/28/76	0	55	Perfect
13-7/28/76	0	60	Perfect
14-7/28/76	0	60	Perfect
1-7/29/76	10	80	Nó good. Formation of Inclined webs
2-7/29/76	4	40	No good
3-7/29/76	15	80	No good. Formation of inclined webs
1-9/13/76	0	55	Very good. It seems like the material close to the wires around the projection is the last to be formed
2-9/13/76	0	60	Perfect
3-9/13/76	0	55	Perfect
4-9/13/76	1	70	Material did not go to the bottom in the vicinity of the flaw
5-9/13/76	0	55	Perfect
6-9/13/76	40	70	Flaws were close together
7-9/13/76	0	50	Perfect
8-9/13/76	12	85	No Good
17-9/13/76	1	55	Material around the flaw formed o.k.
18-9/13/76	0	50	Perfect

Table 18. Mechanical Properties of High Impact Polystyrene As a Function of Heating Time.

Specimen	Cross Section (mm^2)	Heating Time (sec)	Maximum Load (N)	Y.P. Load (N)	Strength (10^{-3} KPa)	Y.P. (10^{-3} KPa)	ΔF (N)	$\Delta\varepsilon$ μ/m	E (10^{-6} KPa)
2-8/27/76	30	108	614	44.5	20.5	1.48	445	0.0103125	1.44
3-8/27/76	29	240	552	35.6	19	1.23	256	0.00875	1.4
4-8/27/76	30	150	623	44.5	20.8	1.48	445	0.01031	1.44
5-8/27/76	30	180	538	44.5	18	1.48	267	0.00606	1.47
6-8/27/76	29	120	609	44.5	21	1.53	356	0.00825	1.49
7-8/27/76	29.5	133	609	44.5	20.6	1.51	213	0.006	1.21
8-8/27/76	29	480	565	44.5	19.5	1.53	356	0.009	1.36
9-8/27/76	29.5	0	632	50.0	21.4	1.69	356	0.075	1.6

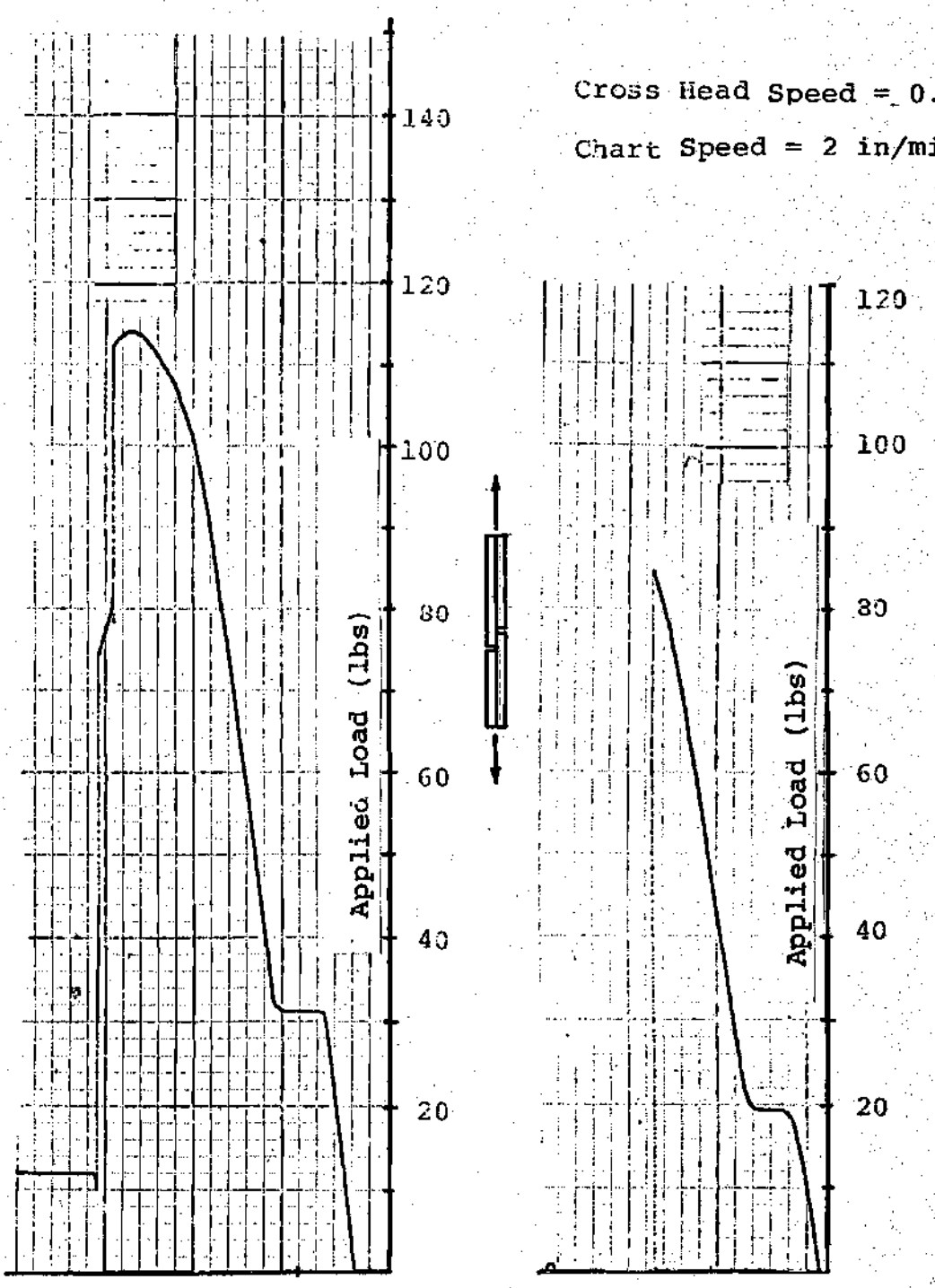

Figure C-1. Typical Shear Test Results of Heat Welded Specimens of High Impact Polystyrene.

Table 19. Heat Welding of Flat Polystyrene Specimens for Shear Test*

No.	Temp. (°F)	Preheat Time (Min)	Heat-Time with Pressure	Observation
1	200	0	8	No bonding at all
2	270	0	12	No bonding
3	270	0	20	No bonding
4	300	0	20	Partial bond, broke by hand pulling
5	350	2	3	Satisfactory
6	350	2	2	Good seal
7	350	2	1	Very good seal
8	350	1	3	Very good seal
9	350	1	2	Very good seal
10	350	1	1	Good seal, no bond
11	325	2	2	Good seal, no bond
12	325	2	4	Looks good
13	325	2	3	Looks good
14	325	2	1	Looks good
15	325	2	2	No bond (oil surface)

*Pressure constant--1.4 KPa (20 psi)

0.762 mm sheet thickness (0.030 in)

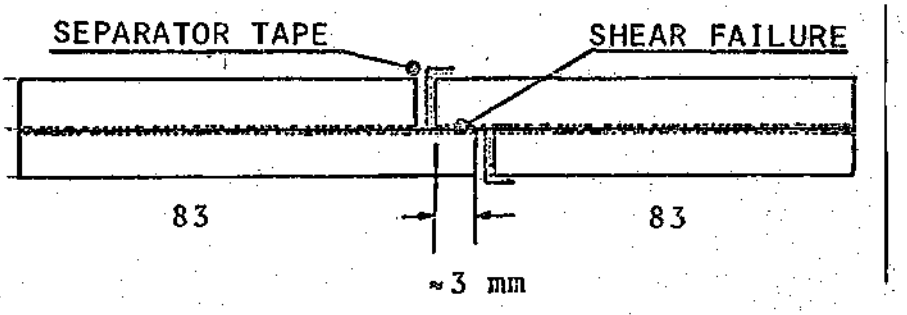

Table 20. Shear Test on Flat Heat Welded Specimens

Specimen Number	Area (in^2)	Force (lbs)	Shear Stress KPa	Preheat Time (min)	Press. Time (min)	Temperature (°C)
5	.0824	45	36.67	2	4	176
6	.0897	102	78.45	2	3	176
7	.0840	113	92.8	2	2	176
8	.0853	110	89	2	1	176
9	.0859	111	89.1	1	3	176
10	.0633	92	100.2	1	2	176
12	.0756	85	77.5	2	4	163
13	.0711	114	110.6	2	3	163
14	.0969	54	38	2	1	163

Table 21. Heat Welding of Semicores Observations*

Test	Preheat Time (min)	Forming Time (min)	Observation
1	0	4	Sheet broke at vicinity of a flaw.
2	2	4	Leakage at a flaw. Bad forming.
4	2	6	No leakage. Good bond. There were no flaws.
4	2	6	Excellent. No leakage was detected, no breaks, and no cracking on bending.

*Semicores were heat welded at a temperature of 176°C (350°F) and a pressure of 1.4 KPa (20 psi).

Table 22. Relation Between Applied Pressure, Sheet Thickness and Forming Time of Zn-22Al.

Number	Sheet Thickness (mm)	Pressure (psi)	Forming Time (sec)	Time For Pressure Drop to 20 psi (sec)	Observations
1-8/24/76	0.075	28	15	40	Very good sealing
2-8/24/76	0.075	28	17	40	Very good sealing
3-8/24/76	0.075	16	80	-	Very good sealing
4-8/24/76	0.075	20	66	-	Very good sealing
5-8/24/76	0.075	24	61	20	Very good sealing
9-7/29/76	0.075	36	25	22	Some leakage
10-7/29/76	0.075	36	15	50	Good sealing
11-7/29/76	0.075	36	22	40	Good sealing
7-7/23/76	0.075	30	30	34	
8-7/23/76	0.075	36	23	30	
3-7/23/76	0.125	36	123	44	Good forming
1-7/23/76	0.125	36	120	25	Not fully formed

APPENDIX D

APPLICATION AND SELECTION OF BONDING MEDIUM

Surface Preparation

The proper application of a bonding medium in a light weight structure is as important as the design of the structure itself. A structure poorly bonded shows low performance. If the core and facings in a sandwich construction are not firmly joined, large relative movements take place at the bonding line and the structure behaves as a group of independent elements or at most loosely bonded. The surface preparation is essential for a good bond.

The procedure used to clean the aluminum facings was as follows [20]

1. Removal of the oil with isopropyl alcohol, or acetone.
2. Immersion in an alkaline cleaner for 8-12 minutes.
3. Rinsing throughly with water .
4. Immersion in an etching solution at 150 ° $\pm$ 5 °F for 10 minutes of the following composition.

   Distilled water 30 parts by weight

   Sulfuric Acid (conc) 10 parts

   Sodium Dichromate ($Na_2CA_2O_7 \cdot 2H_2$) 1 part
5. Rinsing the facing sheets in clear running water.
6. Drying for 10 minutes with air.

The Zn-22Al sheets surface preparation was identical to the recommendations for aluminum honeycomb cores. Aliphatic Naphtha was used at room temperature for five minutes and and the sheets were dried for 10 minutes at 200 °F. As an alternative method, acetone was used to replace the Naphtha.

The High Impact Polystyrene sheets were cleaned with Isopropyl Alcohol, and a few sheets were slightly sanded with 200 grit sandpaper, as recommended by Cagle [20].

Selection of the Adhesive

A number of adhesives were tried out to determine the most suitable product for the core loading plate and core-core interface. The optimum curing conditions that the manufacturer suggested were not always possible to achieve because the curing time and temperature had to be such that did not affect the core shape. The results reported in Figure D-1 correspond to shear test, similar to the loading conditions in the core tensile shear test.

The results indicate that AFEPOXY 2, cured for two hours at 138 °C (280 °F), was about the best product; however, such conditions could not be tolerated by the High Impact Polystyrene without affecting badly its shape. As there were large deformations taking place at the bonding line, as reported in Figure D-2, the AFEPOXY 2 was successfully replaced by RTC Epoxy, and no more adhesive failure were observed.

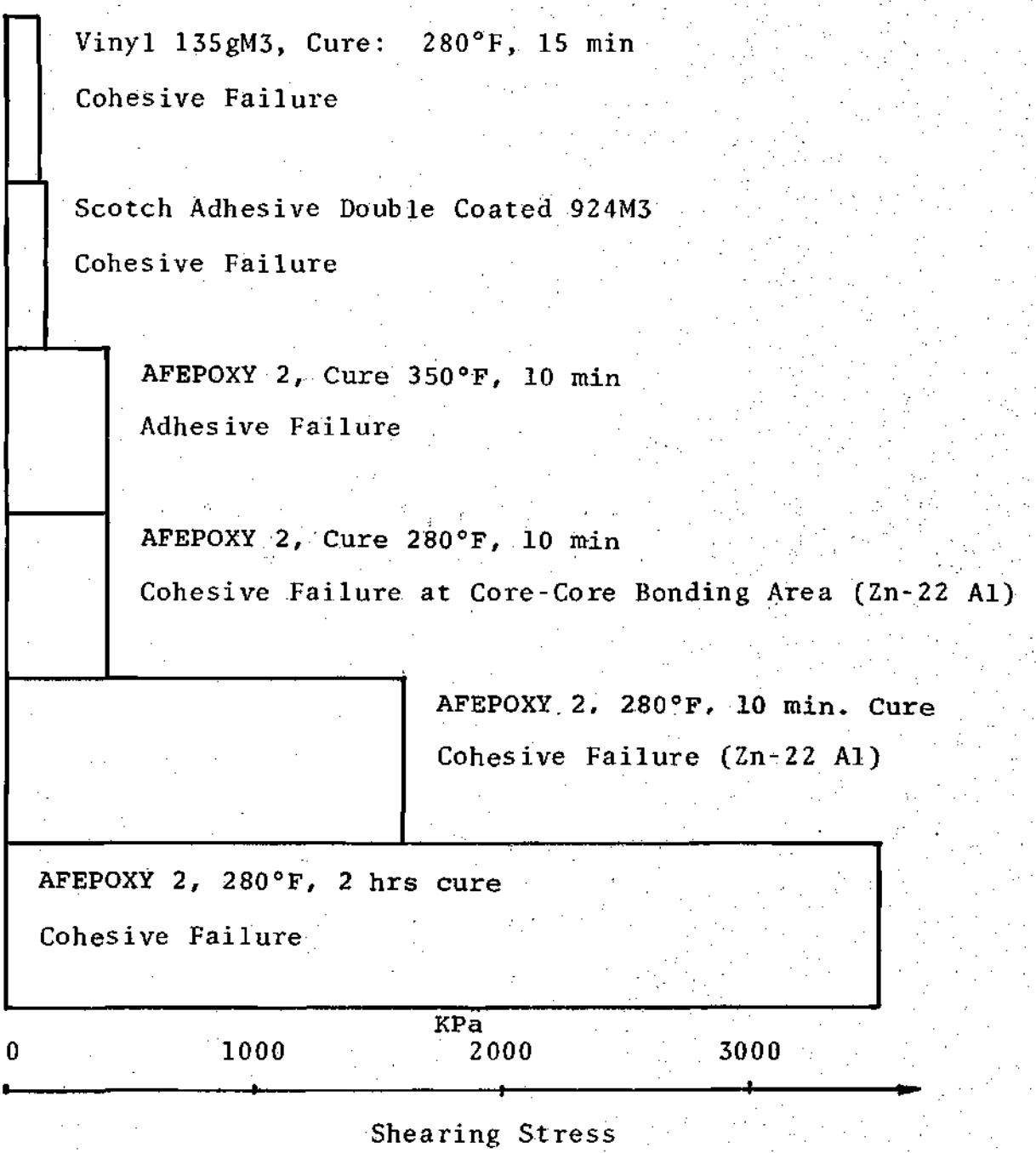

Figure D-1. Selection of Adhesive for Core-Loading Plate Bond

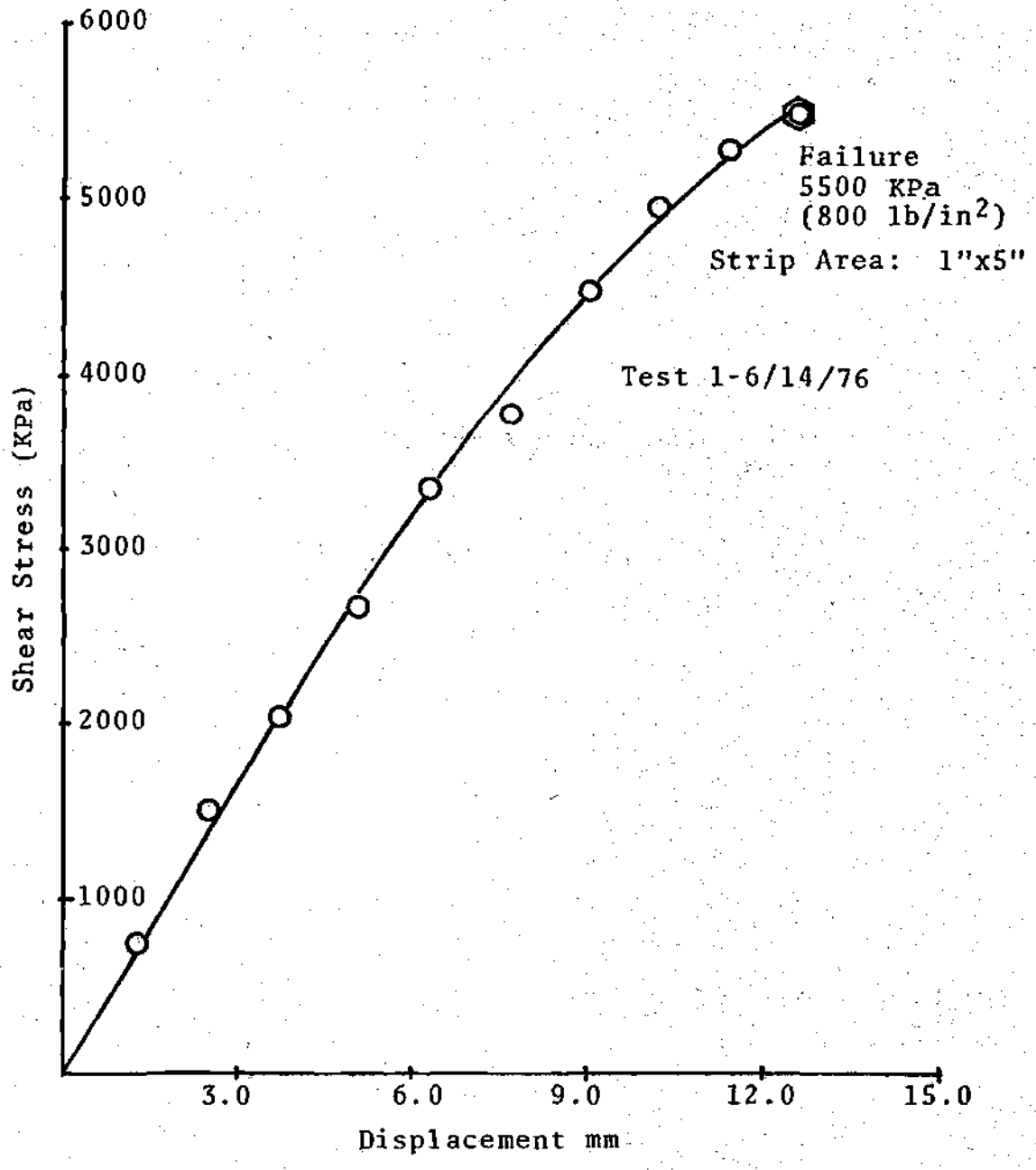

Figure D-2. Shear Strength of Adhesive AFEPOXY 2 Cured at 140°C (285°F) for 2 Hours

Table 23. Adhesive AFEPOXY 2 Shear Test Behavior

Load lbs	Load N	Stress KPa	Displacement mm
550	2,450	760	1.27
1,100	4.900	1,519	2.54
1,500	6,675	2,069	3.81
1,950	8,680	2,690	5.08
2,425	10,800	3,350	6.38
2,750	12,200	3,780	7.62
3,250	14,500	4,500	8.89
3,600	16,000	4,960	10.15
3,850	17,150	5,300	11.43
4,000	17,800	5,500	12.7

*Adhesive was cured at 140 °C (285 °F) for 2 hours.
Cross Head Speed: 1.27 mm/min (0.05 in/min)
Test: 1-6/14/76

APPENDIX E

THE STRAIN GAGE

The strain on the sandwich facings was directly measured by strain gages in the bonding and buckling tests, as mentioned in Chapter III, where the equipment and the electric circuit were illustrated. In order to balance the circuit without much difficulty, four strain gages with nominally the same resistance were used to make the Wheatstone bridge, but only one gage was actually loaded. The strain gage used was type C6-644-260 with a gage factor of 2.21 ± 0.5%, a resistance of 260 ± 0.5 ohms, and manufactured by the Budd Company.

The three unloaded strain gages completing the bridge were mounted on a 5 cmx 20 cm x 1.25 cm piece of 2024 aluminum alloy. The active strain gage was mounted on the 2024 Aluminum T3 alloy facing sheet. Acetone was used to throughly clean the areas where the strain gages were mounted. Eastman 910 Adhesive was used to bond the gages, and the excess of adhesive was carefully squeezed out from the bonding area, to improve the curing and performance of the gages. The mounting plate was grounded to the Instron Universal Testing machine. Figure E-1 illustrates the apparent strain, and gage factor variation that are characteristics to the type of gage used on the experiments.

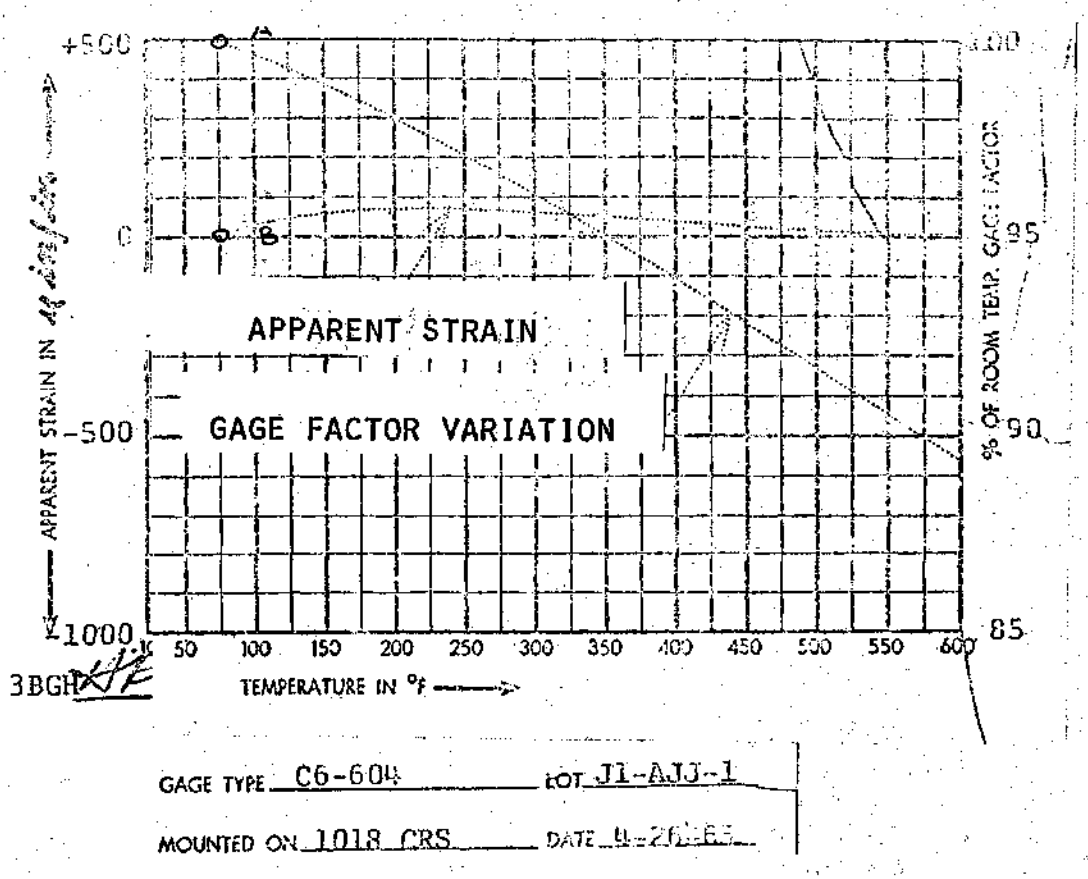

This curve was provided by the manufacturer, the Budd Company.

Figure E-1. Characteristic Curve of Strain Gage Used in Bending and Buckling Tests

APPENDIX F

This appendix is intended as a summary of superplasticity behavior, the understanding of the process, present superplastic technology and its applications.

Superplasticity has been observed in many alloys of eutectic or eutectoid composition, but not exclusively so. All superplastic materials are characterized by having very fine grains, very high strain rate sensitivity and a range of temperature and strain rate in which the phenomenon has been observed. The understanding of this material behavior is not still clear. Most of the work conducted with superplastic alloys have been on the laboratory scale; but great promise is expected because the superplastic materials can deform uniformly sometimes up to 2,000% in terms of original length and no other material can be used to form very complex shapes with great reproduction of details in a single operation.

Superplastic alloys have been discovered in most metallic systems, and in all cases very fine grains have been reported, in the order of .4-10μm [43]. The phenomenon has always been observed in a limited range of temperature and strain rate. Some of the basic metals involved in superplastic alloys are: aluminum, cadmium, copper, iron, zinc, lead, magnesium, nickel, tin, titanium, and zirconium.

Superplasticity: A Useful Property

Superplastic alloys are generally deformed at temperatures above half their melting temperature [28]. At room temperature, they exhibit mechanical properties comparable with conventional materials; therefore, superplasticity can be used to our advantage for parts manufacturing [39]. Super-

plastic metal sheets can be thermoformed by vacuum forming techniques or by applying very low pressure 350-1700 KPa (50-250 psi) [39]. Solid pieces of superplastic alloys can be squeezed into intricate shapes, similar to close die forming or pressure casting. In this way, components with very fine grain, can be obtained, with no microporosity as in the casting of certain alloys, and excellent reproduction of detail.

Superplastic materials, like Zn-22Al alloy, can be used successfully in tooling for plastic injection molding [39]. In this way, female cavities of the mold can be easily produced by pressing a male tool into a blank of eutectoid Zn-22Al. Benefits can be derived from the ability of superplastic alloys to flow readily under low forces in extrusion, rolling, deep drawing, and forming [39]. Materials like superplastic nickel have been rolled, and a significant reduction of rolling forces has been obtained. Nickel base superalloys are also forged superplastically. They are otherwise considered unforgeable.

Metal Forming

Superplastic alloys can be processed by sheet thermoforming, compression molding, and extrusion, as well as blow molding. The merits of using superplastic alloys as opposed to conventional materials, depends on the engineering property requirements of the product, complexity of the shape,

production rate, economy of secondary finishing operations, and tooling cost.

Eutectoid Zn-22Al sheets can be readily formed at a temperature between 268 °C and 274 °C. The process should be completed before the parts reach 278 °C. The forming tools are kept between 305 °C-344 °C (580-650 °F), depending on the sheet thickness. In this way, the whole cycle, including heat treatment, is completed between 3-5 minutes. Thin metal sheets tolerate little or no preheat and they are heated by heat transfer from the tooling. Careful control of preheating temperature and forming time is required to get full benefit of the superplastic condition of the alloy [39]. By using superplastic alloys, parts can be formed into very complex shapes; something that is not possible using other materials. As a result, an assembly of several components made out of conventional alloys are often replaced by a single superplastic part with a more intricate configuration [38].

Although superplastic alloys stretch more uniformly than conventional materials, thinning tends to occur in the last portion to be formed [29]. This effect can be minimized in several ways. First, the pressure could be applied when the material next to the clamping zone is still hotter than the bulk material. In this way, thinning will naturally occur around the clamped material. As the forming proceeds, it will be noticed that the material close to the boundary will be the first to contact the tool cavity and straining will cease.

Another way to reduce thinning is to perform the material in an opposite direction first, then the pressure is reversed. By doing so, and selecting a proper prestretching shape, the material next to the clamping zone will not come into immediate contact with the mold cavity and stretching will be wide-spread.

Plugs of a predetermined shape can also be used for better material distribution. As the bottom of the plug touches a section of the metal sheet, and a force is applied to the plug, the material free of contact will stretch. In this way the sheet can be prestretched at will at specified locations. The parts are subsequently fabricated as the air pressure is applied.

Tooling for Superplastic Alloys

Tool cost can be appreciably reduced when forming blanks and sheets of superplastic alloys because parts can be readily formed at low pressure. The tool material selection depends on production. If production is high, better tool material will be required; so forming time can be reduced at the expense of higher forces to increase the strain rate. On the other hand, if a few parts are going to be formed, then lower strain rate and cheaper tool materials can be afforded.

A tool for pressure thermoforming has, in general, the following features: a pressure clamp, provision for holding tool on press, draft for easy removal, good surface

finishing and texture without interfering with part removal and must be strong and rigid. The tool must have vents to permit the entrapped air to be removed. The vent diameter should be no more than one half the thickness of the sheet. The tool also may have inserted heaters, as well as temperature control sensors. Heat or air-curing ceramic felt or transite can be used as insulating materials. To facilitate part removal, resin-bonded molybdenum disulphide has proven satisfactory.

Tools have been made of steel and aluminum, although steel is preferred because it retains heat better. Sand-cast aluminum alloys have also been used as well as sintered iron, which has the advantage of easy venting. Graphite, a self lubricating material which is easy to machine, is a very good material for superplastic tooling [39].

Mechanical Properties of Superplastic Zn-22Al

Zn-22Al is put in the superplastic condition by heating at 650 °F and water quenching. Under these circumstances, if the alloy is subjected to tension between 475-530 °F it elongates about 2200% before it ruptures. A typical grain size is of the order of 1-2 μm, unresolvable by light microscopy. Further grain size reduction can be obtained by cold rolling. This in turn will reduce the forming pressure even further. For the heat treatment, the parts are brought up to 650 °F and either air or furnace

cooled. The furnace cooled parts exhibit some grain growth and are more resistant to creep at room temperature which is an important factor in superplastic materials.

The Zn-22Al is sensitive to creep at room temperature. The furnace cooled alloy permits much better design stress in terms of creep; however, the yield stress is much higher for the air cooled parts as opposed to the furnace cooled. The creep strength for furnace cooled parts is 43,000 KPa (6,300 psi) compared with 17,000 KPa (2,500 psi) for air cooled parts.

It seems that the principal limitation of Zn-22Al alloy is creep resistance rather than a rupture limitation. The eutectoid Zn-22Al shows an average strength of 90,000 KPa in fatigue, under reversed bending, for 10 million cycles. The Zn-22Al seems to be more resistant to corrosion than 380 Al as cast, when subjected to different environments containing 100% humidity, SO_2, NH_3, NaCl at room temperature.

Controlling Mechanism

For a material to be superplastic, it must be strain rate sensitive. In this way a localized necking will not develop. This is what is observed in some very fine grain alloys as they are stressed above 0.5 T_m. The hardening occurs from strain rate sensitivity rather than from strain hardening. This can be expressed into the following form [34]

$$\sigma = K\dot{\varepsilon}^{m}$$

Rewriting this equation in terms of the area and the applied load, we obtain

$$dA/dt = -1/k(LOAD/E)^{1/m}.A^{(m-1)/m}$$

From here we can see that as m approaches one, dA/dt becomes independent of the area [47]. In practice this means that deformation will not be localized but rather will be well distributed throughout the whole specimen. As the stress is increased in sections where the area has been reduced, the ratio dA/dt will remain about the same in the entire specimen. On the other hand, materials that have an m factor of 0.2 or less show a pronounced necking.

There is no single mechanism that can fully explain superplasticity. Some processes have been advanced as possible superplastic mechanisms, namely: vacancy-migration process, grain boundary sliding, and dynamic-recovery processes.

The vacancy migration hypothesis proposes that there is a directional flow of vacancies along the grain boundary [43] or through the lattice as a result of stress induced migration. There will be a high concentration of vacancies in the boundaries that are perpendiculary oriented to the applied forces and diffusion will occur toward the boundaries that are parrallel to the loading. The diffusion of vacancies will imply a diffusion of atoms [41]. This can be expressed

in the following form:

$$\dot{\varepsilon} = B_1 \Omega\sigma/(L^2 kT) \cdot D_L$$

and

$$\dot{\varepsilon} = B_2 \Omega\sigma \cdot (wD_{g \cdot b})/L^3 kT$$

where $D_{g \cdot b}$ and D_L refer to the diffusion coefficient along the graining boundary and through the lattice, w is the grain boundary width, L is the grain size, Ω the atomic volume, B_1, B_2, k are constants, and σ and T are applied stress and temperature. There are some drawbacks to this superplastic controlling mechanism, for it cannot explain adequately the fact that the grains remain equiaxed and keep their original shape as the material is deformed.

Avery and Backofen [29] have proposed a combined equation that takes into account vacancy migration creep and dislocation climbing, as indicated below:

$$\dot{\varepsilon} = A \frac{\sigma}{L^2} + \sinh(\beta\sigma)$$

where A, B, and β are constants at a given temperatures, $\dot{\varepsilon}$ is the strain rate and σ is the internal stress. Many other variations to the vacancy migration mechanism has been proposed. It seems that at very low strain rate the vacancy migration is the controlling mechanism [43] but at higher strain rates, the role of vacancies is not clearly understood.

Grain boundary sliding may also explain superplasticity. The absence of pronounced change of grain shape gives

support to this hypothesis. It is assumed that the grain boundaries act as a fluid. A complete disorder of atoms as in a noncrystalline state is approached as the grain size becomes very fine. Orowan [52] has suggested that the straing rate would be

$$\dot{\varepsilon} = B_3 \sigma \Omega \cdot D_L / kT$$

where the terms have been defined before.

The full explanation of the superplastic phenomenon using the sliding criterion has been questioned from the fact that not all grain boundaries can move without causing some grain deformation. It has been suggested that diffusion along grain boundaries could accommodate the material at the triple points to permit sliding, as long as the grain size is about 1 μm [42]. Not much attention has been given to the type of boundary that slides. In fact, sliding between two grains of the same phase is more likely to occur because diffusion will provide for the accommodation and stress relief.

Superplasticity has also been explained as a dynamic-recovery process. The idea has been thought taking hot working operation as reference where continuous recrystallization occurs. There is much discussion whether recrystallization occurs continuously during hot working. It is known that some materials do not recrystallize until after the straining is stopped [43]. There is no evidence to indicate

that high strain rate sensitivity is associated with hot working. Continuous recovery of superplastic material has not been proven, and only metallographic evidence has been reported [43].

Survey of Zn-22Al Experiments

Most of the research in superplastic alloys has been centered on Zn-22Al experiments by cold working, hot working, bulging of sheets, blank forming, corrosion resistance and many others.

Nuttal studied the behavior Zn-22Al as quenched and rolled at room temperature [37]. It was found, rather amazingly, that both hardness and tensile stress were reduced with increase in rolling reduction. The microstructure was elongated in a similar manner to most metallic materials. However, the tensile test indicated that the microstructure shape and size does not change. This again indicates that superplasticity is also associated with low strain rate (viz tensile testing). Nuttall also changed the grain size and noticed that as the grain size was increased the loading continued to increase with strain. But for the finer grained material a decrease in loading as strain increased resulted.

It was also observed that aging at room temperature could affect the material properties. After ten days of aging it was found that cold rolled material could be elongated

more than the material that was aged for six months.

Stamping experiments with superplastic Zn-22Al were performed by R. A. Saller and T. L. Duncan [44]. They found more evidences concerning the very high strain rate sensitivity of superplastic alloys. They were able to make a stamping tool from Zn-22Al by using a coin pattern and a small disc weight capable of deforming the Zn-22Al at very low strain rate. The deformed parts could be used later as a tool to make an impression in copper using a high deformation rate. This experiment reaffirms that the flow stress of superplastic materials is highly dependent on the strain rate.

Experiments concerning bulging of Zn-22Al sheets have also been conducted at 250 °C [45]. The variation of the mean strain as a function of grain size, and pressure, were studied. It was found that the bulging characteristics did not change appreciably with pressure over a limited range of pressure; instead, variations were associated with grain size. Bigger elongations and better material distribution were obtained with finer grains. Also, surface roughness of the formed parts increases with grain size, as the strain rate sensitivity is diminished.

Deformations involving severe variations in strain rate, such as forming a sheet around solid projections and wires, have been recently studied by Underwood, Gomez, and Ueng [40].

REMARKS

1. The flow stress of superplastic materials is very sensitive to the strain rate, but not to the strain level. The deformation of the material is very uniform, exhibit no necking under tension, and the engineering strain is 500% or more, before rupture takes place.

2. Superplastic alloys are still in a development stage; but some alloys, as eutectoid Zn-22Al, are finding more and more industrial applications.

3. Superplastic materials can be used to advantage, especially in the manufacturing of complex parts from metal sheets or billets. Neither the degree of filling nor the reproduction of details are matched by conventional materials. Production cost can be reduced as an assembly of several standard components is replaced by only one part made from superplastic alloys.

4. Superplastic materials are found to be very useful in tooling, especially in tools for injection molding.

5. Ceramic, alloys, and single phase superplastic materials have been reported. A common feature to all superplastic materials is that they have a very fine grain. For this reason, most superplastic alloys have a eutectic or eutectoid composition.

6. Superplasticity is only observed in a range of

temperature and strain rate that is characteristic for each alloy.

7. Once the parts are formed in the superplastic condition, they can be heat treated to restore desired mechanical properties at room temperature.

8. The mechanisms to explain the superplastic behavior of some materials is not fully understood. Grain boundary sliding, vacancy migration, and dynamic recovery processes have been suggested as possible mechanisms.

9. As superplasticity is characterized by very fine grains, in the order of 0.4-10 μm, it is expected that crystallization takes place by homogeneous nucleation, as it is the case for Zn-22Al where a spinodal decomposition reaction occurs.

LIST OF REFERENCES

1. A. Voss, "Mechanical Properties of Some Low-Density Materials and Sandwich Cores," Report 1826, Forest Products Laboratory, United States Department of Agriculture, 1952.

2. E. Kuenzi, "Mechanical Properties of Aluminum Honeycomb Cores," Report 1849, Forest Products Laboratory, United States Department of Agriculture, 1955.

3. R. Seidl, E. Kuenzi, and D. Fahey, "Paper Honeycomb for Structural Building Panels," Report 1796, Forest Products Laboratory, 1961.

4. L. J. Markwardt and L. Wood, "Long Term Case Study of Sandwich Panel Construction in FPL Experimental Unit," FPL Report 2165, 1959.

5. P. Jenkins and E. Kuenzi, "Effect of Core Thickness on Shear Properties of Aluminum Honeycomb Core," Report 1886, Forest Products Laboratory, 1962.

6. G. Stevens, "Compressible and Shear Strength of Two Configurations of Sandwich Cores of Corrugated Foils," Report 1889, Forest Products Laboratory, 1962.

7. G. Stevens and E. Kuenzi, "Mechanical Properties of Several Honeycomb Cores," Report 1887, Forest Products Laboratory, 1962.

8. E. Kuenzi, "Mechanical Properties of Diffusion-Bonded Titanium Sandwich Construction," Report 218, Forest Products Laboratory, 1973.

9. W. Kommers and A. Norris, "Effects of Shear Deformations in the Core of a Flat Rectangular Sandwich Panel," Report 1583-A, Forest Products Laboratory, 1962.

10. P. M. Jenkinson, "Compressive and Shear Properties of Polyester and Polyimide Film Honeycomb Cores," Report 75, Forest Products Laboratory, 1967, AD 661107.

11. N. T. Baldanza, "Survey of Plastic Sandwich Construction," Plastic Report 34, 1968, AD 673713.

12. H. R. Ogden, T. Houck, L. Abraham, and R. Taffee, "Formable Sandwich Structures for Aerospace Applications," Materials Science Research, Proceedings of the 1964 Southern Metals/Materials Conference on Advances in Aerospace Materials, Plenum Press, 1965, pp. 177-191.

13. Bendix Corporation Staff, "Energy Absorbing Characteristics of Crushable Aluminum Structures in a Space Environment," Report SPP-65-107, NASA, 1965, N65-31183.

14. C. E. S. Ueng, "A Note on the Similarities Between Analysis of Homogeneous and Sandwich Plates," ASME Transactions, Series E, Journal of Applied Mechanics, Vol. 33, 1966, pp. 681-683, A66-42159.

15. H. G. Allen, "Analysis and Design of Structural Sandwich Panels," Pergamon Press, 1969.

16. F. T. Plantema, "Sandwich Construction, The Bending and Buckling of Sandwich Beams, Plates and Shells," Wiley, 1966.

17. H. Eickner, "Adhesive Bonding Properties of Various Metals as Affected by Chemical and Anodizing Treatments of the Surfaces," Report 1842, Forest Products Laboratory, 1953.

18. T. Black and R. Blomquist, "Development of Improved Structural Epoxy--Resin Adhesives and Bonding Processes for Metals," Ibid.

19. T. C. Fan, "Face Wrinkling Mode of Buckling of Sandwich Panels," Rand Corporation Report P-3202, 1965, AD 619997.

20. Ch. V. Cagle, Handbook of Adhesive Bonding, McGraw Hill Book Co., 1973, p. 11-13.

21. I. Skeist, Handbook of Adhesives, Reinhold Publishing Corporation, 1962, p. 481.

22. N. A. Debruyne, Adhesion and Adhesives, Elsevier Publishing Co., 1965.

23. E. C. Bernhardt, Processing of Thermoplastic Materials, Robert Krieger Publishing Co., 1974.

24. P. Riewald and T. Venkatachalam, "Kevler: Aramid Fiber for Rope and Cable Applications," Offshore Technology Conference, Houston, Texas, 1975.

25. W. Rosenhain, T. Haughton, and K. E. Bingham, Institute of Metals, 1920, 23, 261.

26. A. Sauveur, Trans. Amer. Inst. Min. Met., 1924, 206, 928.

27. E. E. Underwood, Trans. Amer. Inst. Min. Met., 1962, 224, 914.

28. C. Rossard, Rev. Met., 1966, 63 (3), 225.

29. W. A. Backofen, I. R. Turner, and D. Avery, Transaction of American Society of Metals, 1964, 57, 80.

30. E. Hardt, Acta, 1967, 15, 351.

31. A. R. Ragab and T. L. Duncan, "Rate Dependent Transient Extrusion," Int. J. Mech. Sci., Pergamon Press, 1975, Vol. 17, pp. 125-137.

32. A. R. Ragab and T. L. Duncan, "Superplasticity: Constitutive Equations and Forming Problems," Symposium on Foundation of Plasticity, Polish Academy of Science, 1972.

33. T. J. Headley, D. Kalish, and E. E. Underwood, "The Current Status of Applied Superplasticity," Ultrafine Grain Metals, Syracuse University Press, 1970.

34. D. L. Holt, Int. J. Mech. Sci., 1970, Vol. 12, 491, printed in G.B.

35. R. W. K. Honeycombe, "Plasticity and Superplasticity, Institution of Metallurgist Review Course, 1969, Series 2, Number 3, pp. 1-18.

36. R. B. Nicholson, ibid., pp. 19-37.

37. K. Nuttall, Journal of the Inst. of Metals, 1972, 100, 114.

38. H. Naziri and R. Pearce, "A Guide to Superplasticity," Sheet Metal Industries, January, 1969.

39. D. S. Fields, "The Promise of Superplasticity," Information and Technical Publication Department, IBM Document EN.20.0276, July, 1972.

40. E. E. Underwood, A. Gomez and C. E. S. Ueng, "Design and Fabrication of New Core Configurations for Sandwich Panels," Proceedings of IV Conference in Materials Technology, Caracas, 1975.

41. P. G. Shewmon, Diffusion in Solids, McGraw Hill Book Co., p. 44.

42. R. C. Gifkins and K. V. Snowden, Trans. Met. Society, AIME, 1969, 239, 910.

43. R. H. Johnson, Met. Rev., 1970, 15 (146), 115.

44. R. A. Saller and T. L. Duncan, Journal of the Institute of Metals, 1971, 89, 1973.

45. T. Hestbech, E. W. Langer and A. Rosen, Journal of the Institute of Metals, 1971, Vol. 99, 2654.

46. P. G. Shewmon, Transformation in Metals, McGraw Hill Book Co., p. 290

47. D. H. Avery and T. M. Stuart, 14th Sagamore Army Materials Research Conference, Raquette Lake, New York, 1967.

48. Hexcel, Design Hand Book for Honeycomb Sandwich Structures, TSB 123, March 1970.

49. L. Calcote, The Analysis of Laminated Composite Structures, Van Nonstrand Reinhold, 1969.

50. American Society for Testing Materials, Annual Book of ASTM Standards, pt. 16, 1973.

51. Hexcel, Catalogue TSB 120.

52. E. Orowan, Progress in Physics, 1948-49, 12, 185.

VITA

Amílcar José Gómez Fermín was born in San Juan Bauitista, Isla de Margarita, Venezuela, on February 12, 1934. He graduated from El Macaro School of Education in 1951, and served as elementary school teacher until March, 1956. He was awarded a scholarship by the Venezuelan Government and started his engineering education at the University of Genoa, Italy, in September 1956. He transferred to Jackson Junior College, Jackson, Michigan in February 1958, and entered the University of Michigan, Ann Arbor, Michigan in June 1958, where he completed his Bachelor of Science in Mechanical Engineering in February 1961, and later his Master of Science in Mechanical Engineering in February 1962. Since then, he returned to his native country, Venezuela, where he worked first with the Siderurgica del Orinoco (Iron Mills), Puerto Ordaz, and later with Creole Petroleum Corporation, Zulia State, until August 1963. At that time he joined the University of Oriente teaching staff, until September 1973, when he came to the Georgia Institute of Technology under a leave of absence. At the University of Oriente, he held the position of head of the Mechanical Engineering Department for two years and head of the Mechanical and Electronic Technician Department for two more years. He also taught undergraduate level courses at the University of Oriente

in the areas of manufacturing processes, machine design elements, and mathematics. He received In Plant Group Training in Yugoslavia and France from October 1966 to December 1967, sponsored by UNESCO and the French Government. He planned and directed a small business enterprise in which University and teaching staff pooled their capital to manufacture school supplies, in the period 1970-1973.

He has recently accepted a position to work with the Venezuelan Research Institute (IVIC) in Caracas.

He is a member of the American Society for Metals, the Society of Manufacturing Engineers, and Venezuelan Association of Mechanical and Electrical Engineers.

Mr. Gomez is married to the former Paulagene Becky Ross, from Michigan. They have four children, LiLita (16), Randy (15), Joey (13), and Rigi (12).